PHOTO-DRIVEN ONE AND TWO-ELECTRON PROCESSES OF TETRAAZATETRAPYRIDO-PENTACENE AND SUBSTITUTED DIPYRIDOPHENAZINE LIGANDS IN THE PRESENCE OR ABSENCE OF ZINC AND RUTHENIUM COMPLEXATION

by

JOSEPH M. ASLAN

Presented to the Faculty of the Graduate School of

The University of Texas at Arlington in Partial Fulfillment

of the Requirements

for the Degree of

DOCTOR OF PHILOSOPHY

THE UNIVERSITY OF TEXAS AT ARLINGTON

August 2012

ACKNOWLEDGEMENTS

I would like to take this opportunity to sincerely thank my advisor Frederick M. MacDonnell for providing me with the tools for success throughout my graduate school career. From teaching me how to "separate the wheat from the chaff", manage my time wisely, and view the big picture, I have been able to succeed in my graduate school work. I will never forget the lessons you have taught me, and I will try to be an example to others as you have been towards me. I would like to thank Dr. Shreeyukta Singh for teaching me how to handle the "ups and downs" of research. Her character is the definition of patience and wisdom, and I hope I can conduct myself in the same way towards future colleagues and students.

I would also like to thank my mentors at SABIC, Dr. Navinchandra Asthana and Dr. Ganesh Kannan. They both have been taught me how to successfully drive research in a fast-pace setting, and have for enriched my life by showing me how to use chemistry to create an impact in the market.

To Masoud Aslan, Mary Akin, Rex Akin, Jonathan Aslan, and Matthew Aslan, thank you for supporting me through my entire educational process. From the time I researched "greek-fire" in 7th grade, and re-discovered the ancient recipe in the high-school laboratory, everyone knew I was going to end up a mad scientist or a chemist. Thankfully I became a chemist, despite what others may think, and I would not be here without the support of my family. To Casey Freeman, thank you for motivating me to succeed, teaching me how to assert myself as a scientist, and reach beyond my limits to accomplish difficult tasks.

Lastly, I would like to thank God. He is the Father of chemistry. I thank Him for guiding my hands and gifting me with wisdom. To Him I attribute all of my success, and with Him anything is possible. My graduation as a Ph.D. in Inorganic Chemistry is proof.

July 12, 2012

ABSTRACT

PHOTO-DRIVEN ONE AND TWO-ELECTRON PROCESSES OF TETRAAZATETRAPYRIDO-PENTACENE AND SUBSTITUTED DIPYRIDOPHENAZINE LIGANDS IN THE PRESENCE OR ABSENCE OF ZINC AND RUTHENIUM COMPLEXATION

Joseph M. Aslan, Ph.D.

The University of Texas at Arlington, 2012

Supervising Professor: Frederick M. MacDonnell

Herein, we report the interaction of light with Zn(II) and Ru(II) adducts of the polypyridal ligands tetraazatetrapyridopentacene (tatpp) and dipyridophenazine (dppz). For examples where Zn(II) is coordinated to tatpp and dppz, we have established a kinetic isotope effect for photo-oxidation of alcohols using both zinc(II) free and zinc(II) bound complexes of tatpp and dppz. The data supports H-atom transfer mechanism in the absence of Zn(II), and a formal "hydride" transfer in the presence of Zn(II).

We also report herein the synthesis of various $[Ru(phen)_2(dppzX_2)]^{2+}$ complexes, where dppz represents dipyrido-[3,2-a:2',3'-c]phenazine and X = H, Br, and CN substitution in the 10,11,12, and 13 positions of dppz, and have characterized these complexes using NMR, ESI-MS, CHN, and UV/Vis. Solvated ground state MO calculations were performed at the B3LYP level using Gaussian 03 software, which predicts the energy of the orbital localized on the dppz ligand can be lowered with increasing withdrawing group strength, and by substituting withdrawing groups in the 10,13 position of dppz more so than substitution in the 11,12 position, which was validated experimentally using cyclic voltammetry. Both di-cyano

$[Ru(phen)_2(dppz(CN)_2)]^{2+}$ complexes showed multiple reductions during cyclic voltammetry and differential pulse voltammetry experiments, and spectroelectrochemistry was used to characterize the species produced. In both complexes, reductions occurring between -1.1 V and -1.4 V vs. NHE show a decrease in the 450 nm MLCT absorption band, which signifies reduction of the metal bound exterior phen ligands. Reductions occurring between 0 V and -1.0 V vs. NHE result in new optical absorption bands which are unrelated to the MLCT absorption band at 450 nm, and signify reduction of the dppz acceptor ligand. The singly and doubly reduced anions of both di-cyano complexes were singly and doubly protonated using trifluoroacetic acid, and the optical absorption spectra were compared to those obtained during 470 nm photolysis of the complexes under N_2 using triethylamine as the sacrificial reducing agent. The data concludes that withdrawing groups can be used to allow photo-driven multi-electron storage to occur in the 10,13-disubstituted $[Ru(phen)_2(dppz(CN)_2)]^{2+}$ complex.

Finally, we report the synthesis and characterization of the unusual dtatpp ligand, and its tetranuclear ruthenium complex, $[(Ru(phen)_2)_4(dtatpp)](PF_6)_8$, where tatpp represents 9,11,20,22-tetraazatetrapyrido[3,2-a:2’3’-c:3’’,2’’-l:2’’’,3’’’]-pentacene and dtatpp represents the dimerized tatpp monomer. This ligand is a symmetric dimer of the tatpp ligand and has been implicated as a byproduct during the synthesis of the tatpp monomer. Since the ruthenium complex contains two tatpp monomers, which individually can store up to two electrons by photochemical methods, we hope that the successful synthesis of this complex will allow us to elucidate the underlying electronic properties of this and related complexes, especially upon reduction of the tatpp components.

TABLE OF CONTENTS

LIST OF ILLUSTRATIONS

LIST OF TABLES

LIST OF ABBREVIATIONS

10-MeTPZ - 10-methylphenothiazine

ADH - Alcohol Dehydrogenase

Cp - Cyclopentadiene

CV - Cyclic Voltammetry

dpb - 2,3-bis(2-pyridyl)benzoquinoxaline

dpp - 2,3-bis(2-pyridyl)pyrazine

dppz - dipyrido-[3,2-a:2',3'-c]phenazine

dppz-o-Br - 11,12-dibromodipyrido-[3,2-a:2',3'-c]phenazine

dppz-o-CN - 11,12-dicyanodipyrido-[3,2-a:2',3'-c]phenazine

dppz-p-Br - 10,13-dicyanodipyrido-[3,2-a:2',3'-c]phenazine

dppz-p-CN - 10,13-dicyanodipyrido-[3,2-a:2',3'-c]phenazine

DPV - Differential Pulse Voltammetry

ESI - Electrospray Ionization

EtOH - Ethanol

H_2 - Hydrogen

HAT - H-atom Transfer

i-PrOH - 2-propanol

KIE - Kinetic Isotope Effect

MeOH - Methanol

MLCT - Metal to Ligand Charge Transfer

$[MV]^{2+}$ - 1,1'-dimethyl-4,4'-bipyridinium or Methyl-Viologen

N_2 - Nitrogen

P - $[Ru(phen)_2tatppRu(phen)_2]^{4+}$

PCET - Proton Coupled Electron Transfer

phen - 1,10-phenanthroline

Q - $[Ru(phen)_2tatpqRu(phen)_2]^{4+}$

Ru - Ruthenium

tatpp - 9,11,20,22-tetraazatetrapyrido[3,2-a:2'3'-c:3'',2''-l:2''',3''']-pentacene

tatpq - 9,11,20,22-tetraazatetrapyrido[3,2-a:2',3'-c:3",2"-l:2'",3'"-n]-pentacene-10,21-quinone

TEA - Triethylamine

TFA - Trifluoroacetic Acid

UV - Ultraviolet

Vis - Visible

Zn - Zinc

CHAPTER 1

INTRODUCTION

1.1 Perspective

With the increasing demand for energy to power modern society and the depletion and environmental aspects of fossil fuel usage, the search for a renewable energy source has become a topic of major interest. Although there have been many technological advances in obtaining energy from renewable sources such as, solar, hydro, and wind power, as well as deriving power from biomass, many of these alternatives have practical limitations which prevent them from being used on a transformative scale. Some of the major issues are the scale to which these energy sources can be tapped and the costs associated with turning this energy into useable forms. In general, the fuels are produced on too little a scale or the technology required to obtain the alternative fuel is not cost effective, or both.[5-8]

Of these alternative energy sources, solar energy conversion has been widely studied since the quantity of sunlight energy which strikes the earth's surface is abundant (close to 4.3 x 10^{20} J/hr) and free.[9,10] Conversion of this solar energy into a fuel such as H_2 is highly attractive for multiple reasons, some of which are the high energy density of H_2 fuel (141.86 $MJ \cdot kg^{-1}$ as compared to gasoline 46.4 $MJ \cdot kg^{-1}$), the by-product of H_2 combustion is H_2O which is environmentally friendly, and consumption of H_2 does not increase CO_2 emissions which is currently a global concern.[11] Ideally, the perfect photo-catalytic system capable of performing this task would be one which absorbs visible light, is capable of storing multiple electrons, and has the redox potentials necessary to drive the water-splitting reaction shown below, which is further broken down into two half-reactions.

$$2\ H_2O \rightarrow 2\ H_2 + O_2$$

$$2\ H^+ + 2\ e^- \rightarrow H_2 \qquad +79.9\ kJ/\ mol\ H_2,\ pH\ 7$$

$$2\ H_2O \rightarrow O_2 + 4\ H^+ + 4\ e^- \qquad +314.9\ kJ/\ mol\ O_2,\ pH\ 7$$

When comparing the amount of energy required to drive the water-splitting reaction, with the amount of light energy which the earth receives, it is obvious that the potential exists to design a system which is capable of performing such this task.

Although the potential exists to produce H_2 and O_2 from H_2O using visible-light, this has not been realized in any practical system. Some success has been realized in the design of systems capable of driving either the reductive or oxidative half-reactions, which is a simpler task. Our focus has been on developing photocatalysts which can drive the reduction half-reaction by which light energy can be absorbed and efficiently directed to a hydrogen production. One of the first successful examples of photo-driven H_2 production was reported by Meyer et. al. in 1979, by using multiple components such as $[Ru(bpy)_3]^{2+}$, $[MV]^{2+}$, and TEA, where phen represents 2,2'-bypyridine, $[MV]^{2+}$ represents methyl-viologen, and TEA represents triethylamine.[12-14] TEA is a sacrificial reductant and would be replaced by an oxygen-evolving system is any practical system. Otherwise, this system contains the basic components required for solar energy conversion into a fuel, the components of which can be described as the Donor-Chromophore-Acceptor system, or DCA model. In Meyer's three component system, the "chromophore" is $[Ru(bpy)_3]^{2+}$ which absorbs visible light through an MLCT process, which produces an excited state capable of being reduced by the "donor" TEA.. The photochemically generated $[Ru(phen^{\bullet})(phen)_2]^+$ species, transfers this stored energy to an "acceptor" such as $[MV]^{2+}$, to form $[MV^{\bullet}]^+$, which in the presence of a Pt catalyst generates H_2. Figure 1.1 depicts the reaction scheme. Although this catalytic cycle was observed to only last for a few hours due to decomposition of the chromophore, multiple H_2 production strategies have been modeled after this system due to the simplicity of design, with hopes of achieving the ultimate goal of producing H_2 from H_2O, using visible light.

Much work has also been directed at improving certain aspects of the system, one of which is covalently linking the chromophore, donor, and acceptor into one molecule in order to

improve the charge transfer processes.[15,16] An example of a covalently linked molecular assembly is shown in Figure 1.2, where the electron donor is MePTZ or 10-methylphenothiazine, the chromophore is $[Ru(Me_2bpy)_3]^{2+}$ where Me_2bpy is 2,2'-bipyridine-4,4'dimethyl, and the electron acceptor is $[MV]^{2+}$. Photo-excitation of this molecular assembly with visible light leads to charge separation within the same molecule, to form $(MePTZ^{\bullet+})Ru(II)(MV^{\bullet+})$. Unfortunately, this charge separated state was observed to be short-lived (160 ns) due to charge recombination, and further development of these types of systems are necessary before it can be used in fuel production schemes.[16,17]

Another approach to improving the $[Ru(bpy)_3]^{2+}$ system is by adding an acceptor ligand which will direct the photoexcited electron away from the Ru(III) center, which will increase the lifetime of the excited state and prevent decomposition of the photogenerated $[Ru(III)(bpy^{\bullet-})(bpy)_2]^{2+}$ complex. A successful example in combining an acceptor ligand with the Ru(II) metal to improve excited state lifetime and chromophore stability is with complex $[Ru(bpy)_2dppz]^{2+}$ where the acceptor ligand is dppz, which represents dipyrido-[3,2-a:2',3'-c]phenazine.[18,19] This complex is capable of directing the photoexcited electron away from the Ru(III) center due to the energy of the orbitals centered on the dppz ligand being lower in energy compared to the orbitals centered on the bpy ligands. The consequence of the addition of this new orbital, is the bpy orbital is traditionally labeled the LUMO in the $[Ru(bpy)_3]^{2+}$ complex, but must be changed to the LUMO+1 in the $[Ru(bpy)_2dppz]^{2+}$ complex since the new lower energy LUMO orbital is centered on the dppz acceptor ligand. Due to this change, the LUMO in the $[Ru(bpy)_2dppz]^{2+}$ complex is often referred to as the "redox-active" orbital since this is the site of reduction by chemical, electrochemical, and photochemical means, and the LUMO+1 is referred to as the "light-active" orbital since the MLCT transition still occurs between the Ru(II) center and the bpy ligand during photoexcitation.[17-27] Enhanced stability of the photo-generated anion is also due to the aza nitrogens interacting with the solvent via hydrogen bonding, which in turn makes charge recombination difficult.[21] Although the advantage of the $[Ru(bpy)_2dppz]^{2+}$ system is electrons

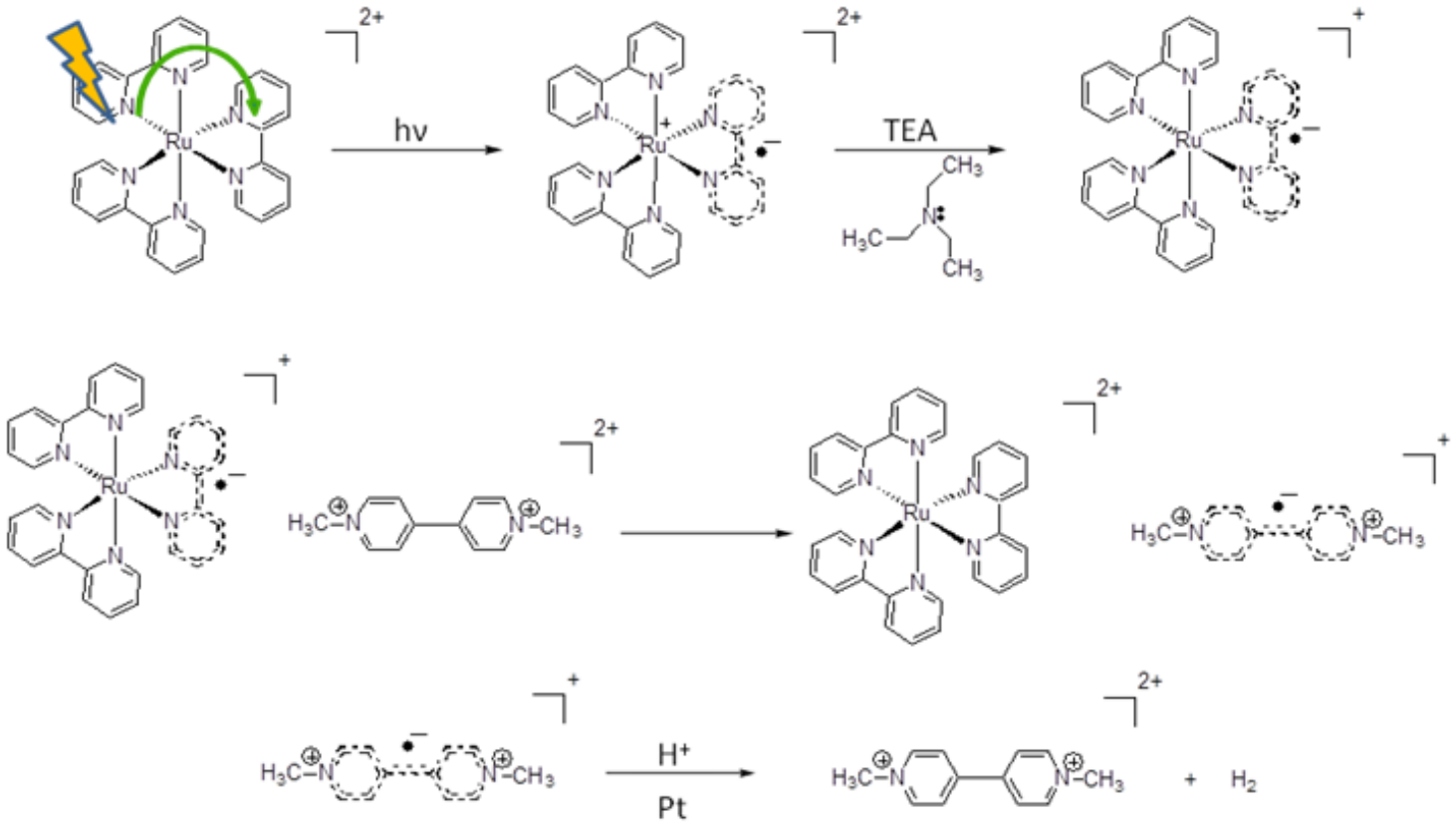

Figure 1.1: Photo-driven H_2 production using visible light and $[Ru(bpy)_3]^{2+}$, $[MV]^{2+}$, and TEA

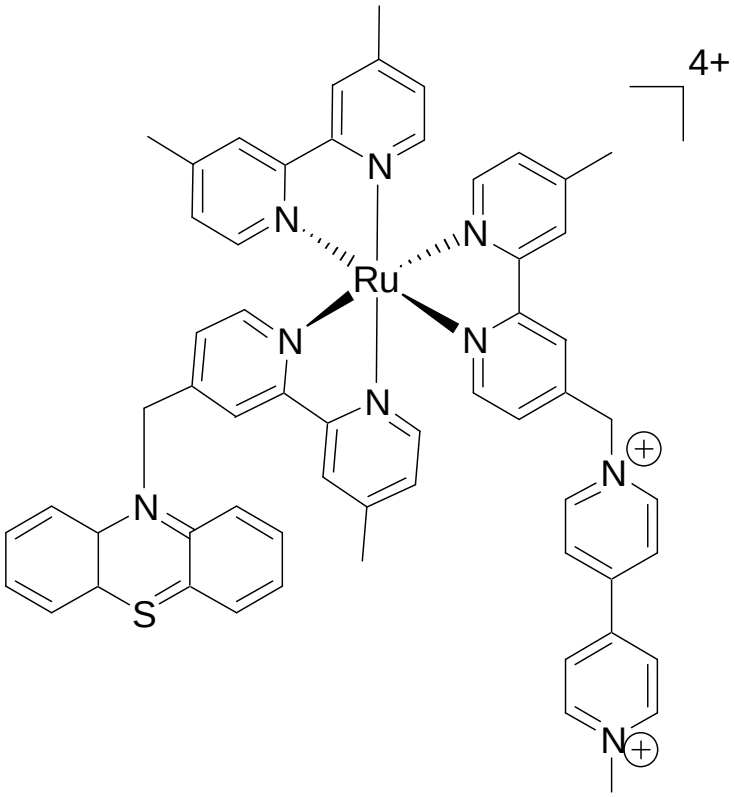

Figure 1.2: Molecular assembly containing MePTZ, $[Ru(Me_2bpy)_3]^{2+}$, and $[MV]^{2+}$

can be stored indefinitely on the dppz ligand without ligand dissociation from the complex, the disadvantage is the potential of the stored electron is lower than that of $[Ru(bpy)_3]^{2+}$, and the potential to produce fuels decreases.

Since the generation of H_2 is a multi-electron process, one approach to increasing the potential of fuel production would be changing to a multi-electron storage system which ideally would transfer two or more electrons simultaneously. One of the first examples of a complex being able to photochemically store more than one electron is shown in Figures 1.3 and 1.4.[3,4] In both cases, Brewer and co-workers have combined multiple metal centers to multiple polypyridal fragments such as bpy, dpp which represents 2,3-bis(2-pyridyl)pyrazine, and dpb, which represents 2,3-bis(2-pyridyl)benzoquinoxaline. The Ru^{2+}-Ir^{3+}-Ru^{2+} complex shown in figure 1.3, is capable of photochemically storing a single electron in each of the metal bound dpb ligands while the Ru^{2+}-Rh^{3+}-Ru^{2+} complex is capable of storing two electrons on the Rh^{3+} metal center to form a Rh^{+} metal, which has been shown to produce H_2 from water via formation of metal-hydrides. [4,28] MacDonnell and coworkers have also developed the multi-electron storage systems $[Ru(phen)_2tatppRu(phen)_2]^{4+}$ or complex P, and $[Ru(phen)_2tatpqRu(phen)_2]^{4+}$ or complex Q, which both store electrons in a similar manner compared to $[Ru(phen)_2dppz]^{2+}$, with the exception of undergoing photo-driven multi-electron storage rather than single electron storage.[17,24,25] Although both complex P and Q are capable of photochemically storing 2 and 4 electrons respectively, only complex Q has been shown to produce H_2, albeit at low TON of 3/day (relative to Q).

Although the use of transition metals with polypyridal systems has proven fruitful in understanding the limits of fuel production and solar energy conversion, one major issue with these systems is the expense associated with using second row transition metals. One route towards multi-electron storage without the use of transition metals has been shown by McGovern and co-workers during the metal free photolysis of dppz in alcohol donor solvents.[2] It has been shown the n-π* excited state of dppz* is responsible for H-atom abstraction of alcohol

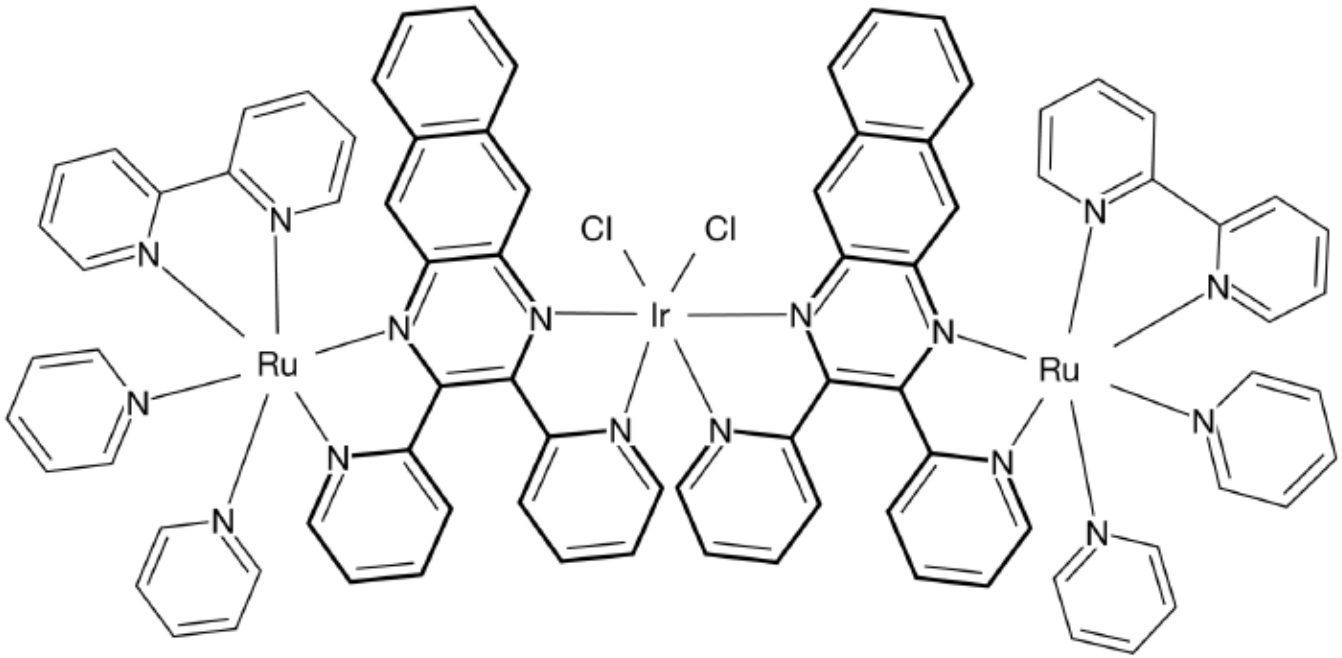

Figure 1.3: The complex as shown $[\{(bpy)_2Ru(dpb)\}_2IrCl_2]^{5+}$, is capable of photochemically storing multiple electrons under N_2, where bpy = 2,2'-bipyridine and dpb = 2,3-bis(2-pyridyl)benzoquinoxaline).[3,4]

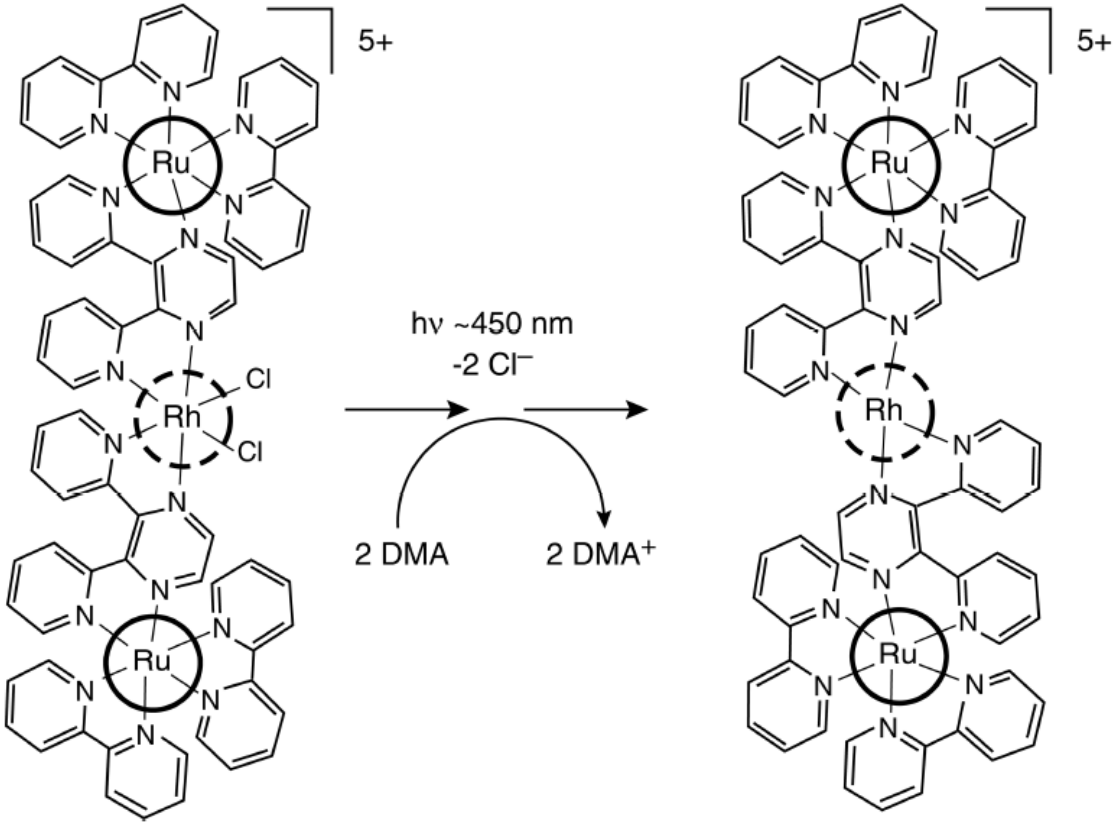

Figure 1.4: Photochemical reduction of the title complex $[\{(bpy)_2Ru(dpp)\}_2RhCl_2]^{5+}$ under N_2, which ultimately results in storage of two electrons on the Rh^{3+} metal center, to form a Rh^{+} metal.[3,4]

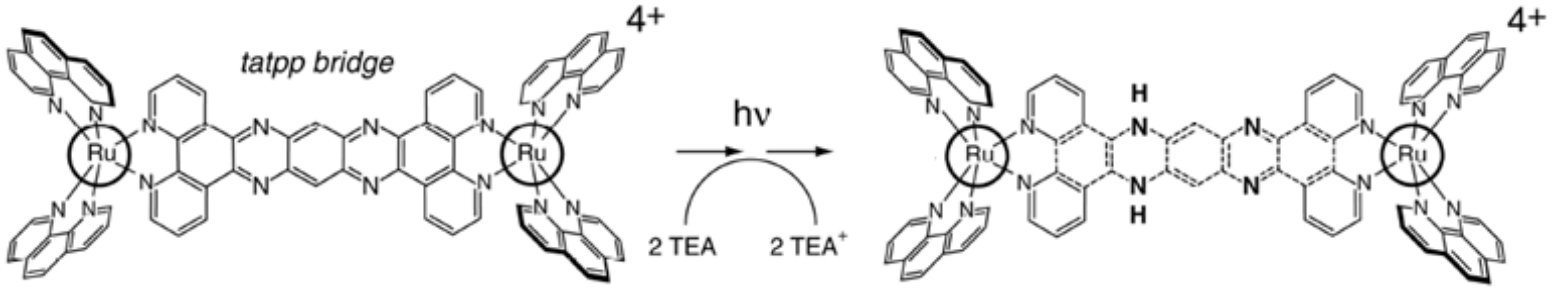

Figure 1.5: Photoreduction of complex P under N_2, which ultimately results in storage of two electrons on the tatpp acceptor ligand.

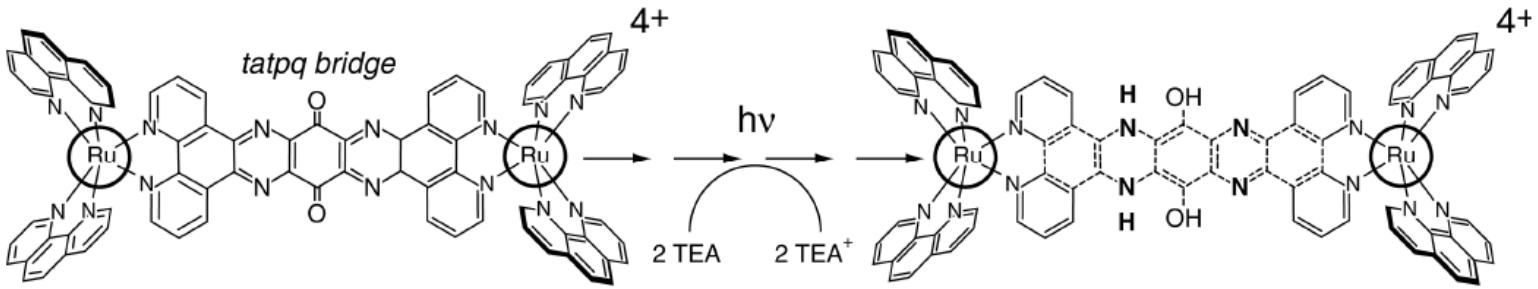

Figure 1.6: Photoreduction of complex Q under N_2, which ultimately results in storage of four electrons on the tatpq acceptor ligand.

to form the $Hdppz^{\bullet -}$ species, which after disproportionation forms the doubly reduced photoproduct H_2dppz and starting material, for an overall two-electron storage process via two-photon excitation. Despite the ability of the ligand to store multiple electrons without the use of expensive transition metals, the quantum yield for this photo-process is quite low (~10^{-3}) and protonation of the di-anion stabilizes the species beyond the point of being applicable towards a large scale hydrogen production process.[1]

Although multiple approaches to improving photo-driven hydrogen production using ruthenium polypyridals exist, in this work we have focused our attention on improving the donor and acceptor components of the DCA model. Specifically, we describe herein the role of Zn(II) in catalyzing the electron transfer reaction between alcohol donor solvents and the photo-generated excited states of the polypyridal ligands dppz and tatpp. We have also examined the role of withdrawing groups in the $[Ru(phen)_2dppz]^{2+}$ complex, in an effort to lower the energy of the acceptor orbital, to allows photochemical storage of multiple electrons. Finally, we will discuss a new material with the potential to store more than two electrons by photochemical methods, which also should show some interesting spectroscopic properties. All of these studies are aimed at expanding the current knowledge of the capabilities of ruthenium polypyridal complexes to harvest light energy, and improving upon the systems previously designed in early studies of the topic.

1.2 Scope of Thesis

Given the challenges associated with using metal bound polypyridal complexes as potential water oxidation and H_2 production catalysts, it is necessary to understand the limits of solar energy conversion so that future systems can be designed which will improve the current technology. Specific areas of research which are available for investigation include, but are not limited to, enhancing the efficiency by which metal bound polypyridal complexes transfer light energy to appropriate reduction catalysts, increasing the number of electrons which can be stored on metal bound polypyridal complexes, optimizing the number of electrons which can be

transferred to a chromophore during photo-excitation, increasing the potential of the photochemically stored electrons etc.. In this study, we have decided to investigate the interactions of polypyridal complexes with Zn(II) in an effort to increase the efficiency and number of electrons transferred between alcohol donor solvents and the photoexcited state of both dppz and tatpp. We have also investigated the use of withdrawing groups on the $[Ru(phen)_2dppz]^{2+}$ complex in order to increase the number of electrons which can be stored by photochemical methods. Lastly, we have discovered a Ru(II) polypyridal complex with the potential to store more than two electrons photochemically, which also should show some interesting spectroscopic properties, as will be discussed in later sections.

The thesis is organized into 4 chapters, with this introduction being the first chapter. A summary of the contents of the following chapters is given below.

Chapter 2: Currently, many such photocatalysts under development utilize precious metals, such as Ru, Re, and Pt, which are scarce and thus expensive. These metals are not easily replaced as the excitation manifold is intimately associated with the transition metal. Complexes like $[(phen)_2Ru(tatpp)Ru(phen)_2]^{4+}$or “P” , have been shown to undergo reversible intramolecular electron transfer upon photoexcitation, which makes it an ideal compound as a potential re-useable hydrogen catalyst.[17,24,25,27] The tatpp bridge of “P” has been shown to be the center of the photochemistry reductions and protonations. Unfortunately, the complex "P" was not able to produce a significant amount of hydrogen with a co-catalyst. It was later discovered that the ligand dppz , was able to be photoreduced in a metal free solution of ethanol.[1] From this work, it was worthwhile to explore the photoactivity of the center bridge in complex "P" without the ruthenium centers. If the neutral tatpp ligand is capable of being photoreduced, it is more likely to generate hydrogen as compared to "P", which has a +4 charge. The advantage to this system is it has the potential to produce hydrogen without the expensive Ruthenium centers. In the second chapter of this work we investigate a photocatalytic system involving Zn(II) adducts of the dppz and tatpp acceptor ligands, which can

be photoreduced using visible light and alcohols as terminal reductants. The excited-state manifold involved in this process is a ligand-centered triplet state, however, the Zn(II) is intimately involved is the alcohol oxidation step, favoring hydride transfer over the more conventional H-atom transfer typical of organic triplet excited states or polyaromatic ring systems. Because of this hydride-transfer mechanism, this photocatalyst is able to undergo a one-photon, two-electron reduction in one step. This ability to drive a multi-electron reaction using a single photon could lead to significant advances and efficiencies in the fuel forming reactions inherent in any solar energy-to-fuel energy scheme.

Chapter 3: One reason the $[Ru(phen)_3]^{2+}$ chromophore is capable of H_2 production is the photogenerated anion of the complex has a relatively high reduction potential (-1.07V vs. NHE). Unfortunately, the reduced complex is susceptible to ligand dissociation over time, which prevents the catalyst from long-term performance. $[Ru(phen)_2dppz]^{2+}$ on the other hand, is stable to ligand dissociation after photoreduction, but the reduction potential of the stored electron (-0.72V vs. NHE) is substantially low compared to $[Ru(phen)_3]^{2+}$, which consequently lowers the quantity of H_2 produced. It is known that substitution of donating and withdrawing groups on aromatic systems greatly affect the orbital energy of the system. One approach to improving the reduction potential of $[Ru(phen)_2dppz]^{2+}$ would be the addition of donating groups to "boost" the energy of the stored electron. An alternative approach would be to turn the single-electron storage system into a multi-electron storage system by adding strong withdrawing groups. With respect to adding donating groups, it is unlikely this approach would be successful for two reasons: (i) If the energy of the dppz orbital is increased to equal or surpass the energy of the metal-bound phen ligand, the complex will store a single electron in the lowest energy orbital, which in this case would be the metal-bound phen orbital rather than the phz orbital of dppz. The consequence is the complex would still generate H_2 in comparable quantities to that of $[Ru(phen)_3]^{2+}$ and ligand dissociation of the $[phen^{\bullet}]^{-}$ anion may still occur (ii) A second approach would be adding donating groups to both the phen and dppz ligands. The

consequence of this change is the lifetime of the d-π* MLCT state and absorption wavelength energy are intimately associated with the phen π* system. By increasing the energy of the orbital, the MLCT absorption band at 450 nm for $[Ru(phen)_3]^{2+}$ would blue shift, possibly into the UV region, making H_2 production a UV driven process, rather than a Visible light driven process. With respect to adding withdrawing groups to dppz, it is possible to lower the orbital energy just to the point at which multi-electron storage would occur. At this potential, the complex would theoretically be one of the first examples of a ruthenium polypyridal system capable of both multi-electron storage, and electron storage at high reduction potentials. In this chapter, we have decided to investigate a series of $[Ru(phen)_2dppzX_2]^{2+}$ analogues, where X = H, Br, CN, in order to investigate the limits of multi-electron storage using ruthenium polypyridal complexes. Specifically, we will show that the use of strong withdrawing groups allows for multiple electrons to be stored photochemically at increased potentials, which will advance the understanding of the limits of ruthenium polypyridal technology.

Chapter 4: Synthetically, it is a challenge to incorporate multiple multi-electron storage systems into a single molecule. Significant advantages of this type of material would include enhanced reduction potentials, an enlarged capacity for the amount of light energy which can be stored in a single molecule, and an increase in the overall efficiency of transferring multiple electrons to a H_2 production catalyst. In this chapter, we discuss the synthesis and crystal structure of the tatpp dimer, also written as dtatpp, and have characterized the material by NMR, X-ray Crystallography, MALDI, and ESI-MS. The tatpp monomer has been shown to store multiple electrons in the parent compound complex P, therefore we have added the $[Ru(phen)_2]^{2+}$ chromophore to the free-ligand dimer to form complex $[(Ru(phen)_2)_4(dtatpp)](PF_6)_8$. The significance of this discovered material is the broad spectrum of applications where it can be used. A few theoretical examples include metal-free H_2 production using alcohols as sacrificial reducing agents, organic semiconductors, and photoactive polymers. Since dtatpp is a by-product formed during the synthesis of the monomer

(<1%), we were unable to obtain enough material to determine which applications it has potential to be used in. Therefore, in this chapter we discuss synthetic routes towards large scale production of the material. We will also discuss the by which we characterizes the dtatpp species as well as the ruthenium complex, $[(Ru(phen)_2)_4(dtatpp)](PF_6)_8$.

CHAPTER 2

PHOTODRIVEN HYDRIDE TRANSFER FROM ALCOHOLS TO POLYAROMATIC HETEROCYCLES USING METAL-ALKOXIDES

2.1. Abstract

The free ligand dipyridophenazine (dppz) is known to react with alcoholic solvents upon photoexcitation at 380 nm to yield dihydrodipyridophenazine (H_2dppz). Mechanistic studies indicate that the photoexcited dppz* abstracts an H atom from the alcohol to form the radical species Hdppz$^{\bullet}$ which then disproportionates. In this report, we demonstrate that this reaction shows a primary kinetic isotope effect (KIE = 4.9) when dppz is photolyzed in methanol or perdeuteromethanol, which is consistent with the mechanistic model above. Significantly, addition of Zn(II) to the dppz solution not only appreciably accelerates the rate of photoreduction, it also appears to change the photoreduction mechanism as evidenced by a significantly smaller KIE of 1.7. We observe a similar KIE of 1.5 for the photoreduction of tatpp in both methanol and 2-propanol in the presence of Zn(II). We postulate that the ability of Zn(II) to coordinate alcohols and activate the C-H hydrogens alpha to the alcohol function towards hydride transfer is responsible for the observed change in KIE. This shift in the mechanism of reduction is significant in that it leads to a photochemical reaction in which absorption of one-photon formally induces a 2 electron transfer reaction. One photon, two electron transfer reactions have significantly greater promise in the development of solar-energy conversion schemes over those which depend on bimolecular disproportionation reactions to achieve doubly-reduced substrates.

2.2. Introduction

Fuel-forming photochemical reactions are of particular interest given the need for a sustainable, environmentally-friendly energy supply.[9-11,17] One potentially promising

photochemical process would be reactions that convert cellulose-based biomaterials to more readily usable fuels, such as hydrogen gas. In 2005, Long *et.al.* showed that upon UV

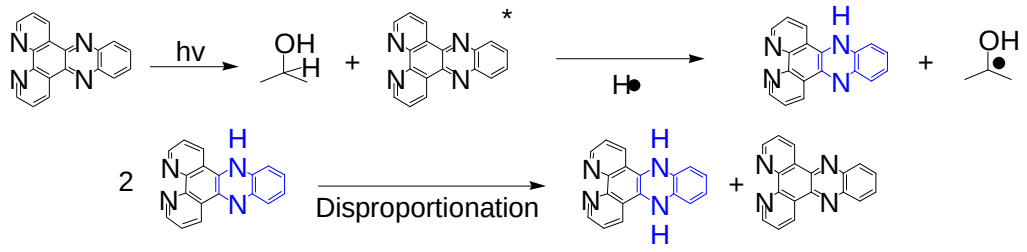

Figure 2.1: Proposed mechanism of dppz photoreduction in isopropanol upon irradiation with UV light.[1,2]

irradiation in the 380 nm region, dipyridophenazine (dppz) reacts with alcohols to form doubly-reduced, doubly- protonated dihydrodipyridophenazine ($dppzH_2$) as shown in Figure 2.1.[2]

While this was not a particularly efficient reaction, it was promising in that release of this stored energy as H_2 would regenerate dppz and thus could lead to a photo catalytic scheme for hydrogen production from cellulosic feedstocks. The reduction potential of dppz to $dppzH_2$ is on the order of -700 mV vs. NHE at pH 7.0 indicating the hydrogen evolution reaction from $dppzH_2$ is clearly exogonic.[18,19] The photochemistry of the uncoordinated dppz was all the more remarkable given the extensive amount of study on the photophysics and photochemistry of ruthenium and rhenium complexes of dppz, which do not form $dppzH_2$ upon photolysis. In these complexes, the photoreduction is limited to singly-reduced products which require the use of more easily oxidized substrates such as triethylamine (TEA) and triethanolamine (TEOA), since alcohols are not attacked. Notably, these transition metal-dppz complexes are mainly studied for their unusual DNA-binding properties in which intercalation of the dppz moiety leads to enhanced luminescence.

The photochemistry of dppz has been studied in detail by Ferraudi and coworkers.[1] They report that the dominant reactivity for the photoexcited dppz occurs through a low-lying $^3(\pi\text{-}\pi^*)$ state which is reductively quenched by triethylamine (TEA) and triethanolamine (TEOA) but not alcohols. The reactivity of dppz* with alcohols is attributed to the role of a higher energy

^{1}(n- π *) state which is capable of H-atom abstraction reactions. The reactivity of this latter state was first described in the closely-related nitrogen-heterocycle, phenazine (phz) and which also demonstrates the ability to use both amines and alcohols as reductive quenchers of its excited-state via the triplet and singlet manifolds, respectively.[18] Reductive quenching via the triplet manifold is more efficient owing to the longer lifetime of the triplet state however the applicability of the singlet state chemistry to more readily available substrates, such as alcohols, sugars, and other types of biomass, suggests the singlet manifold could be more useful.

For both dppz and phz, the ^{1}(n-π*) state is postulated to abstract an H-atom from the alcohol solvent to generate the protonated radical species, dppzH$^\bullet$ and phzH$^\bullet$, respectively, and subsequent disproportionation reactions yield the doubly-reduced product and starting material. This sequence of photogeneration of a radical species followed by disproportionation is frequently observed in the photochemistry of quinones and nitrogen-heterocycles,[18,29] and can represent an obstacle to their effective use in fuel-forming processes because of the bimolecular mechanism with respect to the chromophore.

In this chapter, we have investigated the mechanistic details of the photoreduction of dppz in alcoholic solvents in the presence and absence of Zn(II) ion using a combination of kinetics and kinetic isotope effects (KIE). We also report the KIE of photolysis of tatpp in methanol and 2-propanol in the presence of Zn(II). We observe a significant drop in the observed KIE for reaction of the Zn-dppz adduct relative to the Zn-free dppz case, suggesting a potential change in mechanism from H-atom abstraction for dppz* to hydride transfer for Zn-dppz*. Significantly, this would represent a photochemical process in which a single photonic excitation results in a formal 2-electron reduction of the chromophore in a unimolecular process with respect to the chromophore. This simplification of the reduction scheme could have significant advantages in the development of practical solar fuel formation schemes.

2.3. Experimental

2.3.1. Materials

1,2,4,5-benzenetetraamine-tetrahydrochloride (CAS: 4506-66-5) was purchased from Sigma Aldrich and was purified as described in the literature.[30] Zinc tetrafluoroborate hydrate (CAS: 27860-83-9) was purchased from Alfa Aesar. Deuterated solvents were purchased from Cambridge Isotope Laboratories (D_2O (D, 99.5%), CD_3OD (D, 99.8%), CH_3OD (99%), and d_8 i-PrOD (D, 99.5%)) and were dried by addition of 4Å molecular sieves purchased from Fluka. 9,11,20,22-tetraazatetrapyrido[3,2-a:2'3'-c:3",2"-1:2"',3"'-n]pentacene (tatpp), and dipyrido[3,2-a:2',3'-c]phenazine (dppz) were prepared as previously described.[24,31] Since the total concentration of water in deuterated solvents is much less than what is typically found in a standard 4 L bottle of ACS grade solvent, and the zinc tetrafluoroborate salts contain a significant amount of moisture themselves, we deliberately added a fixed amount of water to all the solvents such that the final concentration of water is relatively similar for each sample. All other materials and reagents were used as received unless otherwise specified. All H_2O was de-ionized unless otherwise specified.

2.3.2. Synthesis

Isotopically labeled solvents and hydrated salts:

$Zn(BF_4)_2 \bullet x\ D_2O$ was prepared by dissolving a 3 g solid sample of $Zn(BF_4)_2 \bullet x\ H_2O$ in 1 mL of D_2O and evaporating the solution to dryness under reduced pressure. This procedure was repeated twice more to ensure any residual hydration consisted of D_2O.

In order to prepare CD_3OH, a 100 mL sample CD_3OD (D, 99.8%) was added to 10 mL H_2O, and the alcohol was distilled into a receiving flask containing 10 mL H_2O, discarding the first and last 10% of distillate prior to use in subsequent distillation. The collected alcohol was re-distilled twice in the same manner. A third distillation in which no water was present was

performed to collect the isotopically labeled sample. 4Å molecular sieves were added to keep the sample dry.

2.3.3. Physical Measurements

General UV/Vis experiments were obtained using a Hewlett Packard 8453 UV-Visible Spectrophotometer. Samples were handled in 1 cm quartz cuvettes which were fitted with a screw cap and septum. These cuvettes were optically transparent at wavelengths above 200 nm. ^{1}H NMR measurements were obtained on a JEOL 500 MHz spectrometer and spectra were referenced vs. acetonitrile.

Kinetic experiments were performed in a custom glass cell (Figure 2.2) which was capable of holding 5 mL of solution when an optical dip probe was inserted, and filters UV light < 320 nm. This was the working volume for all kinetic measurements. An Ocean Optics optical dip probe (UV/SR-VIS TP-300) was attached to fiber optic cable and a USB 4000 diode array detector was use to monitor solution electronic spectra in most kinetic experiments. The cell also was fitted with a water jacket which was maintained at 25°C using a 1140S Heated/Refrigerated Circulator, purchased from VWR.

Figure 2.2: Custom Pyrex® glass cell built by High Tech Scientific Glassblowing Inc. The inner glass tube (8 mm) was joined to an outer tube (48 mm) which allows for cooling of the reaction mixture. This glass cell filters UV light < 320 nm.

2.3.4 Light Sources

The UV light source used for photolysis was an unfiltered, 150 W xenon arc lamp (Oriel, Stratford, CT). The unfiltered photon flux, measured with an Oriel model 70260 Radiant Power/Energy meter, 4 cm from the light source was 210 mW/cm^2 at 375 nm. This lamp configuration is used for all of the kinetic experiments.

In cases where this light source was used to measure quantum yield, a separate set of kinetic experiments were preformed which included the use of a band pass filter which transmitted light between 350 nm - 400 nm. After the filters were set in place, the photon flux was measured using a ferrioxalate actinometer, according to literature methods and procedures.[32] The filtered photon flux was measured at 375 nm, using the same experimental set-up previously described, and was calculated to be 2.82x10^{-8} einsteins/second. After the photon-flux was established, the quantum yield of dppz photolysis in the presence and absence of Zn(II) was then measured by using the same experimental set-up.

The visible light source used for photolysis contained 36, 10 mm LED's with an emission wavelength of 470 nm, purchased from Allied Electronics (VAOL-10GSBY4). The LED's have a 3.6 V 20 mA power requirement, and were assembled together as follows. A 12 V power supply was connected to a splitter circuit board containing two rows of copper tracing, where the + and - terminals of the power supply were soldered to each row respectively. To this splitter board was added 6 individual circuit boards, where each of the boards contained 6 LED's soldered specifically to the manufacturers suggestions. Once the 6 circuit boards were assembled, they were soldered in parallel to the splitter board previously described, and attached to a plastic housing. Figure 2.3 shows pictures of each individual piece, and the final product. As with any custom light source, the magnitude of photon flux will vary depending on multiple factors such as the power supply voltage, circuit design, resistors used etc. Since it would be difficult to assemble two light sources with identical photon-flux, it is necessary to quantify the photon flux using a ferrioxalate actinometer, which was performed according to

literature methods and procedures [32] and experimentally determined to be 7.313E-07 einsteins/second.

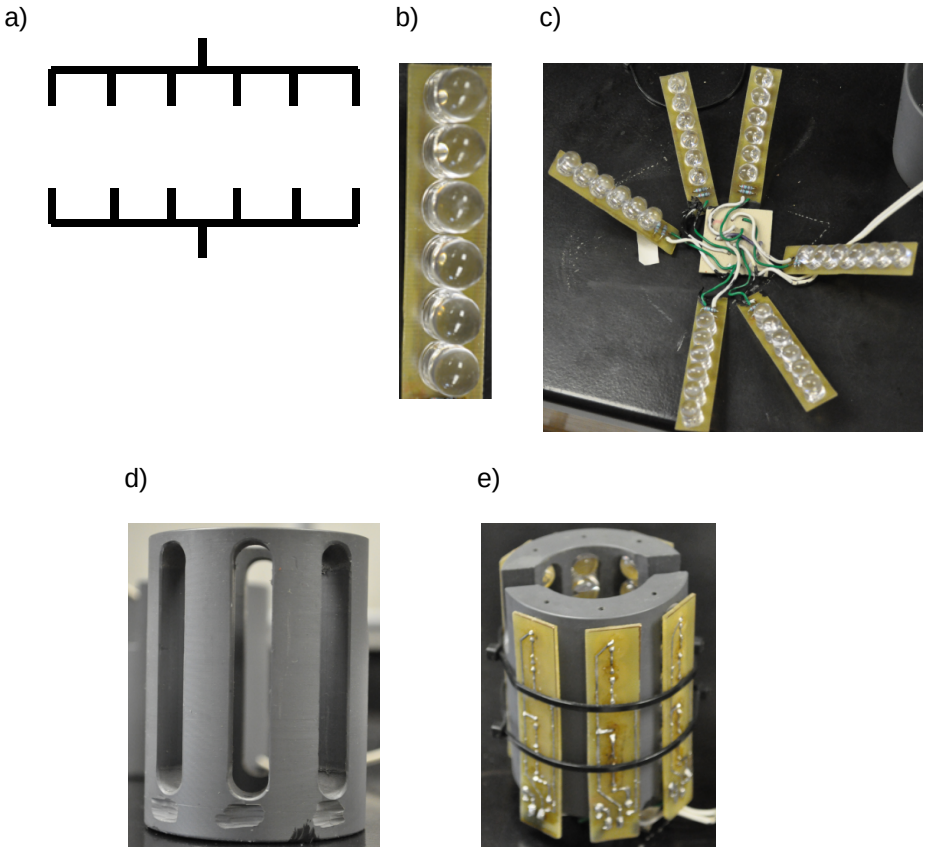

Figure 2.3: a) Splitter board with copper tracing in black. b) 10 mm 470 nm LED's arranged onto a circuit board. c) All 6 LED boards attached to the splitter board. d) Plastic housing made from PVC material. e) Fully assembled photoreactor. Photos and reactor design are credited to Mr. David Boston.

2.4. Results

2.4.1. Initial Observations of Photoreactivity

The electronic adsorption spectra of free dppz and a Zn(II)dppz adduct (5:1 molar ratio) in methanol before and after irradiation with UV light are shown in Figure 2.4. The free dppz is characterized by two sharp intense absorptions peaking at 359 and 378 nm with no significant absorptions above 400 nm. The Zn-dppz adduct is nearly identical but with a slight blue-shift of the two maxima to 357 nm and 375 nm, respectively. Upon irradiation with UV light, the spectra

change significantly as shown in Figure 2.4. The photoproduct of dppz photolysis in alcohols is H_2dppz as reported by Long et. al. and is characterized by the appearance of a broad peak in the visible region, peaking at 470 nm in the Zn-free case.[2] In our experiments, the Zn-dppz adduct showed similar photochemical behavior and spectral changes, with the exception of a broadened absorbance at 500 nm and a notable increase in speed of the photochemical process. Figure 2.5 shows the evolution of the absorption spectra of the Zn-dppz adduct (5:1) as a function of irradiation time in CH_3OH solvent. The spectra do not give a clean a isosbestic point, but instead this point shifts from 380 nm to 390 nm suggesting the process is not a simple direct conversion of reactant to product. Nonetheless, a plot of the increase in absorbance

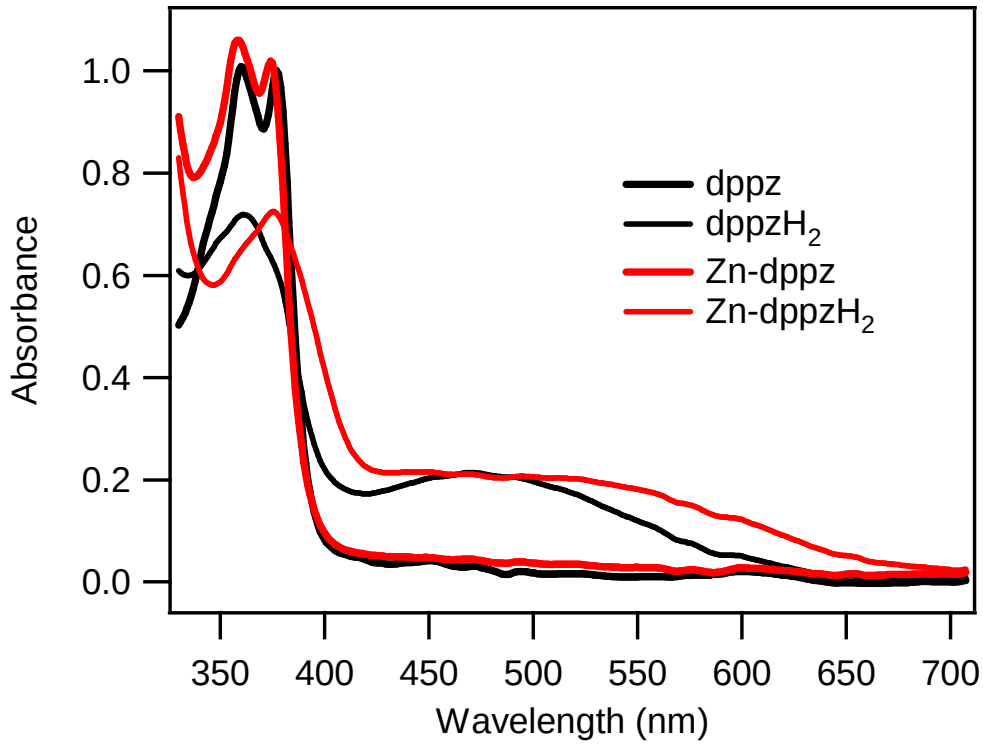

Figure 2.4: Overlay of the absorption spectrum of an 80 µM dppz solution before (black-bold) and after (black) photolysis. Overlay of the absorption spectrum of an 80 µM dppz with 400 µM Zn(II) solution before (red-bold) and after (red) photolysis. Solvent is CH_3OH, and the photolysis was performed using unfiltered UV irradiation from a 150 W xenon arc lamp (Oriel, Stratford, CT) which emits UV light < 400 nm.

(A/A_f) at 550 nm vs. time is linear during the first 10% of reaction as shown in the inset of Figure 2.5. A kinetic analysis was performed to quantify the rates of these processes as a function of the presence or absence of Zn(II), the Zn(II):dppz ratio, and the nature of the alcohol. In addition, perdeuterated alcohols were used to measure kinetic isotope effects to help elucidate the reaction mechanism.

2.4.2. Kinetic Study of Methanol Oxidation in the Presence and Absence of Zn(II)

2.4.2.1. Photolysis of dppz in Alcoholic Solvents

The UV light source, custom glass cell, and optical probe described in the previous section were used for all kinetic measurements. The SpectraSuite software purchased from Ocean Optics was set to collect data at 550 nm with an integration time of 30 ms and 10 scans averaged per data point. The boxcar width was also adjusted to 15. The kinetic data sets obtained using these settings were comprised of absorbance values at specified wavelengths versus time. These data points were loaded into a spreadsheet and converted to percent reaction completion using the formula A/A_f, where A is the absorbance at any given time, A_f corresponds to the final absorbance as calculated using the extinction coefficient at 550 nm, and A/A_f is a measure of the reaction completion as a fractional percent. Since the absorbance of photoproducts can change upon addition of Zn(II), water, etc., the A_f values are calculated for each solution prior to use in data interpretation. After calculation of A/A_f, these values were then plotted vs. time. Using the A_f value the data set was cropped to only include those data with an A/A_f values less than 0.1 A_f which represents the first 10% of the reaction progression. Because the absorbance of the sample changes with time, the number of absorbed photons also changes complicating the kinetic analysis. By convention in most photochemical kinetics, limiting the data set to the first 10% of the absorbance change is used to minimize the effect of this complicating factor.[33-35] Typically, the data sets are linear in this first 10% of absorbance change assuming the reaction follows first or pseudo-first order kinetics. A linear fit to the data is used to extract the rate and an average of 5 data sets.

Using these settings, 4 mM stock solutions of dppz in a specified alcohol were filtered into the custom glass cell, degassed with N_2, and photolyzed using the lamp configuration previously described. In all cases, the dppz chromophore concentration was fixed at 4.0 mM and kinetic data obtained at 550 nm due to baseline curvature at lower wavelengths. The absolute values of these data are highly dependent on the experimental set-up, including the lamp, filters, and sample configuration. While these factors were kept constant, the absolute values are somewhat arbitrary. Our interest is primarily in how the rates change as the system is perturbed and therefore relative rates are reported, with the slowest photochemical system (dppz without added Zn(II)) assigned a rate value of 1.0. These data are collected in Table 2.1.

Since the absolute rate constant of this reaction is largely dependent on light intensity, Zn(II) concentration, H_2O concentration, and instrument set-up, we decided to relate all rate constants to the rate constant obtained under the initial sets of conditions described in run 1 in Table 2.1, for the metal free photolysis of dppz (4.0 mM) in CH_3OH with 55 mM H_2O. The concentration of dppz was chosen on the basis that the H_2dppz photoproduct is difficult to detect at low concentrations with the USB4000 detector. The concentration of H_2O was chosen on the basis that an unopened 4 L bottle of ACS grade CH_3OH contains close to 55 mM H_2O. Since it is difficult to obtain truly anhydrous solvent conditions, and the solubility of the $Zn(BF_4)_2$ salt decreases with decreasing solvent hydration, we decided to use the CH_3OH solvent as received. In order to observe the effect of H_2O on the metal free reaction kinetics, the concentration of H_2O was increased to 5500 mM as shown in run 2. The $rate_{rel}$ for this reaction was determined to be 0.95 when compared to the rate obtained for run 1.

The data in Table 2.1 and Figure 2.6 shows the addition of Zn(II) has a large effect on the $rate_{rel}$. The reaction rate is observed to increase rapidly with added Zn(II) towards a maximum $rate_{rel}$ of 5.9 at a 1:1 Zn:dppz ratio compared to the zinc-free reaction ($rate_{rel}$ = 1.0). Addition of more Zn(II) over this 1:1 ratio shows a modest gradual decrease in $rate_{rel}$ with the highest ratio tested (20:1) having $rate_{rel}$ = 4.2. The data also shows the $rate_{rel}$ increases

noticeably even upon addition of sub-stoichiometic amounts of Zn (1 Zn: 6 dppz) as shown in run 3. If the ratio of Zn:dppz is held at 5:1 and the concentration of H_2O is increased to 110 mM and 165 mM, a slight depreciation in the $rate_{rel}$ is observed as shown in run 7 and 8.

Due to the acidic nature of the Zn(II) ion, the effect of added acid on the relative rate was also studied. A solution of the Zn-dppz adduct (5:1 ratio) was acidified by addition of trifluoroacetic acid (TFA) to make the concentration of $[H^+]$ 2 mM, and then subjected to photolysis. The relative rate for run 9 (3.5 $mol{\cdot}L^{-1}s^{-1}$) compared to run 6 (5.3 $mol{\cdot}L^{-1}s^{-1}$), shows the addition of acid suppresses $rate_{rel}$ in a similar manner to the addition of water. These data show the impact of varying $[H_2O]$ and pH, at least in the acidic range, has a noticeable, but relatively small impact on the rates of photoreduction.

To understand the efficiency of the photoreaction in the presence and absence of Zn(II), it is important to first quantify the photon-flux of the light source, then under the same lamp configuration measure the rate of reaction. Using this methodology, the photon-flux was calculated using filtered λ_{exc} = 375 nm light as described previously, then the quantum yield (φ) for the formation of the H_2dppz upon photolysis of dppz with Zn(II) (5:1) and without Zn(II) was measured and was calculated to be $4.03x10^{-3}$ and $1.14\ x10^{-3}$ respectively, which gives some measure of the overall reaction efficiency. Notably, these quantum yields match well with that reported by Lezna and coworkers who report luminescence quantum yields of dppz in CH_3OH at two excitation wavelengths, $\lambda_{350nm} = 1.9 \times 10^{-4}$ and $\lambda_{400nm} = 1.8 \times 10^{-2}$ [1].

2.4.2.2. Photolysis of tatpp in Alcoholic Solvents

The visible light source, custom glass cell, and optical probe described in the previous section were used for all kinetic measurements. Similar software settings to those for photolysis of dppz were also used. Due to the insolubility of the tatpp ligand in alcoholic solvents, it was necessary to add $Zn(BF_4)_2 \bullet x\ H_2O$ to get the tatpp to dissolve, presumably by coordination to the phenanthroline sites on the tatpp ligand. In general, an molar excess of Zn(II) was added so as to saturate the phenanthroline binding sites. Importantly, the waters of hydration pay a role

in the solubility of the Zn-tatpp adducts as anhydrous $Zn(BF_4)_2$ did not dissolve appreciable amounts of tatpp. We hypothesize that the waters are necessary ligands to complete some of the Zn(II) coordination sphere. These issues complicate the system, which in turn makes it difficult to create identical stock solutions. Therefore, samples for each kinetic run were created on an individual basis, by dissolving 1 mg of tatpp in 5 mL of alcoholic solvent, with 150 mg of zinc tetrafluoroborate. The solutions were then stirred for 3 minutes and filtered into the custom glass cell previously described. After inserting the optical probe the solutions were degassed with N_2 for 5 minutes, then photolyzed using the light source previously described in Figure 2.3.

2.4.3. Kinetic Isotope Effect

McGovern and coworkers showed that the rate of dppz photoreduction increased upon changing the solvent from methanol to ethanol to isopropanol, which is consistent with a reaction mechanism involving H-atom abstraction.[2] This was confirmed in a separate study using pulsed radiolysis by Lezna and co-workers.[1] We examined the effect of deuterium substitution on CH_3OH, and how the isotope affected the kinetics. The ratio of the rates is a measure of the difference in bond dissociation energy, which for H-atom abstraction mechanisms is typically above 2, and for Hydride transfer mechanisms is typically below 2. Using KIEs, Table 2.2 shows in the absence of Zn(II), photolysis of dppz in 55 mM H_2O and the alcohol (CH_3OH or CD_3OD), we observed a significant primary KIE, k_H/k_D of 4.9, which is typical for H-atom transfer reactions according to Balaceanu.[36] When Zn(II) was added to the photolysis solutions at a Zn:dppz ratio of 5:1, a significant drop of the k_H/k_D to 2.6 was observed, and a further decrease to 1.7 when the ratio was increased to 20:1, as shown in Table 2.2.

While the magnitude of the KIE in the Zn(II)-free reaction is consistent with an H-atom abstraction mechanism, the lower values observed upon addition of Zn(II) suggests the mechanism is altered by the Zn(II) ion, possibly involving a hydride-transfer process. Coordination of alcohols to Zn(II) ions is frequently postulated as a mechanism to activate the

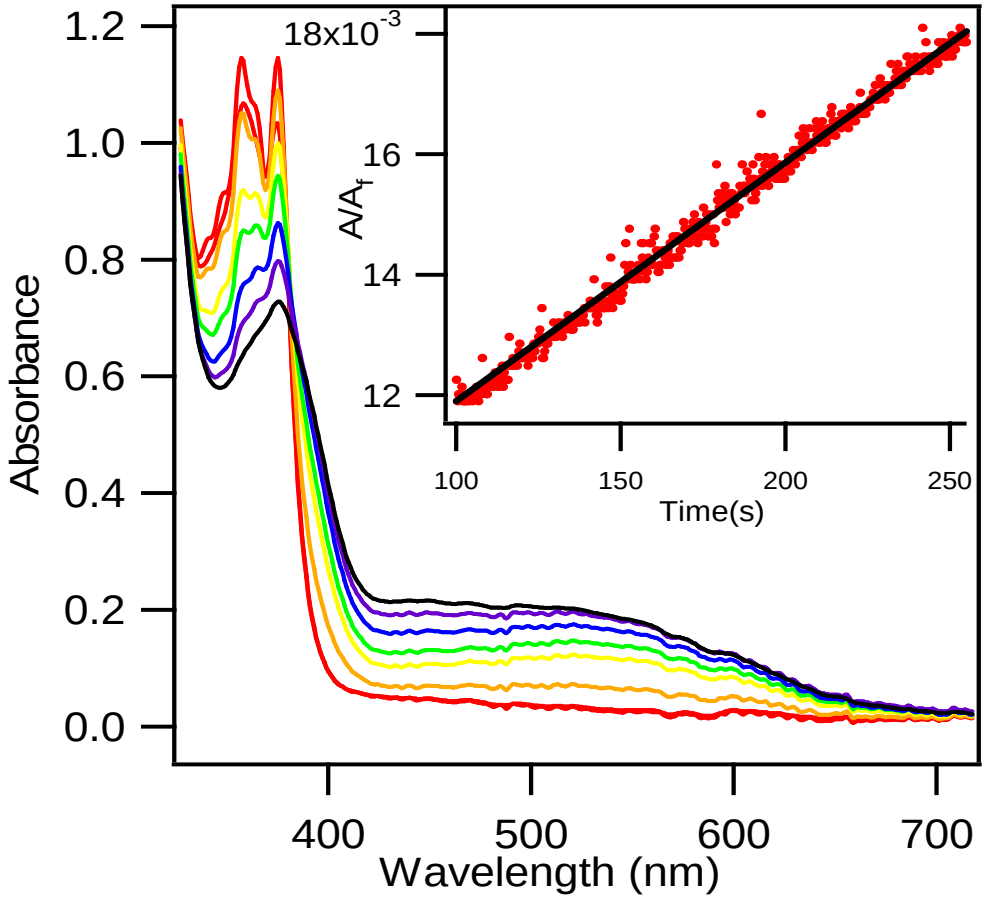

Figure 2.5: Evolution of the absorbance spectrum of dppz (0.1 mM) and $Zn(BF_4)_2 \bullet x\ H_2O$ (1 mM) in MeOH under UV irradiation < 380nm. Inset: Data obtained monitoring change in absorbance at 550 nm vs. time (s) for the first 10% of reaction. Linear fit was performed using y = mx + b, where m represents the rate of reaction.

Table 2.1. Kinetic data for the photoreduction of dppz with CH_3OH in the presence or absence of Zn(II) and water.

		$[Zn(BF_4)_2]$ (mM)	$[H_2O]$ (mM)	$Rate_{rel}$ ($mol \cdot L^{-1}s^{-1}$)	Φ_{375nm} (10^{-3})[b]
dppz (4.0 mM)	1	0.0	55	1.0 ± 0.24	1.2
	2	0.0	5500	0.95 ± 0.21	
	3	0.67	55	1.4 ± 0.54	
	4	1.3	55	4.7 ± 0.85	
	5	4.0	55	5.9 ± 1.2	
	6	20	55	5.3 ± 1.1	4.0
	7	20	110	3.2 ± 0.56	
	8	20	165	3.5 ± 0.71	
	9	20	55 (H^+)[a]	3.5 ± 0.68	
	10	40	55	4.7 ± 1.1	
	11	60	55	4.5 ± 0.79	
	12	80	55	4.2 ± 0.74	

[a] sample contained 55 mM water and 2 mM CF_3COOH [b] Quantum yields were obtained by modification to the light source, using a band pass filters which transmitted light between 350 nm - 400 nm. After the photon flux was calibrated using a ferrioxalate actinometer, the same lamp configuration was used for determination of the reaction quantum yield.

C-H bond α to the alcohol function, towards hydride-transfer.[37-44]

In order to examine the role of the O-H bond, we examined the KIE's at 5:1 Zn:dppz for CH_3OH, CH_3OD, CD_3OH, CD_3OD in the presence of either H_2O or D_2O (55 mM). The results show the KIE's do not deviate significantly from 1.0, signifying the O-H bond is not involved in the reaction mechanism. In order to rule out solvent isotope effects, the KIE was measured in a purely protic environment, as well as a purely deuteric environment, and both values were compared to the KIE of C-H cleavage in H_2O vs. C-D cleavage in D_2O (2.6 ± 0.26). Table 2.2 shows the KIE in protic (2.7 ± 0.35) and deuteric (2.3 ± 0.26) environments are nearly identical to the KIE measured in different isotopic environments, suggesting the solvent environment plays little role in the mechanistic scheme. Significant KIEs are only observed when C-D is exchanged for C-H bonds in the alcoholic substrates, indicating that the substrate, and more specifically the C-H bonds of the substrate, are directly involved in the mechanistic rate determining step.

2.4.4 Kinetic Isotope Effect of tatpp in Alcoholic Solvents

The evolution of the electronic adsorption spectra of tatpp in methanol with excess Zn(II), during irradiation with 470 nm light is shown in Figure 2.7, where the Zn-tatpp adduct is characterized by a structured absorption band between 400 nm and 460 nm. Upon irradiation with visible light, the spectra changes significantly, with appearance of a new absorption band centered at 550 nm and a decrease in the absorption band between 400 nm and 460 nm. The product of tatpp photolysis in DMSO has been reported by Obare et. al. to be H_2tatpp under acidic conditions, and is characterized by a broad peak in the visible region, peaking at 560 nm.[45] Similar to the photolysis of dppz in alcoholic solvents, the spectra do not give a clean a isosbestic point, but instead this point shifts from 479 nm to 473 nm suggesting the process is not a simple direct conversion of reactant to product. Nonetheless, a plot of the increase in absorbance (A/A_f) at 550 nm vs. time is linear during the time interval shown, as seen in the inset of Figure 2.7. The quantum yield for this photo-process was calculated to be $\varphi = 1.6 \times 10^{-3}$

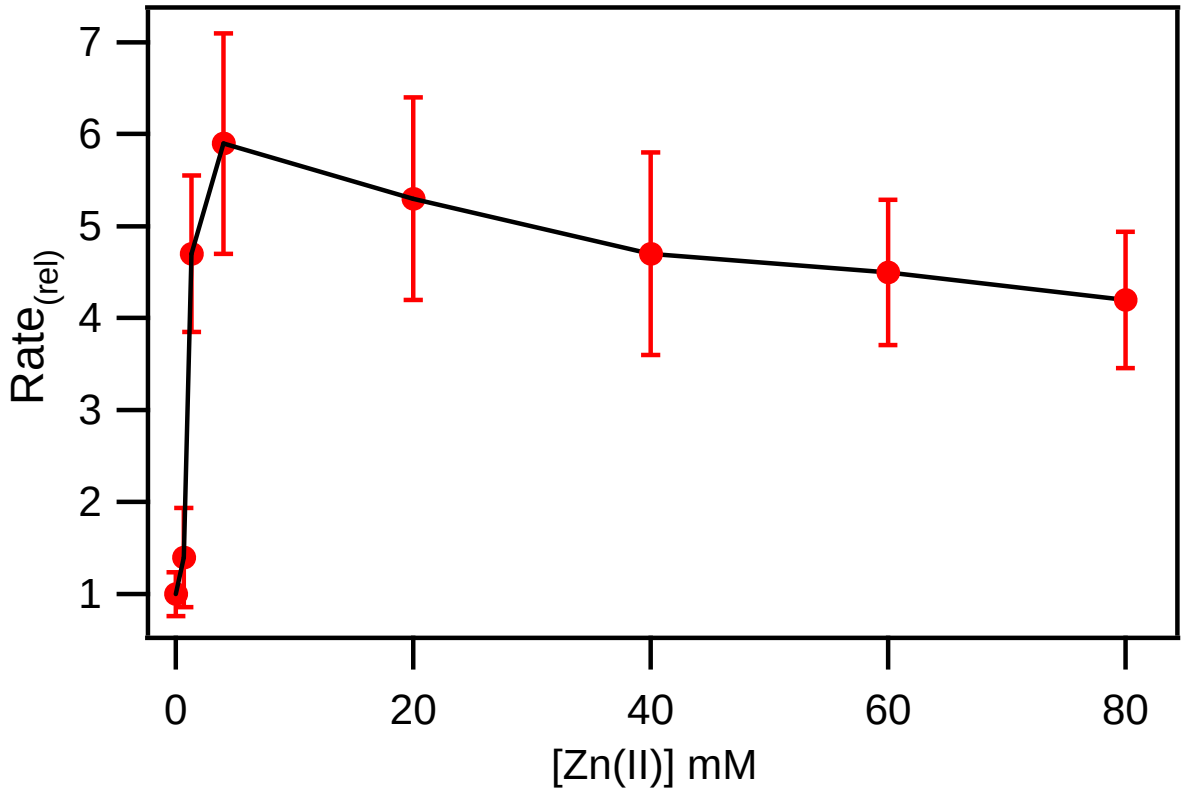

Figure 2.6: Plot of $rate_{(rel)}$ vs. Zn(II) concentration, provided by $Zn(BF_4)_2 \bullet x\ H_2O$, during photolysis of dppz (4 mM) in MeOH under UV irradiation >380nm. Each data point represents an average (n=5) of runs. Error for each data point was calculated from the standard deviation of (n=5) runs.

Table 2.2: Kinetic Isotope Effects for anaerobic photolysis of dppz in various alcoholic solvents.

	Solvent	[Water]	[$Zn(BF_4)_2$] (mM)	KIE
dppz (4.0 mM)	CH_3OH CD_3OD	H_2O D_2O	0 [a] 0 [b]	4.9 ± 1.7
	CH_3OH CD_3OD	H_2O D_2O	20 [a] 20 [b]	2.6 ± 0.26
	CH_3OH CD_3OH	H_2O H_2O	20 [a] 20 [a]	2.7 ± 0.35
	CH_3OD CD_3OD	D_2O D_2O	20 [b] 20 [b]	2.3 ± 0.26
	CH_3OH CH_3OD	H_2O D_2O	20 [a] 20 [b]	1.1 ± 0.13
	CD_3OH CD_3OD	H_2O D_2O	20 [a] 20 [b]	0.98 ± 0.13
	CH_3OH CD_3OD	H_2O D_2O	80 [a] 80 [b]	1.7 ± 0.22

[a] $Zn(BF_4)_2 \bullet x\ H_2O$ was used [b] $Zn(BF_4)_2 \bullet x\ D_2O$ was used

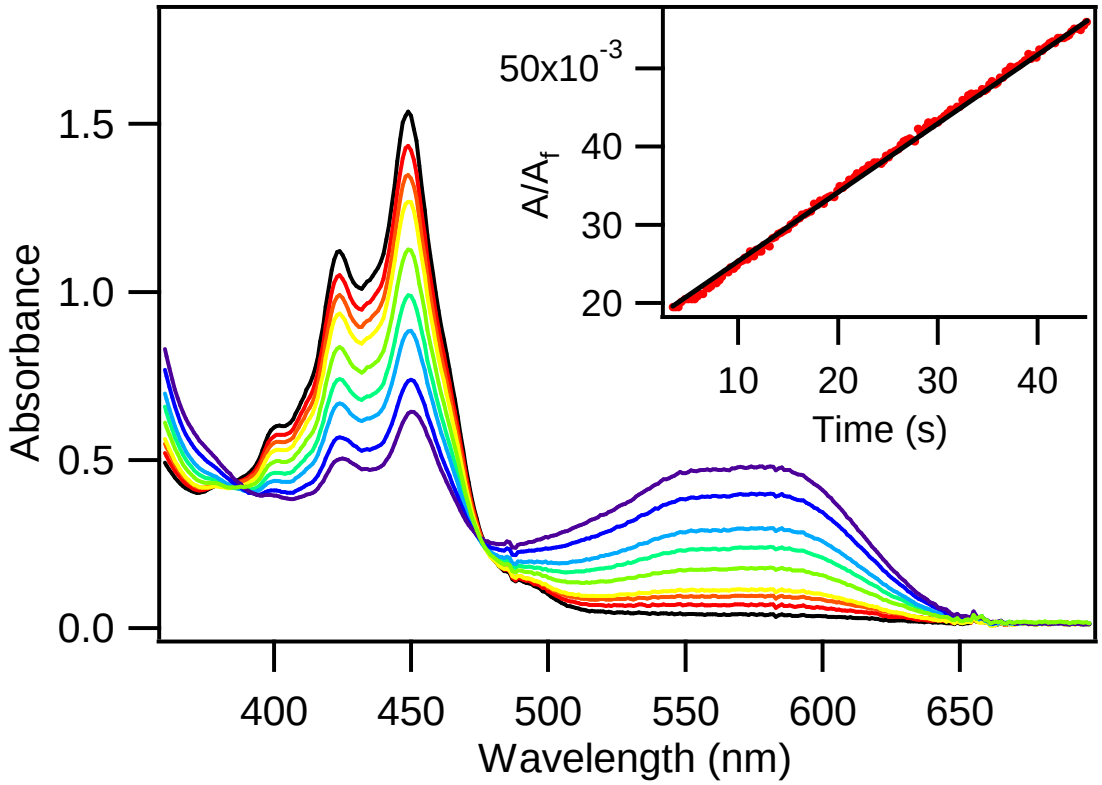

Figure 2.7: Evolution of the absorbance spectrum of tatpp (0.1 mM) and $Zn(BF_4)_2 \bullet x\ H_2O$ (excess) in MeOH under 470 nm irradiation. Inset: Data obtained monitoring change in absorbance at 550 nm vs. time (s) for the first 10% of reaction. Linear fit was performed using y = mx + b, where m represents the rate of reaction.

at 470 nm using the light source described previously.

McGovern and co-workers have shown NMR is useful in characterizing the doubly reduced, doubly protonated H_2dppz species,[2] and an attempt was made to photolyze tatpp under anaerobic conditions in the same manner, the results are shown in Figure 2.8. Upon irradiation with visible light, the initial peaks characteristic for the tatpp ligand disappear along with the appearance of multiple new bands at various δ ppm. After extensive photolysis (10 days), the final NMR spectrum shows multiple peaks, all of which do not appear to be starting material or photoproduct, but rather a series of intermediates. After exposure to air, the spectrum mostly, but not completely, returns to the initial spectrum. The identity of the new products is not known but is speculated to be dimerization products of the type described in Chapter 4.

The insolubility of the tatpp ligand in alcoholic solvents causes multiple practical limitations, one of which is the necessity to add excess Zn(II) to solubilize the ligand, and the subsequent addition of excess moisture to increase the solubility of Zn(II). Due to these constraints, it is difficult to reproduce stock solutions with identical concentrations, and makes it difficult to accurately study the photoreactivity of tatpp in the presence and absence of Zn(II). Since the addition of excess Zn(II) makes it difficult to perform an accurate Zn(II) titration study, we have decided to quantify the k_H/k_D in both methanol and isopropanol solvents. Table 2.3 shows the k_H/k_D is 1.5 in both methanol and isopropanol, which is comparable to the KIE of 1.7 for photolysis of dppz in CH_3OH with 80 mM Zn(II).

2.5. Discussion

2.5.1 Photolysis of dppz in the Absence of Zn(II)

As demonstrated by McGovern et. al., irradiation of dppz in alcoholic solvents with UV light leads to the formation of dihydrodppz (H_2dppz).[2] This process is readily followed by the partial bleaching of several ligand centered (LC) bands between 340 nm and 390 nm and the

concomitant appearance of a large broad peak centered at 590 nm. The 590 nm peak has been assigned as an intramolecular charge-transfer band between the dihydrophenazine-like portion of the molecule and the bipyridine-like portion. The formation of the doubly reduced product has been postulated to occur by disproportionation of the $Hdppz^{\bullet}$ radical, as indicated in reactions 1 to 3.[2,46] From our data, the magnitude of the KIE (4.9) upon switching from CH_3OH to CD_3OD is consistent with the linear transition state (TS1, shown in Figure 2.9) which is commonly postulated in HAT reactions.[36,47] To measure the efficiency of the reaction, the quantum yield was measured and determined to be 1.14×10^{-3} at $\lambda_{exc} = 375$ nm, which falls in between the luminescent quantum yields of 1.9×10^{-4} for $\lambda_{exc} = 350$ nm and 1.8×10^{-2} for $\lambda_{exc} = 400$ nm reported by Lezna et.al. for dppz photolysis in CH_3OH.[1]

dppz → dppz*	very fast	(1)
dppz* + CH_3OH → $dppzH^{\bullet}$ + $CH_2{}^{\bullet}OH$	slow, RDS	(2)
$dppzH^{\bullet}$ + $dppzH^{\bullet}$ → dppz + $dppzH_2$	fast	(3)
$dppzH^{\bullet}$ + $CH_2{}^{\bullet}OH$ → $dppzH^{-}$ + CH_2O + H^{+}	fast	(4)
$dppzH^{-}$ + H^{+} → $dppzH_2$	fast	(5)

By analogy to phenazine, the key photochemical step is postulated to be H-atom abstraction from the alcohol by the n-π* photoexcited singlet state (dppz*)[1,48] which would formally have a hole localized on the phenazine nitrogen. The reactivity of ^{1}π-π* state of dppz* has been shown to be insufficient for driving HAT reactions from alcohols, and is generally limited to electron transfer reactions with amine donors. Although H-atom abstraction reactions can lead to formation of the doubly-reduced, doubly-protonated H_2dppz via an initial one-electron

Table 2.3: The photolysis of tatpp using 450 nm light, in varying solvents with 5.56 M [H_2O] and 85 mM [Zn^{2+}] in all cases.

	Solvent	[Ligand] µM	Rate Constant k (n=5) $x10^{-3}$	k_H/k_D
tatpp	i-PrOH	3.38	33.3	1.5
	d_8 i-PrOD	4.1	22.1	
	MeOH	6.27	45.3	1.5
	d_4 MeOD	6.03	29.9	

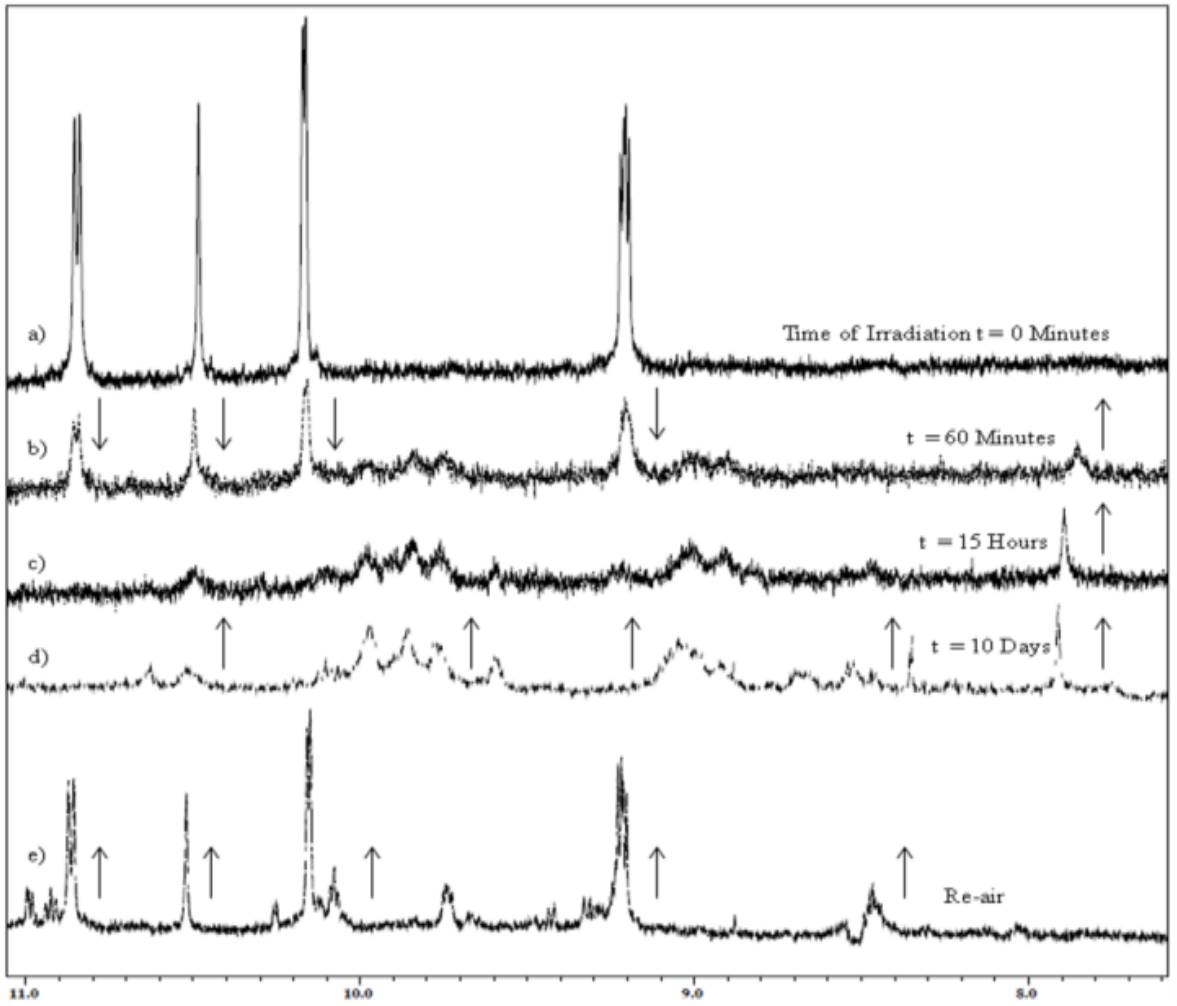

Figure 2.8: Photolysis of Zn_2tatpp adduct in d_3-MeCN with 20% CH_3OH (v/v) using white light from a 100 W tungsten bulb.

reduction followed by disproportionation, reactions 4 and 5 suggest additional routes for the formation of H_2dppz via sequential, one-electron steps. While this scheme does not cover all possible radical decomposition pathways possible, it does reflect the two major pathways by which H_2dppz could be formed.

2.5.2 Photolysis of dppz in the presence of Zn(II)

Understanding the data generated from photolysis of dppz in CH_3OH with Zn(II) present, is not as easily understood. Key observations of the data are (i) addition of Zn(II) increases $rate_{rel}$, but excess Zn(II) does not increase catalytic activity as shown in Figure 2.6, (ii) the KIE decreases with increasing Zn(II), and (iii) the reaction does not proceed unless irradiated with UV light. The small magnitudes of the KIE (2.6 to 1.7) observed in the Zn:dppz adducts are consistent with 'side-on' or other non-linear transition states, such as shown in TS2 or TS3 (Figure 2.9). In TS2, the reaction is an intermolecular process between a Zn:dppz* adducts and a Zn:alcohol adduct with bond cleavage occurring via a triangular TS. In this case, the isotopic substitution has considerably less influence on the activation energy of the bond breaking process and the switch to a hydride-transfer like mechanism is a result of alcohol α C-H bond activation due to coordination to Zn(II) ions. Zinc-catalyzed hydride-transfer from alcohols to various acceptors is a commonly accepted reaction mechanism in a number of biological and chemical reaction systems.[37-42,49-51] For example, alcohol dehydrogenases, which contain a Zn(II) active site, are known to thermally oxidize alcohols, thus transferring an overall "hydride" to an appropriate substrate.[37,38,40,50] However, in most such mechanisms Zn coordination assists with deprotonation of the alcohol prior to hydride transfer. As seen in Table 2.1, entry 9, addition of acid has a small but noticeable effect on the relative rate of dppz photoreduction in the presence of Zn(II). This result indicates that formation of the deprotonated Zn(II)-alkoxide species may play a role here, and that the extent of C-H ‘activation’ by alcohol coordination to the Zn(II) may be attenuated considerably.

Another possibility is the formation of a ternary complex of the alcohol, Zn(II), and dppz as depicted in TS3 in which hydride transfer occurs in an intramolecular fashion. In this case, a 'side-on' transition state with the phenazine nitrogens is not sterically possible, and thus it would require hydride transfer to one of the adjacent carbons atoms in the structure. Subsequent hydrogen migration to the nitrogens and an additional protonation would yield the Zn:H_2dppz product. In this latter mechanism, the $^1\pi$-π^* state would appear to be the reactive species, as the reaction involves initial reduction of the π system.

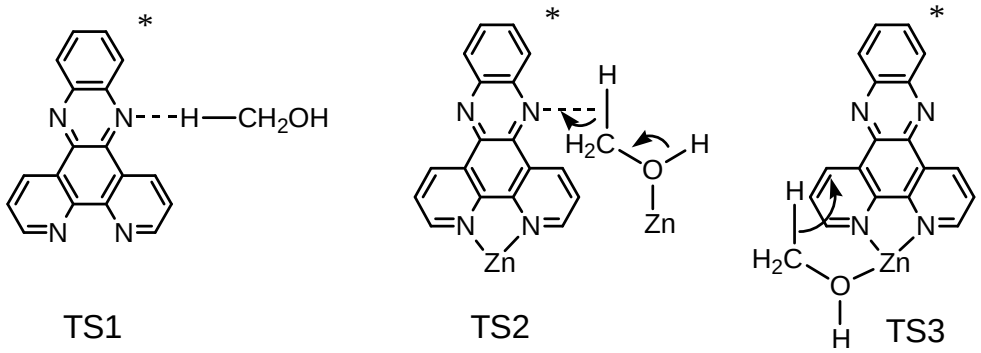

Figure 2.9. Transition states of H-atom abstraction (TS1), Intermolecular oxidation of CH_3OH (TS2), and Intramolecular oxidation of CH_3OH (TS3)

A review of the literature reveals that photochemical reactions involving hydride transfer are relatively rare but not unknown, one of which is the notable case is biosynthesis of chlorophyllide.[49,52-55] Upon photoexcitation of protochlorophyllide (pchlide), NADPH transfers a hydride to C17 of the pchlide to ultimately form chlorophyllide.[49,53-55] The KIE for this process is 1.9 which is in the range of the values we report in our system. This pchlide system is particularly relevant to the Zn:dppz system, as both systems involve a photoexcited chromophore acting as the hydride acceptor. While it may be purely coincidental, it is interesting that the hydride accepting chromophore in both cases in coordinated to a metal ion, Mg^{2+} in pchlide and Zn(II) in the dppz system.

From these data, it is clear that Zn(II) can play a number of potential roles in the observed photoreduction of dppz. It can coordinate and thereby act to activate the hydrogens α

to the alcohol function. It can modify the relative energies and therefore population and reactivity of the dppz ^{1}n-π* and ^{1}π-π* states. It can sterically direct the α-hydrogens of the alcohol to π* system of the dppz acceptor. Or it could be some combination of all three factors. The magnitude of the drop in the KIE in the Zn-free and Zn-dppz photoreductions, suggests a gradual transition from a HAT-type mechanism in the Zn-free case to a hydride-transfer type mechanism in the Zn-dppz case. In the latter, it has been noted in the literature that it is difficult to distinguish between a stepwise electron-proton-electron process or a concerted hydride transfer process, however electron-proton-electron transfer clearly represents an intermediate case between HAT and concerted hydride transfer. Davis and coworkers clearly identify the singly reduced Hphenazine$^\bullet$ radical as the initial photoproduct upon irradiation of phenazine with methanol.[56] This process is much less efficient than the one electron photoreduction with electron donors such as TEA which has been attributed to different reactive states. For TEA and related donors, the ^{1}π-π* state is postulated as the reactive intermediate whereas for alcohols the ^{1}n-π* state is the postulated reactive state. Compared to the reactions with electron donors, lower quantum yields are generally observed for reactions with alcohols with ^{1}n-π* state which is attributed to the partial population of this state by thermal equilibration with the lower-lying ^{1}π-π* state.

The Zn:dppz titration yields some insight into this, but also reveals one additional aspect of the system, the coordination chemistry and speciation of the Zn-dppz system. As was shown in Figure 2.6, the rate of dppz photoreduction rises rapidly from a 0:1 Zn:dppz ratio until a ratio of 1:1 is reached, after which the presence of excess Zn(II) (5:1, 10:1, 20:1) does not further enhance the reaction rate. This data lends some support to the intramolecular process indicated in TS3 at the expense of the intermolecular process (TS2). At lower Zn:dppz ratios, such as 1:2 and 1:3, the solution speciation is complicated by the formation of bis and tris adducts. Chelating diimine ligands such as the closely related 1,10-phenanthroline ligand have large stepwise formation constants (log β) with Zn(II) at 6.4, 5.6, and 5.2 for the mono, bis, and

tris chelate complexes, respectively.[57-59] While the overall coordination number for Zn(II) is flexible between 4 and 6, the number of open coordination sites for the alcohol diminishes as the dppz coordination number increases, lowering the probability of forming the appropriate precursor complex in TS3 for hydride transfer. The complexation of the Zn(II) would similarly effect the probability of formation of TS2, in that lower ratios of Zn(II) would likely lead to increased chelation from dppz, leading to less open coordination sites for alkoxide formation.

2.5.3 Formation of Zn(II) Alkoxide

In biological systems, Zn(II) centered alcohol dehydrogenases are known to thermally oxidize alcohols, thus transferring an overall "hydride" to an appropriate substrate.[37-42,49-55] Multiple studies have been preformed to establish whether the process occurs in a stepwise electron-proton-electron process or a concerted "hydride" transfer process by using tetrahedrally coordinated Zn(II) complexes such as [tris(pyrazolyl)hydroborato]ZnOH, or ZnTpOH, to simulate the alcohol dehydrogenase enzyme center, and various NAD^+ analogues to simulate the hydride acceptor. Both reaction mechanisms suggest the reaction occurs by formation of a metal alkoxide, which labializes the C-H bond α to the alcohol, allowing the unfavorable reaction to proceed. The concentration of the metal-alkoxide is low due to equilibrium with the hydrated solvent environment which forms metal hydroxides, but can be isolated in some cases as the deprotonated metal alkoxide.[37-39] Since the rate of dppz photolysis in CH_3OH is suppressed upon the addition of acid as shown in Table 2.1, entry 9, and the addition of moisture (entries 7 and 8) it is likely metal-alkoxide formation occurs. One consequence of alkoxide formation is a potential change to the solvent environment, specifically changes to acidity and hydrogen bonding effects,[37-39] which in turn might result in a solvent isotope effect. This can be a potential issue when considering the magnitudes of the KIE established in table 2.2, since hydrogen bonding is known to directly affect the orbital energy of dppz, [21,60,61] and changing solvent isotopes may result in varying degrees of hydrogen bonding between dppz and the solvent, yielding inconsistencies in the kinetic data. In order to address

these issues, the solvent hydration was changed from a completely protic environment, to a completely deuteric environment, and the KIE for C-H cleavage was measured. The data in table 2.2 shows the KIE for photolysis of dppz with Zn(II) present (5:1 ratio Zn:dppz) is 2.6 ± 0.26. If the solvent system is changed to a completely protic or deuteric environment, the KIE obtained is 2.7 ± 0.35 and 2.3 ± 0.26 for both protic and deuteric conditions respectively. Since the data shows the magnitudes of the KIE's are not significantly different, the effects caused by alkoxide formation or potential changes to the hydrogen bonding environment can be ignored.

Overall, photolysis of dppz in alcohol donor solvents appears to undergo a one-photon two-electron hydride transfer process when Zn(II) is present. This mechanism is consistent with the observed drop in the KIE, the magnitude of the KIE (1.7 at a Zn:dppz ratio of 20:1), and the substantial rate enhancement observed for photoreduction of the Zn(II) adducts over the Zn-free solutions. If functional, this hydride-transfer mechanism circumvents a number of performance issues that arise when trying to utilize the photochemical H-atom abstraction/disproportionation mechanism in a fuel-forming reaction scheme. It would also be one of the few examples of a photochemically driven, 2-electron transfer process. The decrease in the KIE as the Zn:dppz ratio is increased can be attributed to a transition from the radical mechanism to the hydride transfer mechanism. To a first approximation, the latter mechanism would be first-order in both Zn and dppz and be approaching pseudo 1^{st} order conditions at high Zn:dppz ratios.

2.5.4. Oxidation of Alcohols with tatpp

As demonstrated by Obare and co-workers, irradiation of tatpp in DMSO with UV light produced by a Xenon Arc Lamp ($\lambda > 375$nm) under acidic conditions, leads to the formation of dihydrotatpp (H_2tatpp).[45] This process is readily followed by the partial bleaching of several ligand centered (LC) bands between 400 nm and 460 nm and the concomitant appearance of a large broad peak centered at 550 nm. The absorbance spectrum of the (H_2tatpp) species has also been observed in acetonitrile by MacDonnell and co-workers, during photolysis of the compound [Ru(phen)$_2$tatppRu(phen)$_2$](PF$_6$)$_4$, or complex P.[25] This complex is capable of storing

multiple electrons using multiple photons of visible light via the $MLCT^3$ manifold, which after reductive quenching with a sacrificial reducing agent such as TEA, results in multiple stored electrons on the tatpp bridging ligand. In this chemistry it is well known the decomposition of TEA results in increased solution acidity. Therefore, the doubly reduced P^{2-} is capable of capturing two protons to form the photoproduct H_2P. The optical absorption of the "H_2tatpp" complex resembles that reported by Obare et. al. and is strikingly similar to the spectrum of the photoproduct H_2dppz produced by photolysis of dppz in alcohols. The absorbance spectrum of H_2tatpp in both DMSO and acetonitrile solvents shows a strong (LC) absorption band centered around 560 nm and 580 nm respectively, and is characteristic of the doubly reduced, doubly protonated tatpp species. The observed red-shift in the (LC) absorption band for H_2tatpp upon switching from DMSO to acetonitrile can be attributed to the solvent polarity changing from 7.2 to 5.8 respectively, in which case the DMSO solvent polarity contributes to stabilizing the ground state of H_2tatpp, resulting in a slight blue shift in absorption wavelength as compared to the less polar acetonitrile solvent.

In our data, we also observe the formation of a broad peak at 550 nm upon photolysis of tatpp with 470 nm light, in the presence of Zn(II) and alcohol solvents. This photoproduct has an optical absorption identical to those previously described for H_2tatpp, shown in Figure 2.7, and is presumably H_2tatpp. The quantum yield for this reaction is $\varphi = 1.6 \times 10^{-3}$ using 475 nm light, and compares well to the quantum yield observed for dppz photolysis in alcohols in the presence and absence of Zn(II) as shown in Table 2.1. Although the UV/Vis spectra and quantum yield calculations point to complete conversion of tatpp to H_2tatpp, the NMR data in Figure 2.8 shows other side reactions occur which are not detectable by UV/Vis. Even after long periods of irradiation (10 days) complete conversion of tatpp to H_2tatpp is not observed, and the reaction is not completely reversible as evidenced by new peaks forming which do not relate to the starting material, upon exposure to air. This is not the case with complex P, where the absorbance spectrum shows complete conversion of complex P towards H_2P upon exposure to

visible light, and is completely reversible back to the starting material upon exposure to air. This is also not the case with photolysis of dppz, where McGovern and co-workers show the NMR spectra of H_2dppz upon exposing dppz to UV light, and the spectra of H_2dppz after exposure to O_2. The study shows the reaction is completely reversible since the photoproduct reverts back to the starting material upon exposure to air. Despite the irreversibility observed during photolysis of tatpp and subsequent exposure to air, the instability of the free ligand was not completely unexpected since longer fused chains of aromatic rings tend to be unstable to light and air, and undergo π-π stacking and dimerization processes even at low concentrations.[62-64] This is most likely why reversibility occurs in complex P and dppz, since complex P is capable of avoiding π-π stacking due to the bulky $Ru(phen)_2$ end groups, and dppz contains lesser fused rings compared to tatpp, thus imparting reversibility in both cases.

Due to the insolubility of tatpp and the necessary addition of excess Zn(II) to prevent aggregation, great care was taken to obtain the KIE data in both methanol and isopropanol solvents. Preparation of stock solutions were not possible due to changing concentration of tatpp ligand over time caused by aggregation, therefore fresh solutions were made prior to each run. The data in table 2.3 shows the average concentration of tatpp changes upon switching solvents, even with identical solution preparation conditions for multiple runs. Despite the unavoidable error introduced into the system due to practical limitations, the data shows photolysis of tatpp in methanol and isopropanol both have a KIE of 1.5 which is comparable to that of 1.7 for dppz photolysis in the presence of 80 mM Zn(II). Unfortunately, the accuracy of these values are limited by the solubility of tatpp, and the magnitude of the KIE could not be precisely determined with this experimental set-up. Given these results, we believe the series of reactions which occur during the photolysis of tatpp in alcoholic solvents occurs in an identical fashion to that of dppz in methanol in the presence of Zn(II). Despite the error associated with the KIE's, the value of 1.5 for photolysis of tatpp in both methanol and isopropanol suggest a one-photon two electron hydride transfer occurs, with the use of visible light.

2.6. Conclusions

Although the results for metal-free photolysis of dppz is straightforward, the addition of the Zn(II) ion yields some interesting results and conclusions. In this work, the data shows an enhanced rate effect, due to what we believe is a Zn(II) catalyzed hydride transfer from a metal-bound alcohol species to the photoexcited state of both dppz and tatpp. This process appears to mimic the hydride transfer chemistry seen in biological systems, and has many implications in the development of such chromophores for light-driven fuel formation reactions. If functional, this hydride-transfer mechanism circumvents a number of performance issues that arise when trying to utilize the typical photochemical H-atom abstraction/disproportionation mechanism in photolysis of dppz in the absence of Zn(II), for a fuel-forming reaction scheme. It would also be one of the few examples of a photochemically driven, 2-electron transfer process. Further testing is required to rule out how the two-electron transfer process occurs but the data suggests the H-atom transfer process observed for photolysis of dppz in alcohols in the absence of Zn(II), is enhanced in the presence of the Lewis Acid Zn(II), which may lead to an overall two electron, photo-driven hydride transfer process.

CHAPTER 3

PHOTODRIVEN MULTI-ELECTRON STORAGE IN DI-SUBSTITUTED RU(II) DPPZ ANALOGUES

3.1 Introduction

Compounds that store light energy in the form of high potential electrons are sought after materials.[11,14,17,21,28,65-71] Of the various electron storage systems, Ru polypyridal complexes have attracted much attention due to their useful photophysical, optical, and electronic properties which makes them good chromophores for potential photocatalysts for H_2 production via single and multi-electron storage as well as having interesting DNA binding properties and biological activity.[18,22,24,25,72-75] In recent years, Ru^{2+} multi-electron storage systems such as dinuclear $[(phen)_2\ RutatppRu(phen)_2]^{4+}$ (P) and $[(phen)_2\ RutatpqRu(phen)_2]^{4+}$ (Q) (where phen is 1,10-phenanthroline, tatpp is 9,11,20,22-tetraaza tetrapyrido[3,2-a:2'3'-c:3'',2''-l:2''',3'''-n]-pentacene and tatpq is 9,11,20,22-tetraaza tetrapyrido[3,2-a:2'3'-c:3'',2''-l:2''',3'''-n]-pentacene-10,21-quinone) have been shown to undergo photo-driven multi-electron storage, using TEA as a sacrificial donor.

One of the common ways by which Ru^{2+} polypyridal complexes are used to capture and convert light energy into chemical energy is by reductive quenching of its photoexcited states which effectively traps an electron in a high energy orbital. For example, photoexcitation of $[Ru(phen)_3]^{2+}$ in the MLCT band centered at 450 nm produces a transient charge separated state in which an electron is promoted from a Ru $d\pi$ orbital to one of the unoccupied orbitals of the phen ligand(s) to form $[Ru^{3+}(phen^{\cdot-})(phen)_2]^{2+*}$. This state is both a potent oxidant (E_{ox}^{*} ~1.02 V vs. NHE) and a potent reductant (E_{red}^{*} ~ 0.57 V vs. NHE). When this reacts with an appropriate donor, such as TEA, the hole on the Ru^{3+} ion is filled and the electron is trapped in the ligand LUMO to form $[Ru^{2+}(phen^{\cdot-})(phen)_2]^{+}$, which has a reduction potential (E_{red}) on the order of -1.09 V vs. NHE. Due to coulombic repulsion or self-quenching, such chromophores are typically limited to storing a single electron.

The process by which P, Q, $[Ru(phen)_2dppz]^{2+}$, $[Ru(bpy)_2dppz]^{2+}$, and other ruthenium-polypyridals store light energy is very similar, except the dppz, tatpp and tatpq acceptor ligands, have two or three acceptor orbitals involved in the excited state. Excitation into the MLCT band is seen to occur at energies similar to $[Ru(phen)_3]^{2+}$ (450 nm) which is attributed to excitation of the electron into a phenanthroline-like MO which is higher in energy than the LUMO, which is centered on the polyazine portion of the ligand. After initial population of the phen-like MO, often the LUMO+1, the electron moves to the LUMO and is trapped there upon reductive quenching. Because of the emptying of the phen-like MO, this process can be repeated in P and Q to store up to 2 or 4 electrons, respectively, as apparently the coulombic repulsion in occupying the LUMO is not sufficient to prevent repopulation of the phen-like MO upon another MLCT excitation. Unfortunately, the LUMO in P and Q is significantly lower in energy than the phen-like MO, meaning that the reducing potential of some of these stored electrons is as low as 200 to -200 mV vs. NHE. The net result being that while multiple electrons are stored, they have only modest reduction potentials.

In the dppz complexes, $[Ru(phen)_2dppz]^{2+}$ and $[Ru(bpy)_2dppz]^{2+}$, the orbital picture is similar except that the LUMO is much closer in energy to the phen-like MO and therefore could store higher potential electrons. In practice, only one electron is stored, i.e. $[Ru^{2+}(phen)_2dppz^{\cdot-}]^{+}$ and no doubly reduced products are ever observed. Electrochemistry is typically used to establish the energy of the LUMO which is assigned to the first reductive process and is observed at -720 mV vs. NHE in the $[Ru(bpy)_2dppz]^{2+}$ complex.[18,24] Thus if we could store a second electron in the LUMO of the dppz complex via a photochemical process, we could potentially store two relatively high energy electrons.

It appears that the multi-electron storing capacity of P and Q is related to the large difference in energy between the phen-like MO and the LUMO whereas the single electron storage capacity of $[Ru(phen)_2dppz]^2$+ and related complexes is due to the relatively high energy of the LUMO and its closeness to the phen-like MO.

The question arises as to what is the highest energy LUMO on the acceptor ligand that will allow multi-electron storage? This is the question that is directly addressed in this chapter and we address this by tuning the dppz ligand reduction potential by addition of selected electron withdrawing groups (EWGs) or electron donating groups (EDGs).Fees et. al. have shown the first reduction potential of the $[Ru(bpy)_2dppz]^{2+}$ is related to the phenazine orbital of dppz, and can be destabilized by EDGs. Specifically, when CH_3 groups were substituted in the 11,12-position of dppz. In this case the reduction potential was shifted 100 mV more negative, signifying a destabilization of the LUMO centered on the dppz ligand. Since donating groups have been shown to destabilize the dppz orbital, it is reasonable to assume that EWGs will stabilize the dppz centered LUMO, which would result in lower reduction potentials for the corresponding complexes. This has been observed in a number of $ReCl(CO)_3(dppzX_2)$ analogues, where X = F, Cl, and CF_3.[61] It is also possible to raise the energy of the LUMO in P and Q by addition of EDG and efforts do this by addition of methoxy substituents or changing the geometry of the tatpp ligand from a linear to a 'bent' configuration have been attempted with mixed success.[76] While these changes have modified the reduction potentials of these ligands the photochemistry of the complex with methoxy substituents was complicated by side reaction in which the methoxy groups were expelled. The bent case did lower the reduction potentials but again a side reaction, presumably dimerization of the 'bent' tatpp ligands, limited the usefulness of this system.

DFT calculations of energies and electron distribution of the acceptor orbitals of tatpp, tatpq, and dppz type ligands have proved to be reasonably accurate, in relative terms, with the observed energies and shifts in energies for the relevant acceptor orbitals. In this chapter, we have used DFT calculations of a variety of symmetrically di-substituted dppz ligands in ruthenium complexes of the general formula, $[Ru(phen)_2dppz(X_2)]^{2+}$. From these calculations, it was found that $dppzX_2$ analogues where X = Br and CN in two different, but symmetrical, geometries would be the most promising candidates for multi electron storage of relatively high

energy electrons. In this chapter, we describe the synthesis of selected dppzX2 ligands, their ruthenium complexes, and the testing of these for photodriven multi-electron storage. This is accompanied by electrochemical characterization of the complexes, spectroelectrochemical interrogation of the spectral changes observed upon reduction, and chemical titration to establish the spectra of the reduced and protonated forms of these complexes.

3.2 Experimental

3.2.1 Materials and Reagents

o-Phenylenediamine (Acros, CAS: 95-54-5), HBr (48%, Fluka, CAS: 10035-10-6), Br_2 (99.8% Alfa Aesar, CAS: 7726-95-6), Et_3N (99.5%, Sigma Aldrich, CAS: 121-44-8), $SOCl_2$ (Sigma Aldrich, CAS: 7719-09-7), CuCN (Fluka, CAS: 544-92-3), $NaBH_4$ (Sigma Aldrich, CAS: 16940-66-2), NH_4PF_6 (Oakwood Products, CAS: 16941-11-0), $FeCl_3 \bullet 6\ H_2O$ (Acros, CAS: 7705-08-0) were purchased and used without further purification. 1,10-Phenanthroline-5,6-dione (phendione) was synthesized according to literature procedures.[24] $[Ru(phen)_2]Cl_2$ was prepared according to literature procedures.[73] All synthetic reactions were performed under aerobic conditions unless otherwise specified. All solvents were used without further purification unless otherwise noted. Synthesis of compounds **2**, and **3**, were performed according to literature procedures.[24,77,78]

3.2.2 Instrumentation

H^1 NMR measurements were obtained on a JEOL 500 or 300 MHz spectrometer. IR spectra were obtained using a Bruker Vector 22 FT-IR spectrometer with KBr discs. ESI-MS data was collected using a Thermo Scientific ESI-IT-MS, LCQ DECA-XP, with a flow rate between 5-10 µL/min, and voltage setting of 4.5 kV.

Cyclic voltammetry (CV) and differential pulse voltammetry (DPV) measurements were performed using CH Instruments (1620A) electrochemical workstation, with a platinum wire counter electrode, glassy carbon working electrode, and a Ag/AgCl reference electrode. All potentials are reported vs. NHE unless otherwise specified. Measurements were performed at

room temperature, under N_2, using dry DMF, with $Bu^n_4NPF_6$ (0.1 M) as the supporting electrolyte, and a Ru(II) complex concentration of (0.05 mM). At the end of the experiments, ferrocene was added to provide an internal reference potential, and was referenced with respect to the Fc/Fc^+ couple at 0.64 V vs. NHE. All potentials are reported vs. NHE. Spectroelectrochemistry experiments were performed using both a Hewlett-Packard HP8453A and the CH Instruments (1620A) electrochemical workstation simultaneously, to collect UV/Vis and electrochemical data. The spectroelectrochemical cell kit was purchased from BASi (EF-1351), which included a thin layer quartz cuvette (1 mm pathlength), gold-mesh minigrid working electrode, platinum wire counter electrode, and a Ag/AgCl reference electrode. All spectroelectrochemical experiments were run using anhydrous acetonitrile, with $Bu^n_4NPF_6$ (0.1 M) as the supporting electrolyte, and a Ru(II) complex concentration of (0.5 mM). Photoreduction of complexes $[Ru(phen)_2(dppz\text{-}o\text{-}CN)]^{2+}$ and $[Ru(phen)_2(dppz\text{-}p\text{-}CN)]^{2+}$ were performed using a Hewlett Packard 8453 UV-Visible Spectrophotometer. Screw cap septum sealed, 1 cm glass cuvettes (Starna) were used for all UV/Vis measurements. Photochemically generated anions were created using a light source which emit λ_{max} = 470 nm light, and was previously described in Chapter 2. The photon flux was measured using a ferrioxalate actinometer and determined to be 7.313E-07 Einsteins/Second.

Chemical reductions and protonations were preformed under N_2 in dry acetonitrile, with decamethyl cobaltocene $[((CH_3)_5Cp)_2Co]$ as the reducing agent and trifluoroacetic acid (TFA) as the proton source. Saturated solutions of decamethyl cobaltocene were prepared in a glove-box under anaerobic conditions, and subsequently filtered. The concentration of the stock solution was determined by adding a known volume to a concentrated sample of $[MV](PF_6)_2$ in dry acetonitrile, (where $[MV]^{2+}$ is 1,1'-dimethyl-4,4'-bipyridinium or methyl viologen) and quantification of the $[MV^{\bullet}]^+$ anion generated, using the literature reported molar absorptivity values of ε (396 nm) = 41500 $M^{-1}cm^{-1}$ and ε (608 nm) = 13500 $M^{-1}cm^{-1}$.[79] Since the concentration of $[MV](PF_6)_2$ was in excess compared to the amount of reducing agent added,

we presume the concentration of the $[MV^{\bullet}]^{+}$ anions generated equal the concentration of reducing agent added, and therefore can quantify the true concentration of the decamethyl cobaltocene stock solution.

3.2.3 Synthesis

3.2.3.1 Synthesis of 11,12-dibromodipyrido-[3,2-a:2',3'-c]phenazine **4**

Synthesis was preformed according to literature procedure.[23] Phendione, 0.300 g (1.42 mmol) was suspended in 50 mL EtOH with K_2CO_3 0.200 g (1.44 mmol), with 1,2-diamino-4,5-dibromobenzene (**3**), 0.380 g (1.42 mmol). The solution was refluxed under N_2 for 12 hours. The slurry was filtered using a 0.2 µm nylon membrane. The filter cake was washed with 100 mL hot H_2O, 50 mL acetone, and 20 mL Et_2O then dried in vacuo at 50°C for 12 hr. Yield 0.5 12 g (82%). ^{1}H NMR (500 MHz, $Zn(BF_4)_2$ MeCN-d_3): δ = 8.23 (dd, J = 4.6 Hz and 13.2 Hz, 2H), 8.58 (s, 2H), 9.22 (d, J = 6.9 Hz, 2H), 9.65 (d, J = 9.7 Hz, 2H) ppm.

3.2.3.2 Synthesis of [Ru(phen)$_2$(11,12-dibromodipyrido-[3,2-a:2',3'-c]phenazine)](PF$_6$)$_2$

$[Ru(phen)_2]Cl_2$ 119 mg (0.225 mmol) and **4** 110 mg (0.250 mmol), was added to 30 mL EtOH and 30 mL H_2O. The solution was refluxed under N_2 for 68 hours, filtered and NH_4PF_6 146 mg (0.896 mmol) was added to the filtrate. A red precipitate formed which was filtered and the solid washed with 50 mL H_2O and 50 mL diethyl ether and dried in vacuo at 50° C for 12 h. Yield 0.219 g (82%). CHN Anal. calc. for $[Ru(phen)_2$(11,12-dibromodipyrido-[3,2-a:2',3'-c]phenazine)$](PF_6)_2 \bullet H_2O$ ($C_{42}H_{26}Br_2F_{12}N_8OP_2Ru$) (1209.52 g/mol) : C 41.71; H 2.17; N 9.26; found: C 41.55, H 1.80, N 9.29. ESI-MS: $(M - 2\ (PF_6)^-)^{2+}$: calc: 450.5 m/z, found: 450.536 m/z. ^{1}H NMR (500 MHz, MeCN-d_3): δ = 7.62 (m, 4H), 7.74 (dd, J = 5.4 Hz and 13.8 Hz, 2H), 7.99 (d, J = 6.8 Hz, 2H), 8.09 (d, J = 6.3 Hz, 2H), 8.19 (d, J = 6.9 Hz, 2H), 8.24 (s, 4H), 8.59 (t, J = 7.5 Hz and 6.8 Hz, 4H), 8.79 (s, 2H), 9.52 (d, J = 9.2 Hz, 2H) ppm.

3.2.3.3 Synthesis of 5,6-dibromo-2,1,3-benzothiadiazole **5**, *5,6-dicyano-2,1,3-benzothiadiazole* **6**, *and 1,2-diamino-4,5-dicyanobenzene* **7**

The synthesis of compounds **5**, and **6** were previously reported.[80] Sulfur extrusion of **6** using $NaBH_4$/EtOH as the reducing system, was reported to give **7** in 53% yield. Due to the difficulty in reductive desulfurization of substituted diaminobenzene derivatives, research shows $CoCl_2 \bullet 6\ H_2O$ can be used as a reductive catalyst in $NaBH_4$/EtOH systems, improving yields and reaction time.[81] Adopting this procedure, **7** was prepared by stirring **6** 1.86 g (10.0 mmol), in 100 mL EtOH and 10 mL THF with $CoCl_2 \bullet 6\ H_2O$ 237 mg (0.996 mmol). The suspension was stirred for 15 min, then $NaBH_4$ 1.89 g (50.0 mmol) was added in one portion. The mixture was refluxed for 1.5 h, then $NaBH_4$ 0.750 g (20.0 mmol) was added in one portion to the hot solution. After .5 h the flask was cooled, and filtered through a bed of Celite. The solvent was removed using a rotovap, and the residue was dissolved in 100 mL H_2O. The product was extracted with CH_2Cl_2 (3 x 100 mL), and the organic extracts combined and dried with $MgSO_4$. The organic extracts were filtered and the solvent removed give **7**, which was used immediately in the next step. Yield 1.32 g (84%).

3.2.3.4 Synthesis of 11,12-dicyanodipyrido-[3,2-a:2',3'-c]phenazine **8**

Synthesis was preformed according to literature procedures.[75] 1,2-diamino-4,5-dicyanobenzene **7** 1.32 g (3.97 mmol) was suspended with phendione 0.834 g (3.97 mmol) in 50 mL EtOH with K_2CO_3 0.400 g (2.88 mmol) and refluxed under N_2 for 24 hours. The slurry was filtered and the filter cake was washed with 100 mL hot H_2O, 50 mL acetone, and 20 mL Et_2O then dried in vacuo. Yield 1.02 g (78%). ^{1}HNMR (500 MHz, $Zn(BF_4)_2$ MeCN-d_3): δ = 8.29 (dd, J = 5.2 Hz and 2.7 Hz, 2H), 9.03 (s, 2H), 9.26 (d, J = 6.3 Hz, 2H), 9.83 (d, J = 9.7 Hz, 2H) ppm. IR-(KBr) 2250 cm^{-1} (CN stretch)

3.2.3.5 Synthesis of [Ru(phen)$_2$(11,12-dicyanodipyrido-[3,2-a:2',3'-c]phenazine)](PF$_6$)$_2$

$[Ru(phen)_2]Cl_2$ 119 mg (0.225 mmol) and **8** 83.3 mg (0.250 mmol), was added to 30 mL EtOH and 30 mL H_2O. The solution was refluxed under N_2 for 72 hours and then filtered hot. An

aqueous solution of NH_4PF_6 146 mg (0.896 mmol) in 3.0 mL water was added to the filtrate, causing immediate precipitation of a brown solid. The mixture was filtered and the solid washed with 50 mL H_2O and 50 mL diethyl ether and dried in a vacuo for 24 hours. Yield 0.227 g (93%). CHN Anal. calc. for [Ru(phen)$_2$(11,12-dicyanodipyrido-[3,2-a:2',3'-c]phenazine)](PF$_6$)$_2$ ● 2 H_2O ($C_{44}H_{28}F_{12}N_{10}O_2P_2Ru$) (1101.74 g/mol) : C 47.20; H 2.52; N 12.51 found: C 47.36, H 2.35, N 12.08. ESI-MS: (M - 2(PF_6^-))$^{2+}$: calc 396.9 m/z, found 397.0 m/z. ^{1}H NMR (500 MHz, MeCN-*d$_3$*): δ = 7.63 (m, 4 H), 7.77 (dd, J = 5.4 Hz and 2.9 Hz, 2 H), 7.98 (d, J = 5.2 Hz, 2 H), 8.14 (d, J = 5.2 Hz, 2 H), 8.18 (d, J = 4.0 Hz, 2 H), 8.24 (s, 4 H) 8.60 (t, J = 7.5 Hz and 9.2 Hz, 4 H) 9.07 (s, 2 H) 9.56 (d, J = 9.7 Hz, 2 H) ppm. IR-(KBr) 2250 cm^{-1} (CN stretch)

*3.2.3.6 Synthesis of 2,1,3-benzothiadiazole **9**, 4,7-dibromo-2,1,3-benzothiadiazole **10**, 1,2-diamino-3,6-dibromobenzene **11**, and 10,13-dibromodipyrido-[3,2-a:2',3'-c]phenazine **12***

The synthesis of compounds **9**, **10** and **11** were previously reported.[81,82] Synthesis of **11** was performed according to literature methods using $CoCl_2$ ● 6 H_2O as a reductive catalyst with $NaBH_4$/EtOH, and immediately used to synthesize **12** according to literature procedures.[83] Compound **11** 1.32 g (5.00 mmol) was added to phendione 1.06 g (5.02 mmol) and K_2CO_3 0.400 g (2.88 mmol) in 50 mL EtOH and refluxed under N_2 for 12 hours. The slurry was filtered and the filter cake was washed with 100 mL hot H_2O, 50 mL acetone, and 20 mL Et_2O. The filter cake was dried in vacuo. Yield 1.89 g (86%). ^{1}HNMR (500 MHz, Zn(BF_4)$_2$ MeCN-*d$_3$*) δ = 8.00 (s, 2 H), 8.25 (dd, J = 4.7 Hz and 13.2 Hz, 2 H), 9.25 (d, J = 6.3 Hz, 2 H) 9.69 (d, J = 8.6 Hz, 2 H) ppm.

3.2.3.7 Synthesis of [Ru(phen)$_2$ (10,13-dibromodipyrido-[3,2-a:2',3'-c]phenazine)](PF$_6$)$_2$

[Ru(phen)$_2$]Cl_2 119 mg (0.225 mmol) and **12** 110 mg (0.250 mmol), was added to 30 mL EtOH and 30 mL H_2O. The solution was refluxed under N_2 for 48 hours, and NH_4PF_6 146 mg (0.896 mmol) was added to the filtered solution. A red precipitate formed, which was filtered and washed with 50 mL H_2O and 50 mL diethyl ether, then dried in a vacuo at 50°C for 24 hours. Yield 0.15g (56%). CHN Anal. calc. for [Ru(Phen)$_2$(10,13-dibromodipyrido-[3,2-a:2',3'-

c]phenazine)]$(PF_6)_2$ ● H_2O ($C_{42}H_{24}Br_2F_{12}N_8P_2Ru$) (1209.52 g/mol) : C 41.71; H 2.17; N 9.26; found: C 41.70; H 1.95; N 9.19. ESI-MS: $(M\text{-}2(PF_6))^{2+}$: calc: 450.75 m/z found: 450.469 m/z. ^{1}H NMR (500 MHz, MeCN-d_3): δ = 7.63 (m, 4 H), 7.78 (dd, J = 5.4 Hz and 13.2 Hz, 2 H), 7.99 (d, J = 6.3 Hz, 2 H), 8.13 (d, J = 6.9 Hz, 2 H), 8.20 (d, J = 6.9 Hz, 2 H), 8.24 (s, 4 H) 8.30 (s, 2 H) 8.60 (t, J = 8.6 Hz and 8.6 Hz, 4 H) 9.64 (d, J = 9.2 Hz, 2 H) ppm

3.2.3.8 Synthesis of 4,7-dicyano-2,1,3-benzothiadiazole ***13***

4,7-dibromo-2,1,3-benzothiadiazole **10** 2.87 g (9.76 mmol) was added to CuCN 2.84 g (31.7 mmol) in 40 mL DMF. The slurry was thoroughly degassed with N_2 and refluxed for 3 h. A separate solution of $FeCl_3$ ● 6 H_2O 13.0 g (48.1 mmol) was added to 3.5 mL concentrated HCl and 20 mL H_2O. Once the refluxed mixture cooled to r.t. the $FeCl_3$ ● 6 H_2O solution was added to the cooled reaction solution and stirred at 20° C for 0.5 h. The product was extracted with CH_2Cl_2 (2 x 100 mL) and the combined organic layers were washed with 6 M HCl (3 x 100 mL), H_2O (50 mL), and brine (50 mL). The organic layer was then dried with $MgSO_4$ and the solvent was removed under reduced pressure. Yield 1.12g (62%). ^{1}H NMR (500 MHz, Acetone-d_6): δ = 8.5 (s, 2 H) ppm.

3.2.3.9 Synthesis of 1,2-diamino-3,6-dicyanobenzene ***14***

4,7-dicyano-2,1,3-benzothiadiazole 1.86 g (10 mmol) was suspended in 100 mL EtOH and 10 mL THF with $CoCl_2$ ● 6 H_2O 237 mg (1.00 mmol). The suspension was stirred for 15 min, and $NaBH_4$ 1.89 g (50.0 mmol) was added in one portion. The mixture was refluxed for 1.5 h, and additional $NaBH_4$ 0.750 g (20.0 mmol) was added in one portion to the hot solution and heated for 0.5 h. The solution was filtered through a bed of celite and the solvent removed under reduced pressure. The residue was dissolved in 100 mL H_2O and extracted with CH_2Cl_2 (3 x 100 mL). The organic extracts were combined, dried with $MgSO_4$ and the solvent removed under reduced pressure. The crude solid was immediately used in the next step. Yield 1.01g (64%)

*3.2.3.10 Synthesis of 10,13-dicyanodipyrido-[3,2-a:2',3'-c]phenazine **15***

Crude 1,2-diamino-3,6-dicyanobenzene **14** 1.01 g (6.4 mmol) was suspended with phendione 1.34 g (6.4 mmol) in 50 mL EtOH with K_2CO_3 0.4 g (2.88 mmol) and refluxed under N_2 for 24 hours. The slurry was filtered using and the filter cake was washed with 100 mL hot H_2O, 50 mL acetone, and 20 mL Et_2O. The filter cake was dried in vacuo. Yield 1.76 g (83%). ^{1}HNMR (500 MHz, $Zn(BF_4)_2$ MeCN-d_3): δ = 8.31 (dd, J = 4.8 Hz and 5.7 Hz, 2H), 8.59 (s, 2H), 9.29 (d, J = 6.9 Hz, 2H), 9.88 (d, J = 9.7 Hz, 2H) ppm. IR-(KBr) 2250 cm^{-1} (CN stretch)

3.2.3.11 Synthesis of [Ru(phen)$_2$(10,13-dicyanodipyrido-[3,2-a:2',3'-c]phenazine)](PF$_6$)$_2$

$[Ru(phen)_2]Cl_2$ 119 mg (0.225 mmol) and **15** 83.3 mg (0.250 mmol), was added to 30 mL EtOH and 30 mL H_2O. Due to the insolubility of **15** in 1:1 EtOH/H_2O. The solution was refluxed under N_2 for 72 hours, filtered, and NH_4PF_6 146 mg (0.896 mmol) was added to the filtered solution. A brown precipitate formed, and was filtered and washed with 50 mL H_2O and 50 mL diethyl ether, then dried in a vacuo at 50°C for 24 hours. Yield 0.221g (91%). CHN Anal. calc. for [Ru(phen)$_2$(10,13-dicyanodipyrido-[3,2-a:2',3'-c]phenazine)](PF$_6$)$_2$ ● 3 H_2O ($C_{44}H_{30}F_{12}N_{10}O_3P_2Ru$ (1137.77 g/mol) : C 46.45; H 2.66; N 12.31 found: C 46.51, H 2.38, N 11.73. ESI-MS: (M-2(PF$_6$))$^{2+}$: calc: 396.8 m/z found: 397.0 m/z. ^{1}H NMR (500 MHz, MeCN-d_3): δ = 7.63 (m, 4 H), 7.79 (dd, J = 5.2 Hz and 2.9 Hz, 2 H), 7.99 (d, J = 6.3 Hz, 2 H), 8.176 (d, J = 6.3 Hz, 2 H), 8.21 (d, J = 5.2 Hz, 2 H), 8.25 (s, 4 H) 8.61 (t, J = 9.7 Hz and 9.7 Hz, 4 H) 8.63 (s, 2 H) 9.63 (d, J = 9.7 Hz, 2 H) ppm. IR-(KBr) 2252 cm^{-1} (CN stretch)

3.3 Results

3.3.1 Synthesis of Various [Ru(phen)$_2$(dppzX$_2$)]$^{2+}$ analogues

The synthetic preparation of the materials used for these studies are shown schematically in Figures 3.1, 3.2, and 3.3. Although the preparation of materials 4, 5, and 12 has already been previously established,[23,30,75,78,80-83] the preparation of 15 and the complexation of these four acceptor ligands to $[Ru(phen)_2]^{2+}$ has not been previously performed, to the best of our knowledge. All of the dppz acceptor ligands were prepared by a simple

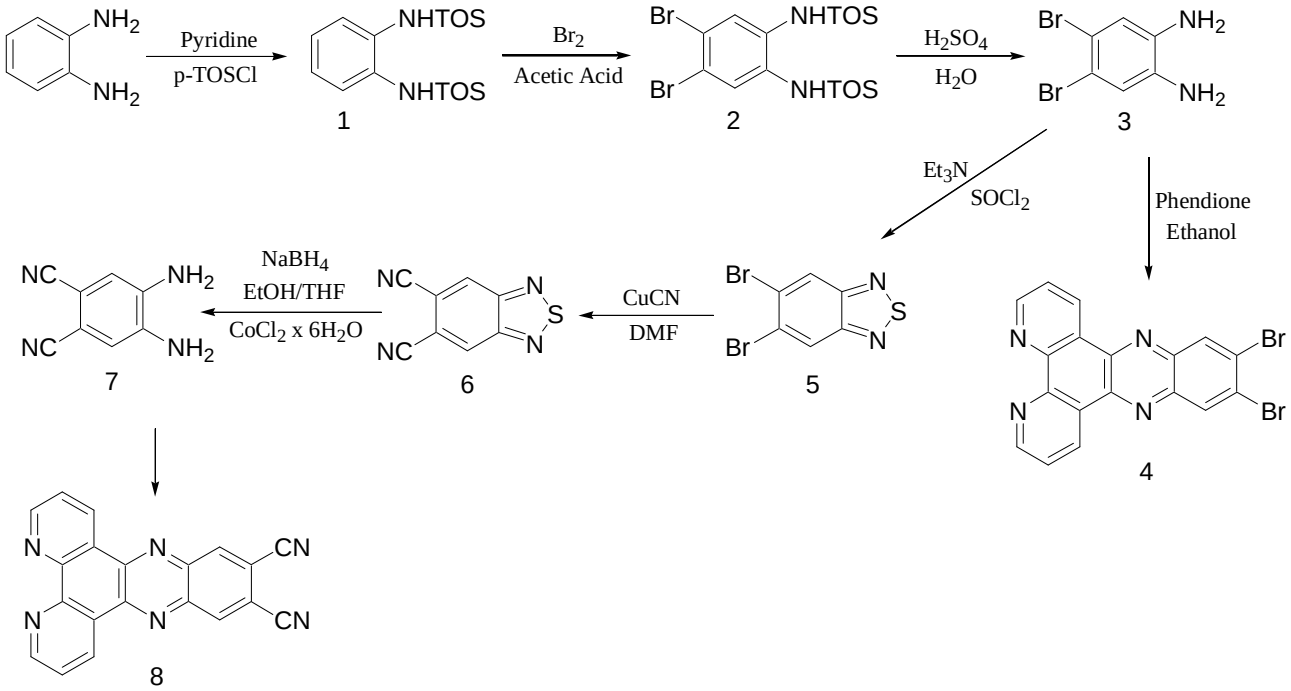

Figure 3.1: Synthetic route towards the 11,12-disubstituted dppz analogues

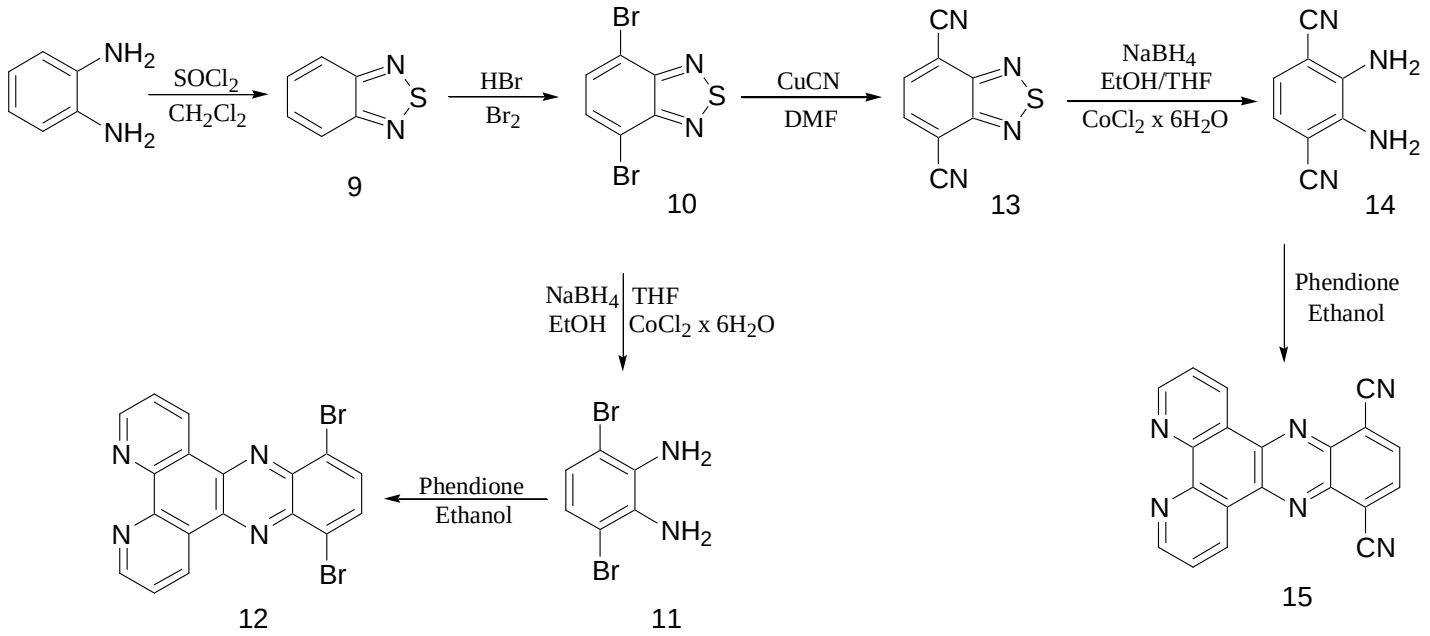

Figure 3.2: Synthetic route towards the 10,13-disubstituted dppz analogues

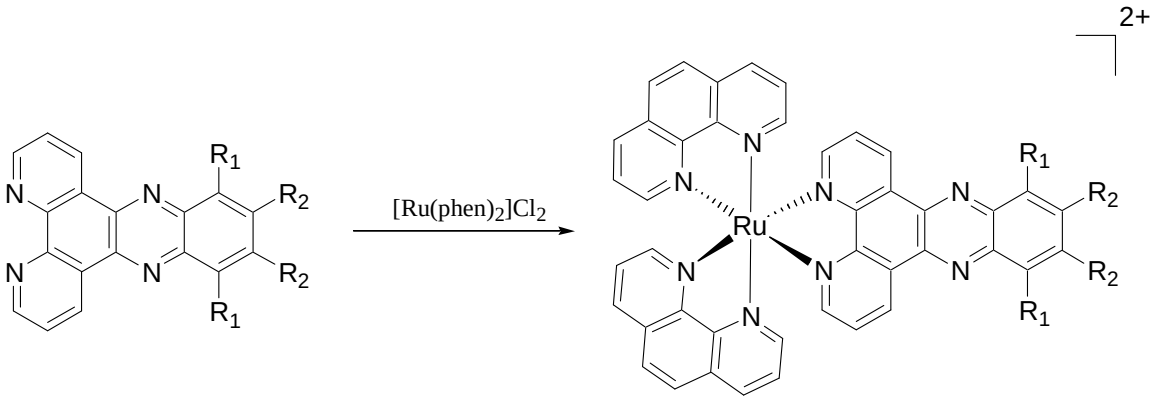

Compound	R_1	R_2
$[Ru(phen)_2(dppz\text{-}o\text{-}Br)]^{2+}$	H	Br
$[Ru(phen)_2(dppz\text{-}o\text{-}CN)]^{2+}$	H	CN
$[Ru(phen)_2(dppz\text{-}p\text{-}Br)]^{2+}$	Br	H
$[Ru(phen)_2(dppz\text{-}p\text{-}CN)]^{2+}$	CN	H

Figure 3.3: Synthesis of the final complexes by addition of $[Ru(phen)_2]Cl_2$

condensation reaction between phendione and the corresponding di-substituted 1,2-phenylenediamines. In cases where a sulfur-extrusion was necessary to achieve the di-substituted 1,2-phenylenediamines, a Co(II)/$NaBH_4$ reduction system designed by Neto et. al was used, to afford the diamines in relatively high yields.[81,82] Both di-cyano substituted 1,2-phenylenediamines were prepared from their respective di-bromo 1,2-phenylenediamine analogues using CuCN in DMF.[80,84]

3.3.2 Calculations

Solvated, ground state DFT calculations of various $[Ru(phen)_2(dppzX_2)]^{2+}$ analogues where X = H, CH_3, Br, and CN, were performed at the B3LYP level using Gaussian 03, and acetonitrile as the solvent. The overall charge of each complex was set to (+2) to account for the Ru(II) metal. In order to make comparisons between the orbital energies of the LUMO and LUMO+1 between various $[Ru(phen)_2(dppzX_2)]^{2+}$ analogues, we decided to set the Ru dπ based HOMO to 0.0 eV since the energy of this orbital should remain relatively similar in each complex. The results are shown in Figure 3.4. In every complex, the lowest energy acceptor orbitals are localized on the dppz and tatpp ligands, which is shown pictorially in Figure 3.5. One MO, typically the dppz centered LUMO, has very similar symmetry and orbital density to the LUMO for phenazine and thus we call this MO the phenazine-like MO. One of the other MOs, typically the LUMO+1, has similar symmetry and orbital density to that of the LUMO for 2,2'-bipyridine or 1,10-phenanthroline and thus we call this the phen-like MO. Fees and coworkers have shown that the MLCT optical absorption properties of $[Ru(phen)_2(dppz)]^{2+}$ primarily involve excitation of the Ru dπ electrons into the phen-like LUMO+1 because its absorption spectrum is nearly identical to that of $[Ru(phen)_3]^{2+}$ and $[Ru(bpy)_3]^{2+}$, both of which exhibit a absorption maximum between 450 nm and 480 nm. Interestingly, no appreciable lower energy absorption is seen in $[Ru(phen)_2(dppz)]^{2+}$ which would correspond to the expected HOMO - LUMO MLCT transition between the Ru dπ orbital and the dppz centered LUMO. A similar situation is observed with P and Q, as neither shows significant absorbtions below the

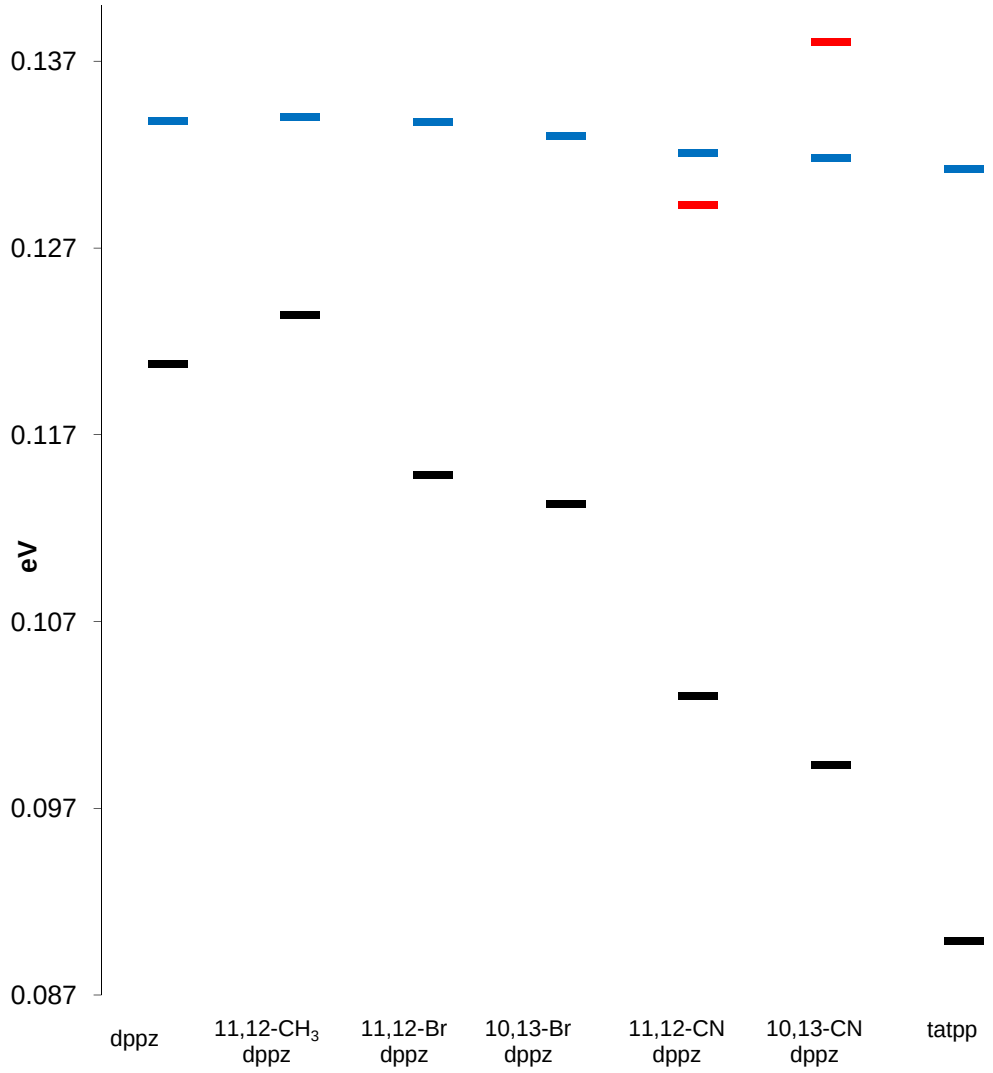

Figure 3.4: DFT calculations of orbital energies of various Ru(II) complexes. Solvated, ground state calculations were performed at the B3LYP level using MeCN as the solvent. The HOMO is centered on the Ru(II) center for each of the complexes and was set to 0 = eV for this diagram. The MO's centered on dppz and its di-substituted analogues and tatpp are the LUMO orbitals (black). The phen centered MO's are typically the LUMO+1 (blue) for most complexes. 11,12-dicyanodppz, and 10,13-dicyanodppz have more than one dppz centered orbital (red).

$[Ru(phen)_3]^{2+}$	$[Ru(phen)_2dppz]^{2+}$	$[Ru(phen)_2(dppz\text{-}o\text{-}CN)]^{2+}$	$[Ru(phen)_2(dppz\text{-}p\text{-}CN)]^{2+}$	Complex **P**
		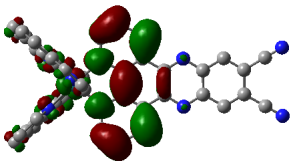	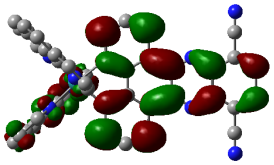	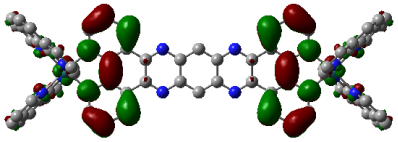
		LUMO+2	LUMO+3 [a]	LUMO+2
	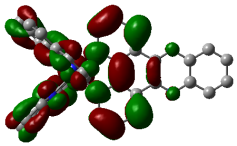	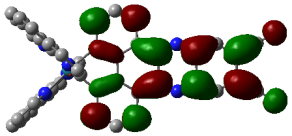	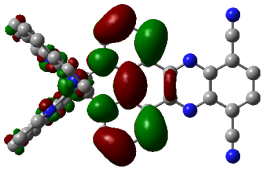	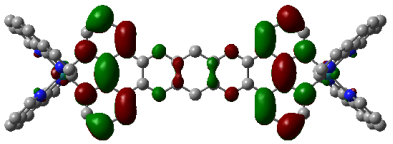
	LUMO+1	LUMO+1	LUMO+1	LUMO+1
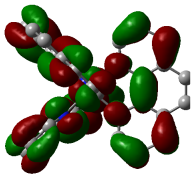	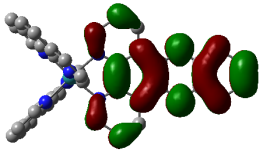	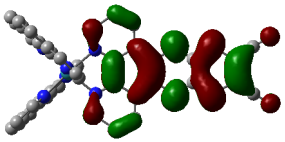	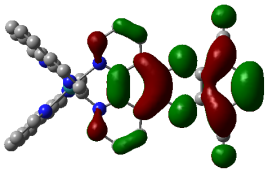	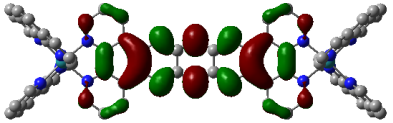
LUMO	LUMO	LUMO	LUMO	LUMO

Figure 3.5: MO pictures for the relevant orbitals described in Figure 3.4. [a)] The LUMO+2 orbital (~0.139 eV) is energetically almost equal to the energy of the LUMO +3 orbital, and was removed for clarity.

480 nm MLCT band. Because of this unusual behavior, the phen-like MO in these complexes is referred to as the 'optical' orbital. Conversely, electrochemical reduction of $[Ru(phen)_2(dppz)]^{2+}$ occurs at much more positive potentials than is seen in $[Ru(phen)_3]^{2+}$ or $[Ru(bpy)_3]^{2+}$, indicating that the phenazine-like LUMO is the first orbital populated upon reduction. Fees et. al. refer to it as the redox MO. This uncoupling of the optical orbital and the redox orbital yields these interesting photo-physical properties which is one of the primary reasons for our interest in this system.

As expected, the data shows that strong electron withdrawing groups, such as CN, greatly stabilize or lower the energy of the phenazine (phz) centered dppz orbital (the LUMO), with only minor influence on the phen-like MO. Bromo substituents are both EWD and EDG but the predominant effect is withdrawing and the LUMO is found at values between those for dppz and $dppz(CN)_2$. The position of the substituents on the distal ring of the dppz also had a small but observable effect of the orbital energies. Substituting electron-withdrawing groups in the 10,13 positions, also showed a slight increase in the stabilization of the ligand centered orbitals compared to orbitals with same substitution in the 11,12 positions. One interesting observation is the MO calculations predict a new ligand centered orbital is present on both dicyano dppz analogues. The energy of this new MO is closer to the phen-like MO than the LUMO and it unclear how its presence affects the overall photophysics, if at all. Figure 3.5 depicts the relevant orbitals for all of the complexes. It is important to note the calculations predict an MO exists at ~0.139 eV in all of the complexes, which was omitted from Figure 3.5 for clarity, and appears to indicate the LUMOs on the additional phenanthroline ligands. The CH_3 and Br substituted analogues were omitted from Figure 3.6 for clarity, since the orbital diagrams are nearly identical to that of $[Ru(phen)_2dppz]^{2+}$.

3.3.3 Electrochemistry

Fees et. al. have shown the first reduction of $[Ru(bpy)_2(dppz)]^{2+}$ in dry DMF occurs at -0.72 V vs. NHE, which corresponds to reduction of the dppz ligand to form the corresponding

coordinated anion, i.e. $[(bpy)_2Ru(dppz^{\bullet-})]^{2+}$.[18,19] The second and third reductions of $[Ru(bpy)_2dppz]^{2+}$ occur at -1.15 V and -1.35 V vs. NHE, and can be attributed to sequential one-electron reductions of the metal bound bpy co-ligands. The second and third reduction potentials differ by about ~0.16V, which the authors attribute to coulombic repulsion.

In this work, the electrochemical reduction of $[Ru(phen)_2dppz]^{2+}$ in DMF closely matches the results obtained by Fees*. et. al.* as shown in Table 3.1. The first reduction occurs at -0.72 V vs. NHE, with the second and third reductions occurring at -1.11 V and -1.32 V. Substitution of Br in complexes $[Ru(phen)_2(dppz\text{-}o\text{-}Br)]^{2+}$ and $[Ru(phen)_2(dppz\text{-}p\text{-}Br)]^{2+}$ show the first reduction is shifted to positive potentials, with $[Ru(phen)_2(dppz\text{-}p\text{-}Br)]^{2+}$ having an additional 40 mV shift compared to $[Ru(phen)_2(dppz\text{-}o\text{-}Br)]^{2+}$, indicating enhanced orbital stabilization which was predicted by DFT calculations. The second and third reductions of both complexes are very similar to that obtained for $[Ru(phen)_2dppz]^{2+}$, which are presumed to be one-electron reductions of the metal bound phen ligands. Both potentials are separated by ~0.16V, as was seen for $[Ru(bpy)_2dppz]^{2+}$. CV scans of the dicyano complexes, $[Ru(phen)_2(dppz\text{-}o\text{-}CN)]^{2+}$ and $[Ru(phen)_2(dppz\text{-}p\text{-}CN)]^{2+}$ showed multiple reduction peaks in the region between -0.15 V and -0.90 V, as shown in Figure 3.6. The DPV data, shown in Figure 3.7, more clearly resolves these processes. The first reduction process of $[Ru(phen)_2(dppz\text{-}o\text{-}CN)]^{2+}$ is observed at -0.26V vs. NHE. A second quasi-reversible reduction is observed with two additional reductions seen -1.16V and -1.33V respectively. The latter two reduction potentials are separated by ~0.16 V, and closely match the second and third reduction potentials of $[Ru(phen)_2dppz]^{2+}$. CV and DPV scans of $[Ru(phen)_2(dppz\text{-}p\text{-}CN)]^{2+}$ shows three reductive processes occur prior to the phen-based reductions at -1.19 V and -1.35 V. The first is a clean, reversible one-electron processes occurring at -0.18 V (vs. NHE) which is 80 mV more positive compared to the first reduction in $[Ru(phen)_2(dppz\text{-}o\text{-}CN)]^{2+}$ (Figure 3.7). A second partly reversible reduction process occurs at -0.5 V. Interestingly, a third reversible one-electron process is observed at -0.84 V. This new

Table 3.1: Reduction potentials of ruthenium-dppz complexes and related analogues. Reductions of the metal bound phen or bpy ligands are highlighted in bold.

Complexes[a]	^{1}E	^{2}E	^{3}E	^{4}E	^{5}E
$[Ru(phen)_3]^{2+}$	-1.05V	-1.25V	-1.5V		
$[Ru(bpy)_2dppz]^{2+}$ [10]	-0.72V	**-1.15V**	**-1.35V**		
$[Ru(phen)_2dppz]^{2+}$	-0.72V	**-1.11V**	**-1.32V**		
$[Ru(phen)_2(dppz\text{-}o\text{-}Br)]^{2+}$	-0.53V	**-1.17V**[d]	**-1.33V**		
$[Ru(phen)_2(dppz\text{-}p\text{-}Br)]^{2+}$	-0.49V	**-1.18V**[d]	**-1.34V**		
$[Ru(phen)_2(dppz\text{-}o\text{-}CN)]^{2+}$	-0.26V	-0.90V[c,d]		**-1.16V**	**-1.33V**
$[Ru(phen)_2(dppz\text{-}p\text{-}CN)]^{2+}$	-0.18V	-0.5V[b,d]	-0.84V	**-1.19V**	**-1.35V**
$Co(Cp(CH_3)_5)_2$ [16]	-1.3V				

[a] obtained from CV data collected using the hexaflurophosphate salts in N_2 purged, dry DMF, with Ag/Ag^+ reference electrode, Pt counter electrode, and $Bu^n{}_4NPF_6$ (0.1 M) supporting electrolyte. CVs were run at 50 mV/s and reduction potentials are reported vs. NHE (Fc^+/Fc internal reference).
[b] non reversible reduction/oxidation step; [c] small wave; reversible; [d] partly irreversible

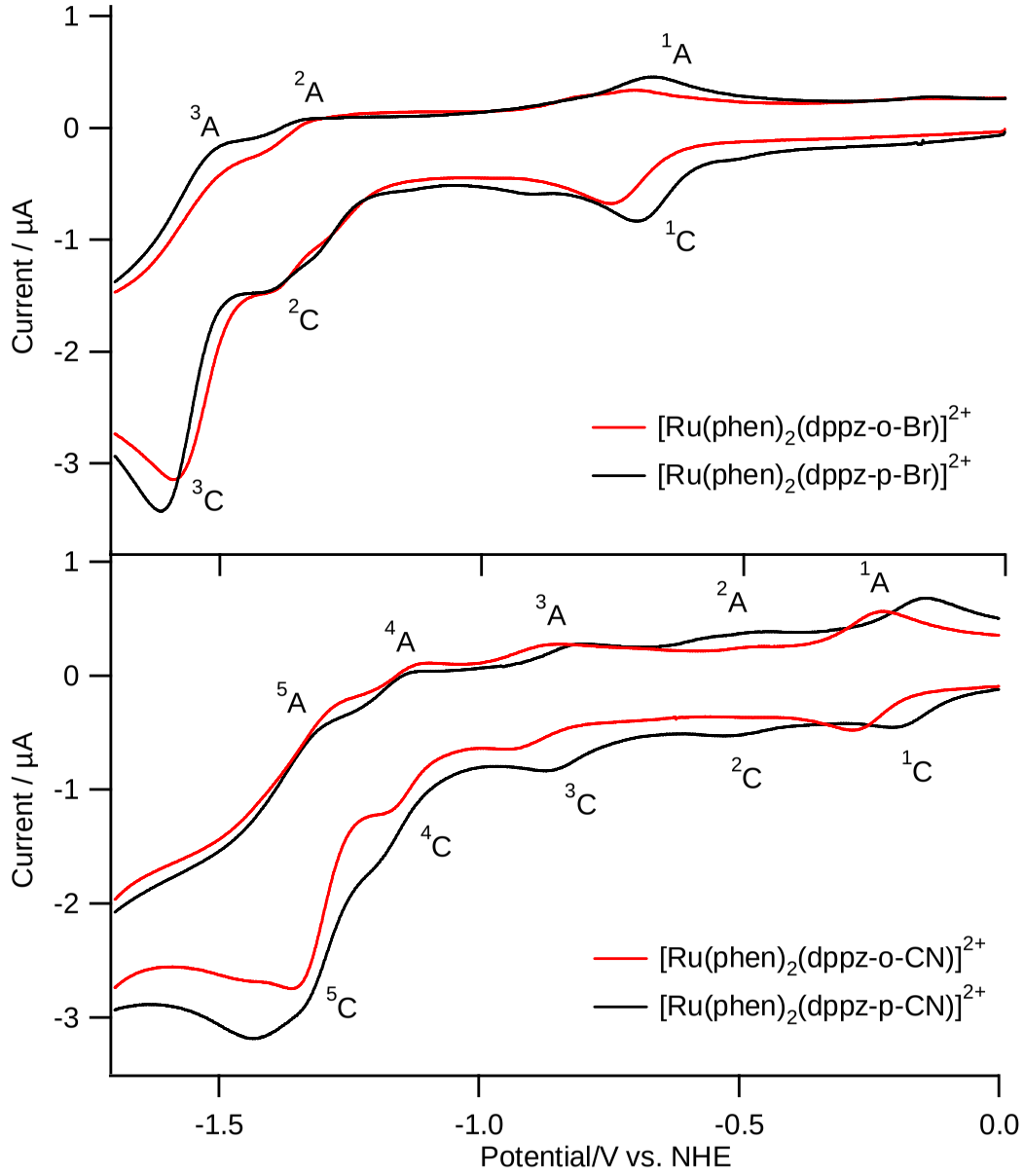

Figure 3.6: CV scans of $[Ru(phen)_2(dppz\text{-}o\text{-}Br)]^{2+}$and $[Ru(phen)_2(dppz\text{-}p\text{-}Br)]^{2+}$ (top) and $[Ru(phen)_2(dppz\text{-}o\text{-}CN)]^{2+}$ and $[Ru(phen)_2(dppz\text{-}p\text{-}CN)]^{2+}$ (bottom). Potentials reported vs. NHE. Data was obtained in dry DMF using Ag/Ag^+ reference electrode, $Bu^n{}_4NPF_6$ (0.1 M) supporting electrolyte, glassy carbon (1.5 mm I.D.) working electrode, and Pt counter electrode with a scan rate of 50mV/s

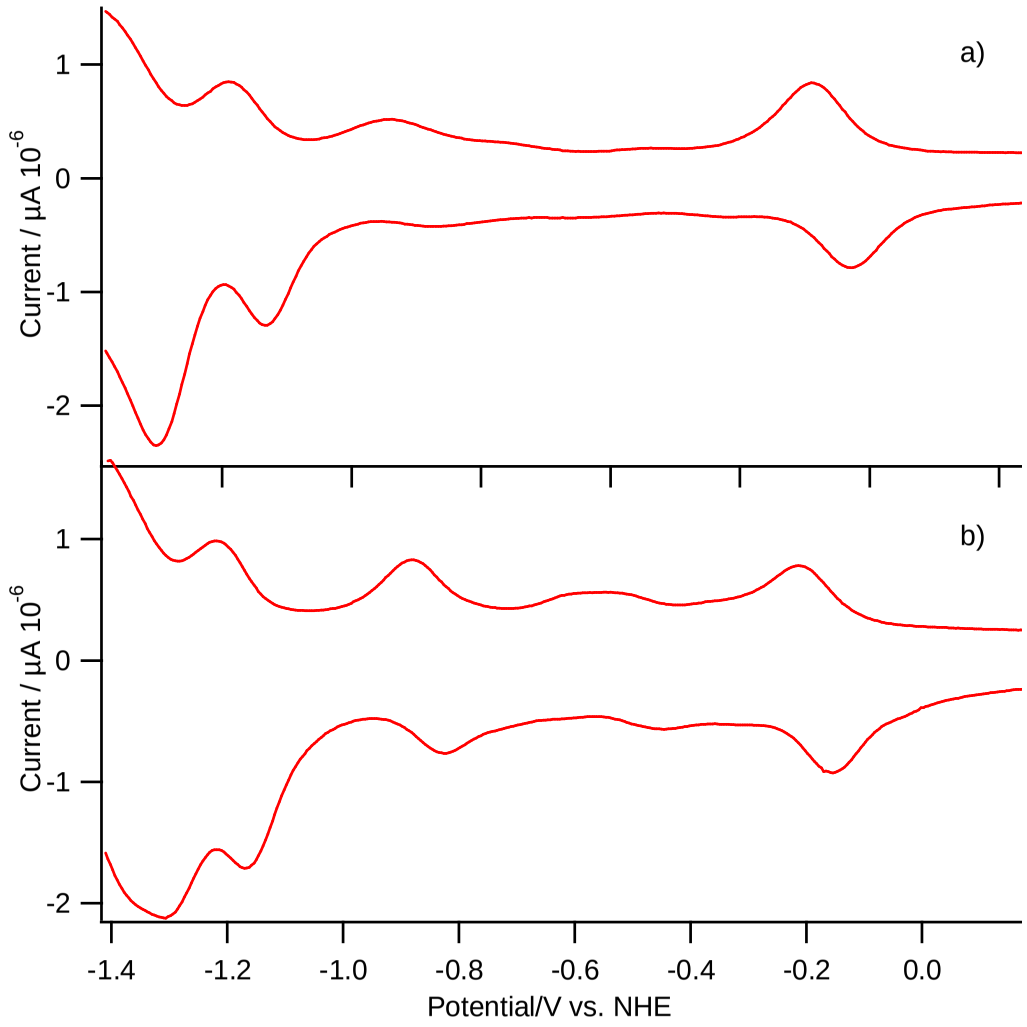

Figure 3.7: DPV scans of $[Ru(phen)_2(dppz\text{-}o\text{-}CN)]^{2+}$ (a) and $[Ru(phen)_2(dppz\text{-}p\text{-}CN)]^{2+}$ (b) in dry DMF under N_2. Potentials reported vs. NHE using Ag/Ag^+ reference electrode, Pt counter electrode, glassy carbon (1.5 mm I.D.) working electrode, and $Bu^n{}_4NPF_6$ (0.1 M) as the supporting electrolyte, with a potential pulse amplitude = 0.05 V, pulse period = 0.2 V, pulse duration = 0.05 s, and step size = 0.004 V.

reduction at -0.84 V appears to be a second one-electron reduction of the dppz ligand, which is confirmed, in part, by reductive titrations and spectroelectrochemical data to be presented.

3.3.4 Chemical Reduction Titration

The electronic absorption spectra of the reduced forms of both dicyano complexes were collected by both chemical titrations and by generating the reduced species electrochemically in a spectroelectrochemical cell. For the titration data, the optical absorption spectra of the reducing agent $[((CH_3)_5Cp)_2Co]$ must be considered and has been previously reported in acetonitrile solutions.[85] Although the electronic absorption spectra of the 19-electron $[((CH_3)_5Cp)_2Co]$ species was reported to be rather featureless, the 18-electron $[((CH_3)_5Cp)_2Co]^+$ species was reported to show small absorption bands at 250 nm (ε = 1170 $M^{-1}\,cm^{-1}$), 338 nm (ε = 1430 $M^{-1}\,cm^{-1}$), 420 nm (ε = 330 $M^{-1}\,cm^{-1}$), 469 nm (ε = 8 $M^{-1}\,cm^{-1}$), 540 nm (ε = 0.8 $M^{-1}\,cm^{-1}$), and 787 nm (ε = 0.2 $M^{-1}\,cm^{-1}$). Since the largest molar absorptivity observed between 300 nm - 800 nm for the $[((CH_3)_5Cp)_2Co]^+$ species is ε = 1430 $M^{-1}\,cm^{-1}$, and typical molar absorptivities of ruthenium-polypyridals is in the range of ε = 15,000 - 20,000 $M^{-1}\,cm^{-1}$, it is unlikely that generation of the $[((CH_3)_5Cp)_2Co]^+$ cation will give any significant contribution to the final absorption spectra of chemically reduced complexes. The absorption spectra of the singly and doubly reduced anions of both dicyano complexes are shown in Figure 3.8 and 3.10 respectively. These species were also protonated by addition of one or two equivalents of trifluoroacetic acid (TFA).

The absorption spectra of complex $[Ru(phen)_2(dppz\text{-}o\text{-}CN)]^{2+}$ shows an absorption band between 350 nm - 460 nm, which is characteristic of the d-π* transition between Ru(II)-dppz species. It is well known the MLCT process occurs between the Ru(II) metal and the LUMO+1 orbital which is centralized around the phen portion of the dppz ligand, and for this reason it is commonly referred to as the optical orbital. The lower energy LUMO orbital is

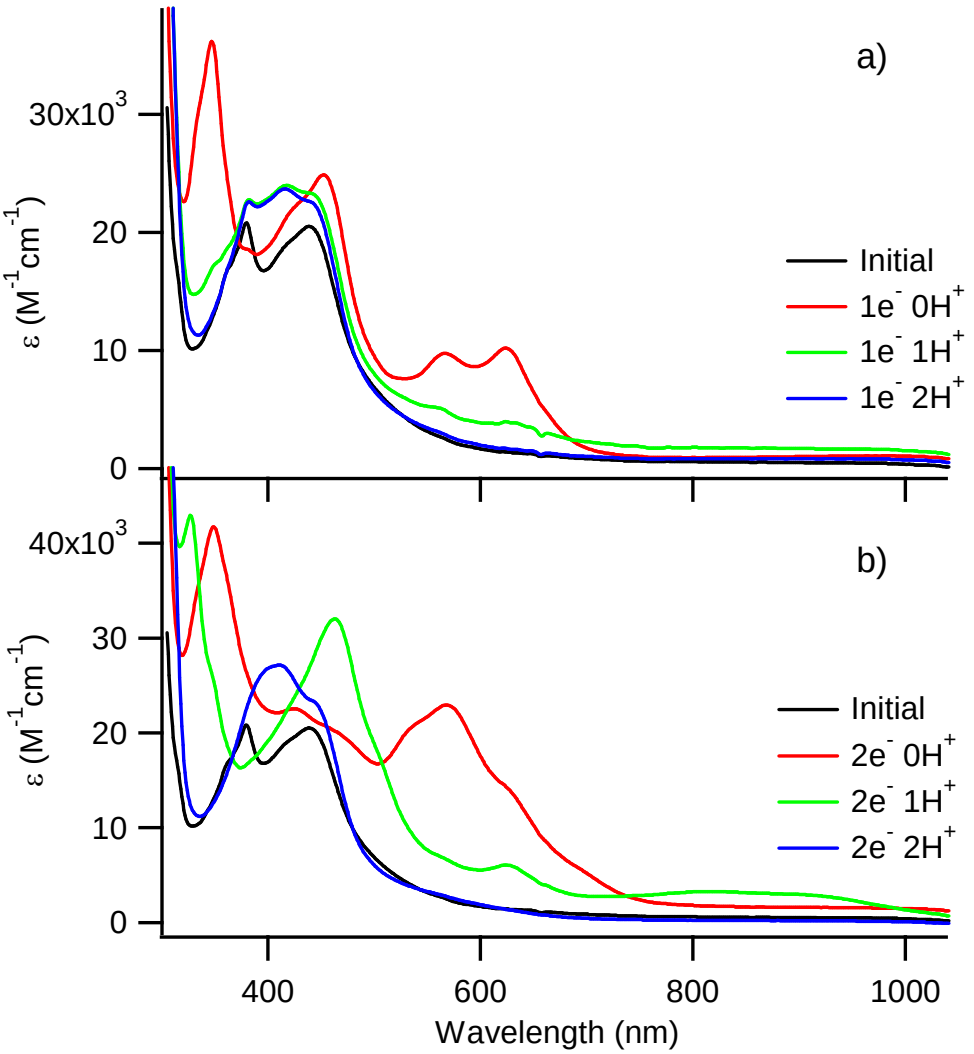

Figure 3.8: Spectral changes of $[Ru(phen)_2(dppz\text{-}o\text{-}CN)]^{2+}$ upon chemical reduction and protonations using $[((CH_3)_5Cp)_2Co]$ as the reducing agent, and trifluoroacetic acid as the proton source. All samples were prepared under N_2 atmosphere in a glove-box. a) Protonations of the singly reduced complex b) Protonations of the doubly reduced complex

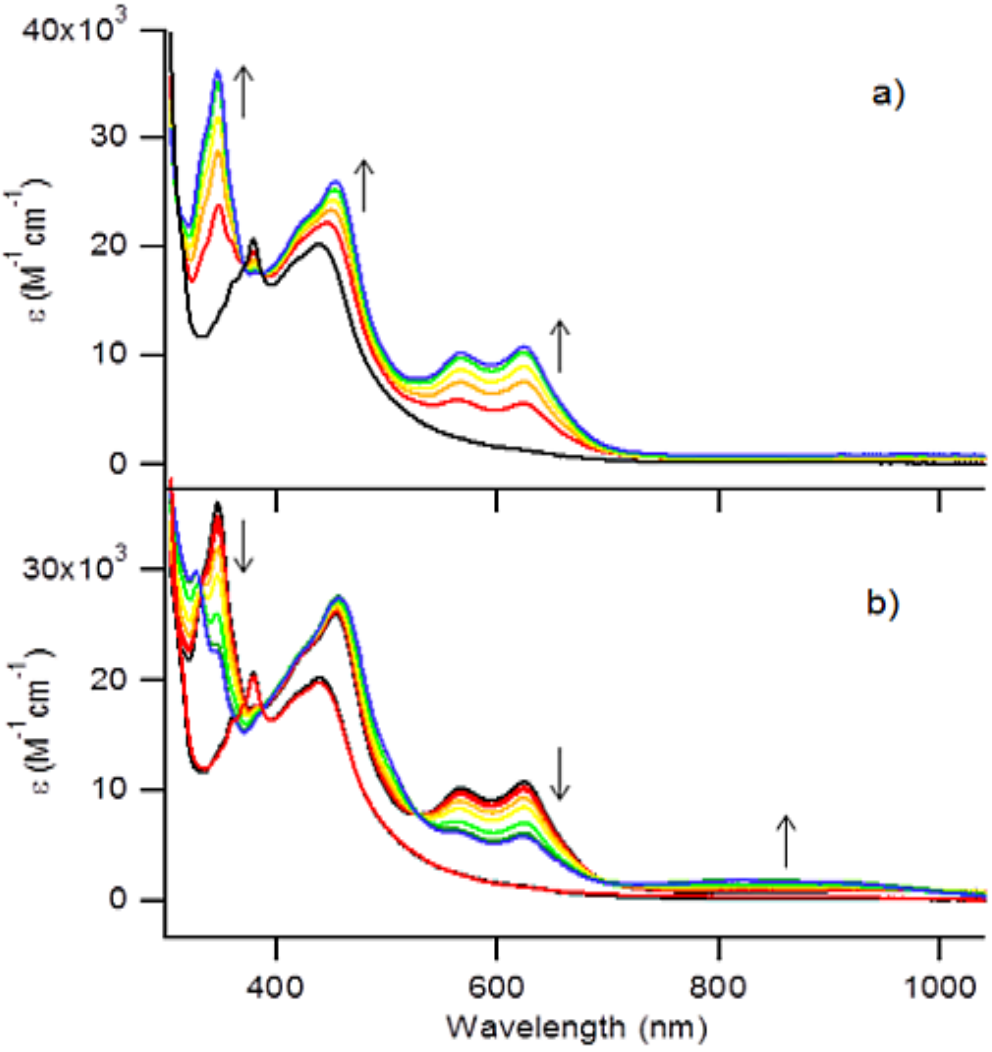

Figure 3.9: Photoreduction of $[Ru(phen)_2(dppz\text{-}o\text{-}CN)]^{2+}$ (50µM) in N_2 purged MeCN (3.0 mL ttl. volume) with TEA (0.2 M), using 470 nm light with a photon-flux of 7.313 x 10^{-07} einsteins/s. a) First observed photoprocess b) Second observed photoprocess

centralized around the phenazine portion of dppz, and commonly referred to as the redox orbital since this is the site of electron storage after reduction occurs. When one electron equivalent is added to $[Ru(phen)_2(dppz\text{-}o\text{-}CN)]^{2+}$, a new absorption band appears with maxima at 570 nm and 630 nm, along with a new absorption band at 350 nm. There is also a slight red-shift to the original MLCT band at 450 nm, which has increased absorbance. Singly protonating this anion completely bleaches the absorption spectra, leaving a structured absorption band between 380 nm - 460 nm, which is different than the absorption spectra of the starting material. The same effect is observed upon adding two proton equivalents. When two electron equivalents are added to $[Ru(phen)_2(dppz\text{-}o\text{-}CN)]^{2+}$, a new absorption band appears between 510 nm - 700 nm and 360 nm. After singly protonating the di-anion, the absorption at 360 nm shifts to 330 nm, and the absorption band at 510 nm - 700 nm is almost completely bleached, leaving new absorption bands at 470 nm and between 700 nm -1000 nm, as shown in Figure 3.8. Doubly protonating the di-anion completely bleaches the spectrum, leaving an absorption band between 350 nm - 500 nm which is different than the spectra of the starting material. Spectroelectrochemistry of $[Ru(phen)_2(dppz\text{-}o\text{-}CN)]^{2+}$ showed similar spectra as shown in Figure 3.11. When the potential was increased towards the first reduction process (-0.26 V vs. NHE in DMF), a new absorption band appears between 550 nm - 670 nm which matches the spectra observed for the chemically generated singly reduced species. No changes in the absorption spectra are observed during the second reduction process (-0.9V), which in DPV studies appeared to be a half-wave reduction process (Figure 3.7). After the potential is increased towards the third reduction process (-1.16 V), the band at 450 nm starts to decrease in absorbance, and the overall spectra begins to resemble the doubly reduced doubly protonated spectra produced by chemical methods. Further increase in potential leads to further bleaching of the absorption spectra.

The initial absorption spectra of $[Ru(phen)_2(dppz\text{-}p\text{-}CN)]^{2+}$is comparable in all aspects to the initial absorption spectra of $[Ru(phen)_2(dppz\text{-}o\text{-}CN)]^{2+}$. Adding one electron equivalent

shows a new broad absorption band between 600-900 nm and 340 nm (Figure 3.10). Addition of one proton equivalent decreases the absorption bands between 600 nm - 900 nm and 340 nm, and addition of the second proton equivalent completely bleaches the spectrum leaving an absorption band at 450 nm. Adding two electron equivalents to $[Ru(phen)_2(dppz\text{-}p\text{-}CN)]^{2+}$ results in the growth of a structured absorption band between 500 nm - 720 nm, which is strikingly different than the spectra observed for the singly reduced species. Adding one proton equivalent to this di-anion results in partial bleaching of the band between 500 nm- 720 nm and an increase in the absorbance at 450 nm. Addition of the second proton equivalent completely bleaches the spectra leaving the absorption band at 450 nm. Spectroelectrochemistry of the $[Ru(phen)_2(dppz\text{-}p\text{-}CN)]^{2+}$ complex showed similar results as shown in Figure 3.11. When the potential is increased towards the first reduction process (-0.18 V vs. NHE), the absorption band between 500 nm - 720 nm begins to appear, which matches the spectra observed for the chemically generated singly reduced species. No changes in the absorption spectra were observed when the potential is increased towards the second reduction process (-0.5 V), which in DPV studies appeared to be a half-wave reduction process (Figure 3.7). When the potential is increased towards the third reduction process (-0.84 V), the absorption band at 450 nm stays constant and a new absorption band between 500 nm - 720 nm appears, which matches the absorption spectra of the chemically generated doubly reduced species. A further increase in reduction potential leads to a further increase in the absorption between 500 nm - 720 nm and a decrease in the absorption at 450 nm.

3.3.5 Photoreduction of $[Ru(phen)_2(dppz\text{-}o\text{-}CN)]^{2+}$ and $[Ru(phen)_2(dppz\text{-}p\text{-}CN)]^{2+}$

The UV/Vis spectra obtained during photolysis of $[Ru(phen)_2(dppz\text{-}o\text{-}CN)]^{2+}$ in acetonitrile, under N_2 using TEA as the sacrificial reducing agent, are shown in Figure 3.9. Two reduction processes are observed, the first of which matches the spectrum of the singly reduced species generated by chemical methods, with absorption bands at 570 nm and 625 nm (Figure 3.8). As the photoreaction proceeds, the second reduction process begins to resemble the final

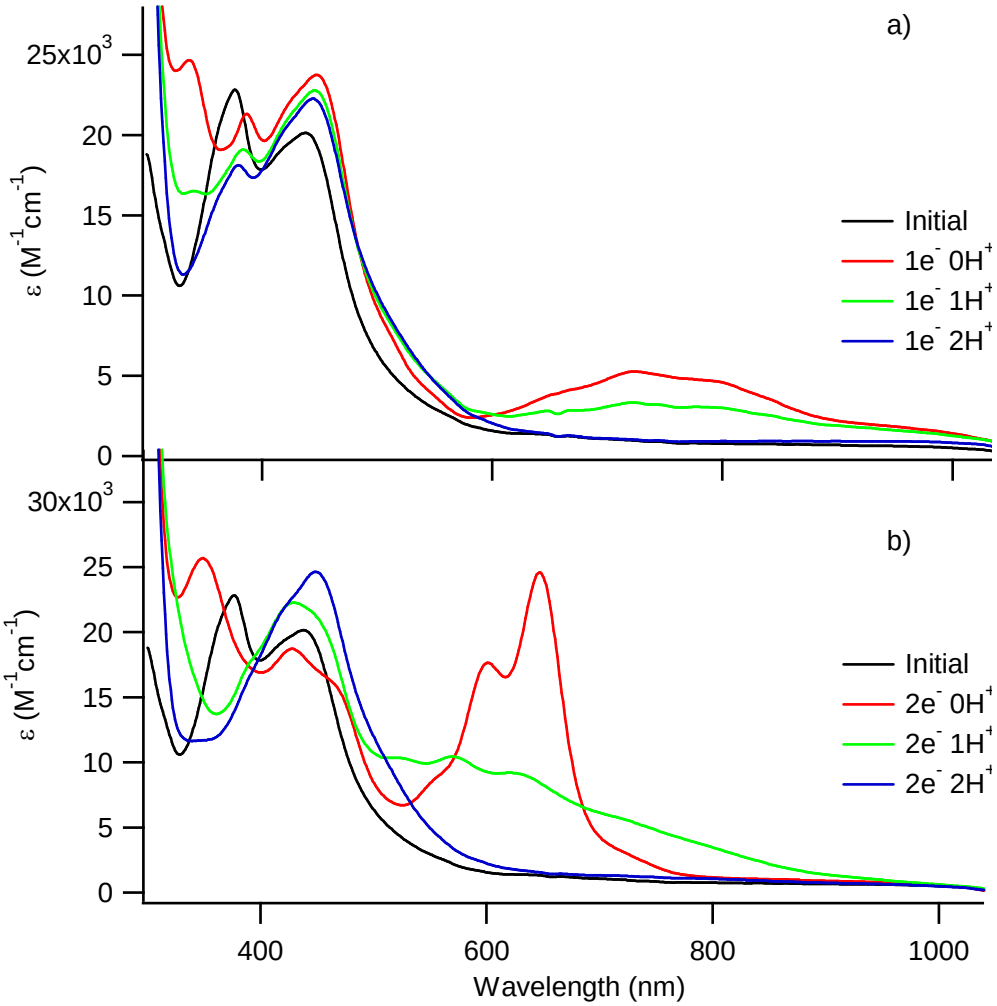

Figure 3.10: Spectral changes of $[Ru(phen)_2(dppz\text{-}p\text{-}CN)]^{2+}$ upon chemical reduction and protonations using $[((CH_3)_5Cp)_2Co]$ as the reducing agent, and trifluoroacetic acid as the proton source. All samples were prepared under N_2 atmosphere in a glove-box. a) Protonations of the singly reduced complex b) Protonations of the doubly reduced complex.

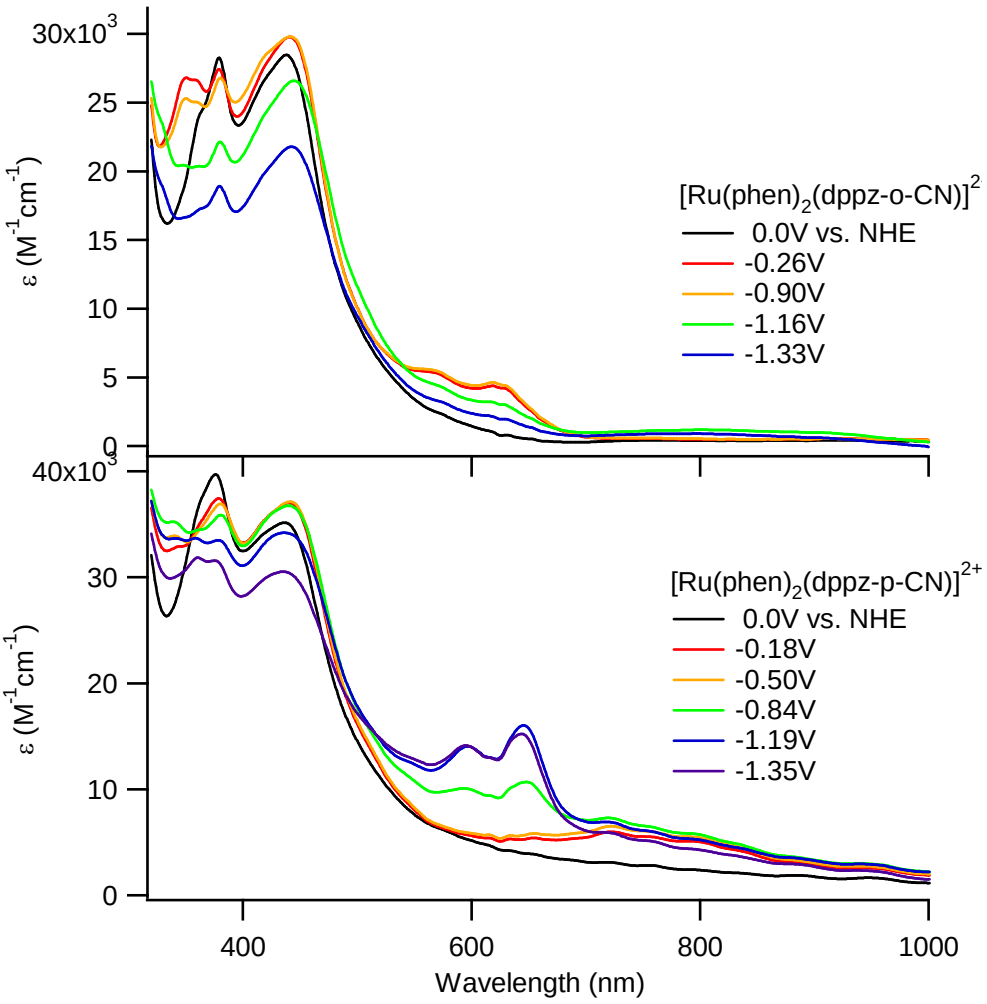

Figure 3.11: Spectroelectrochemistry of complex $[Ru(phen)_2(dppz\text{-}o\text{-}CN)]^{2+}$ (top) and $[Ru(phen)_2(dppz\text{-}p\text{-}CN)]^{2+}$ (bottom) in argon purged MeCN using Ag/Ag^+ reference electrode, Pt counter electrode, Gold mesh working electrode with $Bu^n{}_4NPF_6$ (0.1 M) supporting electrolyte. Potentials listed in the figure were referenced to CV data in DMF for clarity.

spectrum of the chemically generated doubly reduced, singly protonated species, with a broad absorption band between 700 nm - 900 nm, a decrease in absorbance at the 570 nm - 625 nm band, and a slight increase in the UV/Vis spectra obtained during photolysis of $[Ru(phen)_2(dppz\text{-}p\text{-}CN)]^{2+}$ under the same conditions as described above (Figure 3.12). During irradiation, there is observed growth in the absorption band between 700 nm - 900 nm. Further irradiation leads to an increase in absorption at 650 nm but the absorption intensity between 800 nm -1000 nm stays relatively constant. The final absorption spectra appears to resemble the doubly reduced, singly protonated spectrum generated by chemical methods (Figure 10).

3.4 Discussion

MO calculations predict the first reduction potential of the $[Ru(phen)_2dppz]^{2+}$ complex shifts to more positive potentials with increasing withdrawing group strength, and a slightly larger shift to more positive potentials upon substituting in the 10,13 position, as compared to the 11,12 position (Figure 3.4). Experimentally, CV scans for both $[Ru(phen)_2dppzBr_2]^{2+}$ and $[Ru(phen)_2dppzCN_2]^{2+}$ isomers agree with these predictions. Table 3.1 clearly shows a trend in the first reduction potential of each complex, where the potential shifts to more positive values in the order of increasing withdrawing group strength, and a slight shift to more positive potentials upon changing substitution from the 11,12 position to the 10,13 position respectively.

Further reductions in both dibromo dppz complexes closely resemble the previously reported potentials for $[Ru(bpy)_2dppz]^{2+}$ and $[Ru(phen)_2dppz]^{2+}$ complexes, and can be attributed to reduction of the exterior phen co-ligands.[18] Although the withdrawing group effect does lower the first reduction potential in these complexes, no further reductions to the dppz ligand are observed prior to reduction of the metal bound phen ligands.

The post-primary reduction processes for both dicyano dppz complexes are much more interesting. DPV scans for $[Ru(phen)_2(dppz\text{-}o\text{-}CN)]^{2+}$ and $[Ru(phen)_2(dppz\text{-}p\text{-}CN)]^{2+}$ show the first one-electron reduction process occurs at -0.26 V and -0.18 V vs. NHE respectively, which can attributed to formation of the singly reduced $[Ru(phen)_2(dppzCN_2^{\bullet -})]^{+}$ or $[Ru(phen)_2(dppz\text{-}o\text{-}$

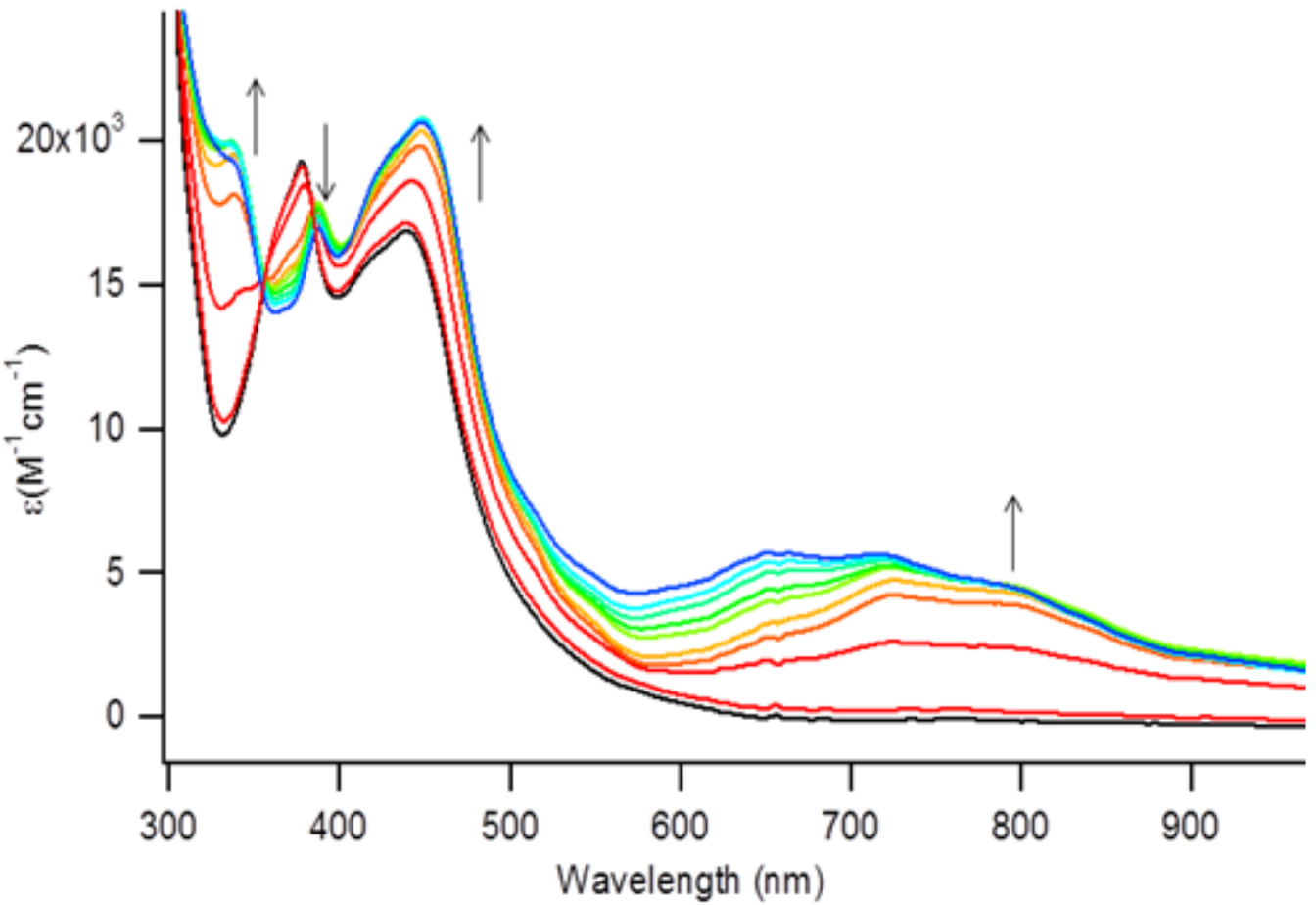

Figure 3.12: Photoreduction of $[Ru(phen)_2(dppz\text{-}p\text{-}CN)]^{2+}$ (50 µM) in N_2 purged MeCN (3.0 mL total volume) with TEA (0.2 M), using 470 nm light with a photon-flux of 7.313 x 10^{-07} einsteins/s.

$CN^{\bullet-}$)]$^{+}$ and [Ru(phen)$_2$(dppz-p-$CN^{\bullet-}$)]$^{+}$ in both cases. Figure 3.7 shows the second reduction process for both dicyano dppz complexes appear to be half-reductions, which occur at -0.9 V and -0.5 V vs. NHE respectively. UV/Vis spectra obtained by spectroelectrochemistry show minima to no change at these potentials for both isomers, suggesting an electrochemical process occurs which is not distinguishable by UV/Vis. One explanation for the observation of the half-wave reduction, is singly reduced polyaromatic heterocycles are known to form π-π stacked dimers to stabilize the radical species.[27] Once this dimer species forms, it is possible the half-wave reduction processes represents separation of the singly reduced dimer into two mono-reduced anions which is similar to the reduction processes described for [Ru(phen)$_2$(tatpp$^{\bullet-}$)]$^{+}$.[26] Since the spectra for both [Ru(phen)$_2$(dppzCN$^{\bullet-}$)]$^{+}$ isomers qualitatively do not change, it is likely a stacking phenomena occurs. After the half-reduction process, the third and fourth reduction processes of [Ru(phen)$_2$(dppz-o-CN)]$^{2+}$ occurring at -1.16 V and -1.33 V vs. NHE, closely resemble the second and third reduction potentials for [Ru(phen)$_2$(dppz)]$^{2+}$, and can be attributed to reduction of the metal bound phen ligands. The UV/Vis spectra obtained at these potentials show absorption at 450 nm decreases. This absorption band is known represents the Ru-phen MLCT transition, and a decrease in absorption at these potentials signifies reduction of the phen ligands.[18]

In complex [Ru(phen)$_2$(dppz-p-CN)]$^{2+}$, after the half-reduction process occurs, a new reduction process is observed to occur (-0.84 V) prior to the reduction of the metal bound phen ligand (-1.19 V). This process shows distinct changes in the absorbtion spectrum shown in Figure 3.11. New absorption bands at 600 nm and 650 nm appear, but no changes are observed in the absorption at 450 nm. Only after increasing the reduction potential to reach the fourth and fifth reduction processes does the absorption band at 450 nm start to decrease, which is similar to the results observed for complex [Ru(phen)$_2$(dppz-o-CN)]$^{2+}$ during reduction of the exterior metal bound phen co-ligands. From these observations it can be concluded that the species formed during this process is not the [Ru(phen)(phen$^{\bullet-}$)(dppz-p-$CN^{\bullet-}$)] species, but

rather the doubly reduced [Ru(phen)$_2$(dppz-p-CN^{2-})] species based on two observations: (i) the magnitude of the fourth and fifth reduction processes of complex [Ru(phen)$_2$(dppz-p-CN)]$^{2+}$ closely match the second and third reduction potentials of the [Ru(bpy)$_2$dppz]$^{2+}$ and [Ru(phen)$_2$dppz]$^{2+}$ complexes, which indicates the new reduction process occurring at -0.84 V is not reduction of the exterior metal bound phen-ligands, and (ii) the absorbance at 450 nm decreases during the fourth and fifth reduction processes, but not during the third reduction process, signifying the reduction at -0.84 V vs. NHE is clearly a second sequential reduction of the dppz ligand. Using these results, it is then possible to explain the observations of the photo-reduction of both dicyano dppz complexes.

The photochemistry of [Ru(phen)$_2$(dppz-o-CN)]$^{2+}$ in dry degassed acetonitrile using TEA as a sacrificial reducing agent shows two photo-processes, the first of which resembles the chemically generated singly reduced spectra, and the second which resembles the doubly reduced singly protonated spectra. The first photo-process shows absorption bands at 570 nm and 625 nm which is characteristic of the [Ru(phen)$_2$(dppz-o-CN$^{\bullet-}$)]$^{+}$ species as determined by spectroelectrochemical and chemical reductions. During the second photo-process new absorption bands at 325 nm and 700 nm - 900 nm appear with decreasing absorbance in the 345 nm, 570 nm, 625 nm bands, with a final absorption spectra that appears to be the doubly reduced, singly protonated product. Although this data initially suggests the complex undergoes sequential multi-electron storage, two other explanations are possible. The first is the decomposition of TEA during photolysis leads to H^{+} generation, which may lead to the formation of the protonated radical, H[Ru(phen)$_2$(dppz-o-CN$^{\bullet}$)]$^{2+}$. If this species forms, it is possible for disproportionation to occur to form the doubly reduced H$_2$[Ru(phen)$_2$(dppz-o-CN)]$^{2+}$ species which can then de-protonate to form H[Ru(phen)$_2$(dppz-o-CN^{-})]$^{+}$. This disproportionation process has been commonly observed for other systems during protonation of a singly reduced polyaromatic heterocycle.[2,25] The second explanation is [Ru(phen)$_2$(dppz-o-CN$^{\bullet-}$)]$^{+}$ can form π-π stacked dimers, which in conjunction with H^{+} generation may give an optical absorption

spectra which resembles the doubly reduced singly protonated species. Due to the unavoidable decomposition of TEA and subsequent generation of H^+, it is difficult to determine by what process the final photoproduct forms. Further experimentation is needed to address these issues.

Photolysis of $[Ru(phen)_2(dppz\text{-}p\text{-}CN)]^{2+}$ in dry degassed acetonitrile using TEA as a sacrificial reducing agent also shows two photo-processes occur. The first photo-process shows a broad absorption band between 600 nm - 850 nm characteristic of formation of the $[Ru(phen)_2(dppz\text{-}o\text{-}CN^{\bullet -})]^+$ species. As the photoreaction proceeds the final spectra closely matches the UV/Vis spectra of the chemically generated doubly reduced singly-protonated spectra shown in Figure 3.8. Since a new reduction potential is observed at -0.84 V vs. NHE, which is lower than the potential for the first reduction of the metal bound phen ligand (-1.19 V vs. NHE), it is likely a second electron is photochemically stored in the acceptor ligand. Unfortunately, similar arguments to those previously described for the second photo-process in the photoreduction of $[Ru(phen)_2(dppz\text{-}o\text{-}CN)]^{2+}$ are applicable here. Since sequential multi-electron storage, disproportionation, or π-π stacked anion dimers are all reasonable explanations for the final spectra of the photo-product appearing to be the doubly reduced singly protonated species, no direct conclusion of the species generated during this photo-process can be made. Further experiments are needed to address this issue.

3.5 Conclusion

To conclude, various $[Ru(phen)_2dppzX_2]^{2+}$ analogues have been synthesized and studied using electrochemical and photochemical techniques. DFT predictions were confirmed by the experimental results, and show substitution in the 10,13-position has a slight increase in stabilization of the phz orbital compared to substituting in the 11,12-position. We have also shown that use of strong withdrawing groups stabilize the phz orbital on the dppz ligand, allows a new one-electron process to occur electrochemically, which is presumably the formation of a doubly reduced $[Ru(phen)_2(dppz\text{-}p\text{-}CN)]^{2-}$ species. Formation of this species has shown it is

possible to tune the orbital energy of a single-electron storage system to allow a multi-electron process at high reduction potentials.

CHAPTER 4

SYNTHESIS AND CHARACTERIZATION OF A DIMERIC TETRAAZATETRAPYRIDOPENTACENE LIGAND AND THE CORRESPONDING TETRA-RUTHANATED COMPLEX

4.1 Abstract

A low-yield byproduct of the synthesis of 9,11,20,22-tetra-aza-tetrapyrido[3,2-a:2'3'-c:3'',2''-l:2''',3''']-pentacene (tatpp) ligand is the symmetrical dimer of this ligand in which a C-C bond is formed between two tatpp ligands at the 10 position. This dimer, dtatpp, is of interest as the lone pair repulsion of the adjacent aza groups should force the two tatpp π systems to be orthogonal, or nearly so, to each other. This chapter describes our characterization of this interesting compound, our efforts to improve synthetic yield of this compound, and our use of this tetra-topic chelating ligand to prepare tetranuclear ruthenium (II) complexes. Dtatpp can be prepared in 0.07% yield from benzenetetramine. The compound in much more soluble than tatpp and has been crystallized from 3:1 CH_2Cl_2/Toluene The X-ray crystal structure has been solved in space group P-1 with the an agreement factor of 0.1580 ($I>2\sigma$). The dihedral angle between tatpp units is 73.34° deg. The synthesis and characterization of the tetranuclear ruthenium complex, $[((phen)_2Ru)_4(dtatpp)]^{8+}$ (Ru_4), is also reported.

4.2 Introduction

Stable bi-radical systems are of interest to the scientific community due to the interesting physical properties which they hold, one of which is the possibility of storing two or more radicals on the same molecule, in separate π-systems.[86-90] In a material such as complex P, where photo-driven multi-electron storage is known to occur,[24] it is possible the sequential electron storage can be tuned in such a way, which will allow a stable bi-radical to form. For

example, if complex P was to dimerize to form two orthogonal π-systems, such as complex $[(Ru(phen)_2)_4(dtatpp)](PF_6)_8$, it would be possible to double the number of electrons which can be stored photochemically, while at the same time providing an organic framework for which spin-alignment may occur. Ideally, this molecule would exhibit some interesting paramagnetism which would be observed by storing $2e^-$ separately on the molecule, on separate tatpp orbitals. Since the synthesis of complex $[(Ru(phen)_2)_4(dtatpp)](PF_6)_8$ would be useful in increasing the capacity of photo-driven multi-electron storage, as well as provide science with a potentially photoactive and stable bi-radical complex, we have decided to study the synthetic routes towards the free-ligand dtatpp, and the Ru(II) complex $[(Ru(phen)_2)_4(dtatpp)](PF_6)_8$. Herein, we report the synthesis and characterization of both the free-ligand dtatpp, and complex $[(Ru(phen)_2)_4(dtatpp)](PF_6)_8$, using various analytical techniques such as NMR, X-ray Crystallography, MALDI, and ESI-MS. We have also included a discussion on an alternative synthetic pathway towards gram-scale synthesis of the dtatpp dimer, for future synthesis of the material in larger quantities.

4.3 Experimental

4.3.1 Materials

Benzenetetraamine tetrahydrochloride (BTA) (Sigma Aldrich, CAS: 4506-66-5) was purified according to literature procedures.[30] 2.0 g of BTA was dissolved in 5.0 mL $HCl_{(conc)}$ and 50 mL D.I. water. Activated Carbon (1.4g) is added in one portion to the stirred suspension, heated until reflux, then filtered hot over a bed of celite. The filtrate is immediately placed in an ice bath and purged with N_2 and 25 mL $HCl_{(conc)}$ is added to the filtrate. A white precipitate forms, which was filtered and washed with acetone (15 mL) then ether (15 mL). After drying by vacuum filtration for 1 hr, the solid is immediately used for synthesis. Phendione was synthesized and purified according to literature procedures.[24,91] All reactions were performed under aerobic conditions unless otherwise specified. All solvents were used without further purification.

4.3.2 Synthesis of dtatpp

2.0 g of recrystallized BTA was added to a 200 mL round bottom flask with 4.5 g phendione (21.4 mmol), and 100-150 mL of dry ethanol. This solution was refluxed under N_2 for 6 days. The slurry was filtered using a fritted funnel with medium porosity, and the filter cake was washed with hot ethanol until no color eluted from solvent washings. The filter cake was then washed with 100 mL Acetone and dried in a vacuo at 50°C for 24 hr. The filtrate and washings containing the dtatpp were set aside for later use.

1 g of the dry filter cake was added to a large 500 mL beaker, and 8-10 g of $Zn(BF_4)_2 \bullet H_2O$ was added to the solid. Both solids were mulled together using a glass rod. 300 mL MeCN was added to the beaker and the solution was heated until reflux. In order to aid solubility of the Zn(II) ion, 1-5 mL of H_2O was added during heating. When the solution is mostly homogeneous, it is filtered hot, and the filtrate placed in a separatory funnel. NaOH 10 M (75 mL), was carefully added to the separatory funnel, and vigorously shaken. A solid precipitates and was filtered onto a fritted funnel with medium porosity, then washed with copious amounts of hot water. The filter cake was dried in a vacuo at 50°C for 24 hr .

The dry filter cake is then crushed into a powder and washed with hot ethanol (3 x 100 mL), and a 1:1 mixture of dichloromethane/chloroform (3 x 100 mL). These washings were placed in a rotovap flask and combined with the filtrate obtained after filtering the cooled reflux solution. The solvent was removed under reduced pressure, and the solids obtained were dissolved in minimal ethanol (5 mL). Excess acetone (100 mL) was then slowly added to precipitate a brown solid. The slurry was then filtered, and the filter cake was dried in a vacuo at 50°C for 24 hr. The dry solid was then re-dissolve d in a minimal amount of dichloromethane (5 mL). The concentrated solution was filtered, and the filter cake was washed with DCM (2 x 5 mL). The filtrate and washings were combined, then carefully concentrated to a minimum volume (1-2 mL) under reduced pressure. A dark red solid precipitates, and was filtered using a 0.2 µm nylon membrane. The filter cake was washed with 10 mL 90:10 acetone/ethanol, then

dried in a vacuo at 50° C for 24 hr to yield dtatpp 55 mg (0.73% yield) (MW = 970 g/mol). MALDI-TOF: $[(M + 2 Na^+)]^+$: calc: 1016.9 m/z, found: 1017.6 m/z. ^{1}H NMR (500 MHz, $CDCl_3$-*d_1*): δ = 9.95 (s, 2 H), 9.87 (d, J = 9.6, 4 H), 9.26 (d, J = 6.2 Hz, 4 H), 8.93 (d, J = 6.5 Hz, 4 H), 8.21 (d, J = 9.6 Hz, 4 H), 7.89 (dd, J = 12.7 Hz and 3.8 Hz, 4 H), 7.17 (dd, J = 12.7 Hz and 3.4 Hz, 4H) ppm.

4.3.3 Synthesis of $[(Ru(phen)_2)_4(dtatpp)](PF_6)_8$

90.0 mg of dtatpp (92.8 µmol) was added to freshly prepared $[Ru(phen)_2]Cl_2$ 230 mg (432 mmol) [73] in 100 mL of EtOH under N_2, and refluxed for 48 hours. The solution was cooled, filtered with a nylon 0.2 µM membrane, and 100 mL H_2O was added to the filtrate. NH_4PF_6 was added in excess to precipitate a nearly black solid which was filtered with a 0.2 µM membrane and dried in a vacuo at 50 ℃ for 24 hr. The produc t was purified by dissolving in acetone (20 mL), and adding tetrabutylammonium chloride (Bu^n_4NCl) 450 mg (1.62 mmol) to precipitate a solid which was filtered and dried in a vacuo at 50 ℃ for 24 hr. The nearly black solid was dissolved in 20 mL D.I. H_2O, filtered, and NH_4PF_6 265 mg (1.62 mmol) was added in one portion to precipitate a solid which was filtered and dried in a vacuo at 50 ℃ for 24 hr. This process was repeated two more times to afford $[(Ru(phen)_2)_4(dtatpp)](PF_6)_8$ 325 mg (86 % yield) (MW = 3976.76 g/mol) ESI-MS: $(M - 3 PF_6)^{3+}$, $(M - 4 PF_6)^{4+}$, $(M - 5 PF_6)^{5+}$, $(M - 6 PF_6)^{6+}$, $(M - 7 PF_6)^{7+}$, $(M - 8 PF_6)^{8+}$ calc: 1181.67, 850.07, 651.73, 518.47, 423.73 m/z found: 1181.67, 850.07, 651.73, 518.47, 423.73, 352.67 m/z. ^{1}HNMR (500 MHz, MeCN-*d_3*): δ = 10.07 (s, 2 H), 9.75-9.67 (m, 5 H), 8.6-7.08 (m, 134 H) ppm

4.3.4 X-ray Crystallography

Crystals of dtatpp were grown by layering toluene on CH_2Cl_2, and crystals grew at the interface of the solvent layers. The solvent system was highly volatile therefore the crystals were acutely air-sensitive. Crystals began to desolvate only seconds after removing from the mother liquor and mounting of the crystals needed to be done hastily. Crystals were drawn out of their vials using a pipette, and placed onto a glass slide that had previously been stored in a

freezer. The crystals themselves were visibly twinned, however time did not allow proper removal of twinned crystals by cutting. A large twinned crystal was mounted onto the x-ray machine equipped with cold nitrogen flow to stabilize the crystals. A unit cell determination expectedly failed because of the twinning problem, however the data was detwinned using the software Cell_Now provided by Bruker-AXS.[92] A reasonable cell was selected by calculating the volume of the putative structure and data was collected for a period of 18 hours. The completed data set was processed using the SAINT (version 6.45) and TWINABS software provided by Bruker-AXS. [92] An hklf4 and hklf5 reflection file was generated and the hklf4 file was used to solve the structure. Later, towards the end of the refinement, the hklf5 reflection file was used to finalize the refinement.

The main molecule showed no visible signs of disorder and refined well with good anisotropic parameters. Several solvent molecules appeared in the unit cell and were badly disorded. The solvent molecules were treated with a combination of restraints that fixed the distances, angles, and anisotropic parameters of the solvent molecules. Interestingly, packing diagrams showed that the main molecule forms a channel when packed together and the channel space is nicely occupied by the solvent molecules. Full crystallographic details and tables containing bond distances and angles are located in Appendix B.

4.4 Results

The NMR of tatpp is shown in Figure 4.1, and is identical to the spectra reported in literature.[24] The spectra obtained for dtatpp is shown in Figure 4.2. The noticeable difference between the tatpp monomer and dimer are splitting of the H_a, H_b, and H_c peaks into two separate sets of peaks. The inner $H_{a'}$, $H_{b'}$, and $H_{c'}$ peaks of the dtatpp dimer are positioned directly in front of the orthogonal π-systems, which causes a shielding effect that shifts the protons with respect to the outer H_a, H_b, and H_c signals. Integration of each peak is 1:1, with the exception of the singlet proton H_d, which integrates 2:1. A crystal of the free ligand was grown by dissolving dtatpp in CH_2Cl_2, and carefully layering toluene above the CH_2Cl_2 phase. Due to

the difficulty of crystallization by this method, it was necessary to set up a 96-well plate with varying ratios of CH_2Cl_2 to toluene. A suitable crystal was obtained from a 3:1 CH_2Cl_2/toluene ratio, and X-Ray crystallography was used to determine the structure (Figure 4.3). The C-C bond distance between both monomers was measured to be 1.496 Å, which is strikingly similar to the bond distance reported for an anthracene dimer.[93] The dihedral angle between the C-C bond of both monomers of dtatpp is 73.34° which dev iates from 90°, by about ± 15°, whereas the anthracene dimer is 80.54° and deviates by only ± 10°. The increased twisting of monomers is most likely due to lone pair interactions from the phenazine nitrogens. MALDI-TOF of the free ligand was also obtained, and the results are shown in Figure 4.4. The free ligand (MW = 970) appears to form sodium adducts with final m/z charges of 1017 and 1041, which represent the $[M + Na^+]^+$ and $[M + 2\ Na^+]^+$ species.

Since the crystal structure, MALDI-TOF, and NMR experiments suggest the dtatpp dimer is free of impurities, we decided to add $[Ru(phen)_2]^{2+}$ to the free ligand to form complex $[(Ru(phen)_2)_4(dtatpp)](PF_6)_8$ as described in the section 4.3.2. The NMR of the complex is shown in Figure 4.5. Compared to the dtatpp monomer in d_1-$CDCl_3$, the spectra is much more complex and difficult to assign. The only peaks which can be deciphered are the singlet (10.07 δ ppm) and multiplet (9.75-9.67 δppm) which most likely represent the H_d proton (9.95 δppm) and H_c proton (9.26 δppm) of the dtatpp monomer. The slight downfield shift of these two protons compared to the free-ligand precursor, is probably due to coordination of the Ru(II) metal. Other peaks are difficult to distinguish since the $[Ru(phen)_2]^{2+}$ fragment exists in both Δ and Λ forms. Due to multiple chiral centers being present on the ends of the $[(Ru(phen)_2)_4(dtatpp)](PF_6)_8$ complex, the overall symmetry in the molecule is broken which leads to multiple splitting of the exterior phen protons. Combined with the shielding effects of the orthogonal π-systems, the exterior phen protons can face "inner" or "outer" directions, similar to what is observed for the free-ligand dtatpp, which further complicates peak assignment. ESI-MS of the $[(Ru(phen)_2)_4(dtatpp)](PF_6)_8$ (MW = 3976.88 g/mol) complex is shown in Figure 4.6. Since

the complex exists as a 8^+ cation, with PF_6^- as the anion, several different mass peaks identify the complex. Theoretically, the calculated m/z ratios to expect are $[M - 3\ PF_6^-]^{3+}$ = m/z 1181.67, $[M - 4\ PF_6^-]^{4+}$ = m/z 850.07, $[M - 5\ PF_6^-]^{5+}$ = m/z 651.73, $[M - 6\ PF_6^-]^{6+}$ = m/z 518.47, $[M - 7\ PF_6^-]^{7+}$ = m/z 423.73, $[M -8\ PF_6^-]^{8+}$ = m/z 352.67. The observed m/z ratios are shown in Figure 4.6 and agree with the calculated values. Although other peaks are observed in the mass spectra which do not resemble the products m/z values, it is most likely due to contamination of the solvent "blank" as shown in Figure 4.7. Despite the instrumental error, most of the observed m/z signals match the calculated values, which identifies the final complex is $[(Ru(phen)_2)_4(dtatpp)](PF_6)_8$. Further work is needed to improve the overall yield of dtatpp dimer, and increasing the quality of the final complex $[(Ru(phen)_2)_4(dtatpp)](PF_6)_8$, which will be discussed in the next section.

4.5 Discussion

Since the removal of 2 e^- and 2 H^+ is necessary to form the C-C bond between both tatpp monomers, we postulate either O_2 or phendione is responsible for the oxidation of tatpp. In order to understand how the dtatpp species is produced, several reactions under varying conditions were performed as described in section 4.3.2, Table 1 summarizes the results.

Table 4.1: Study of the BTA:Phendione ratio under varying conditions

	BTA (g)	Phendione (g)	Atmosphere	K_2CO_3 (g)	Dimer Yield (mg)
1)	2.0	5.9	O_2	1.0	0.0
2)	2.0	5.9	N_2	1.0	0.0
3)	2.0	2.7	N_2	1.0	0.0
4)	3.0	8.9	N_2	0	20
5)	3.0	17	N_2	0	50

In runs 1-3, changes to the atmosphere and ratio of BTA:phendione show no improvement in the overall yield of reaction. In runs 4 and 5 however, when K_2CO_3 is not present, it is possible to isolate small quantities of dtatpp. The data also shows an increase in the ratio of phendione to BTA causes an increase in the overall yield of dtatpp. Since quinones

are known to act as mild oxidizing agents, and the presence of acid is known to enhance the oxidative capabilities of quinones, we postulate phendione undergoes a $2e^-$ reduction and protonation in the absence of K_2CO_3, to form phendiol and the dtatpp dimer. Figure 4.8 shows the possible routes by which phendione oxidizes either the starting material, intermediates, products, or a combination of all three, to form the C-C bond between dtatpp. In the first oxidative pathway, BTA is very electron-rich and it is unstable to air and heat. Although the HCl salt is what stabilizes the tetraamine towards oxidation, it is this instability that increases the driving force for electron transfer towards phendione. After the C-C bond forms, the octaamine is then able to form dtatpp by a condensation reaction with 4 eq. of phendione. In the second pathway, the intermediate dppzdiamine is less electron rich as compared to BTA, due to the extended aromatic π-system. Formation of dppzdiamine also releases HCl into the solvent environment, since the nitrogen heterocycle is less basic compared to BTA. This release of HCl enhances the oxidative potential of phendione since protonated quinones are more easily reduced compared to their unprotonated form. After an electron transfer process occurs, dppzdiamine dimerizes to form the C-C bond, which after further condensation with phendione produces dtatpp. Lastly, the third reaction pathway is the oxidative coupling of two tatpp monomers. The tatpp ligand is very stable towards oxidation, and heat; therefore oxidation of the tatpp ligand would be driven by the large excess of HCl being released into solution upon the condensation reaction between BTA and phendione. Although the reaction as written appears to be a viable pathway, it should be mentioned the solubility of tatpp is so poor that it immediately precipitates out of solution once it has been formed. The consequence of this is the oxidation of the tatpp monomer would be a heterogeneous reaction between tatpp in the solid state and the acidic phendione solution, which most likely would produce less dtatpp as compared to the first two pathways. Although these three reaction pathways have been described as homo-coupling dimerization reactions, it is also possible for C-C bond formation to occur between any of the species in solution. However the oxidative coupling occurs, what is

definite is the data collected by NMR, X-ray crystallography, and MALDI strongly support formation of the dtatpp species. Addition of 4 eq of $[Ru(phen)_2]^{2+}$, one Ru(II) for each bidentate endgroup on dtatpp, yields an ESI-MS and NMR spectra which suggests the final complex $[(Ru(phen)_2)_4(dtatpp)](PF_6)_8$ has also been made. Although the data does not definitively prove the structure of the complex, it is likely that $[(Ru(phen)_2)_4(dtatpp)](PF_6)_8$ has been synthesized since chelation of $[Ru(phen)_2]^{2+}$ to bidentate ligands such as phen, dppz, tatpp, etc. is routinely preformed with minimal side products.[18,21,24,94]

Since the synthesis of dtatpp is a by-product formed during the condensation reaction between phendione and BTA, further work is to be conducted developing a straightforward synthesis towards the final complex $[(Ru(phen)_2)_4(dtatpp)](PF_6)_8$. Figure 4.9 shows one possible route, which uses well-established organic transformations to synthesize the final product. Since the formation of **3** is known in the literature,[78] direct homo-coupling of this material would lead to the formation of a tetra-nitro, tetra-amine species which would ideally form dtatpp after a hydrogenation step, and condensation with phendione. Unfortunately, a direct homo-coupling of this material is not easily preformed due to the instability of primary amines, and the ability to chelate with metal catalysts used in homo-aryl coupling reactions. Therefore, protection of the amine groups with $SOCl_2$ would yield **4** as 5,6-dinitro-2,1,3-benzothiodiazole, which can then undergo a trivial mono-bromination with n-bromosuccinimide to form **5**. Once this material is made, there are a few ways in which a cross-coupling reaction can be preformed. Ullmann coupling reactions typically use a Cu(0) catalyst at high temperatures to form CuX_2, where X= Br^-, Cl^-, Negishi and Kumada couplings use Pd(0) catalysts with Grignard and organozinc compounds respectively, or a Suzuki coupling can be performed which couples boronic acids to aryl halides using a Pd(0) catalyst in the presence of a base.[95-98] Since Negishi coupling reactions are typically mild, catalytic, and Ni(0) can be substituted for the expensive Pd(0) metal, this method of cross-coupling would be an ideal starting point. After formation of the C-C bond to form **6** has been performed, the protecting group can be removed using $NaBH_4$ and a

cobalt catalyst to yield **7.**[81] After an initial condensation reaction with phendione, hydrogenation, and a second condensation reaction with phendione, the final dtatpp dimer would be produced.

4.6 Conclusion

Herein, we have established the synthesis and characterization of the newly formed dtatpp and $[(Ru(phen)_2)_4(dtatpp)](PF_6)_8$ species. Further experimentation is to be performed to understand the limits of multi-electron storage in these new molecules, as well as establish if any paramagnetic effects are observed upon reduction, either by chemical, electrochemical, or photochemical methods. Although the dtatpp species can be obtained in very low yield, we have discussed an alternative pathway to synthesize the target compound which should afford larger scale production of the compound.

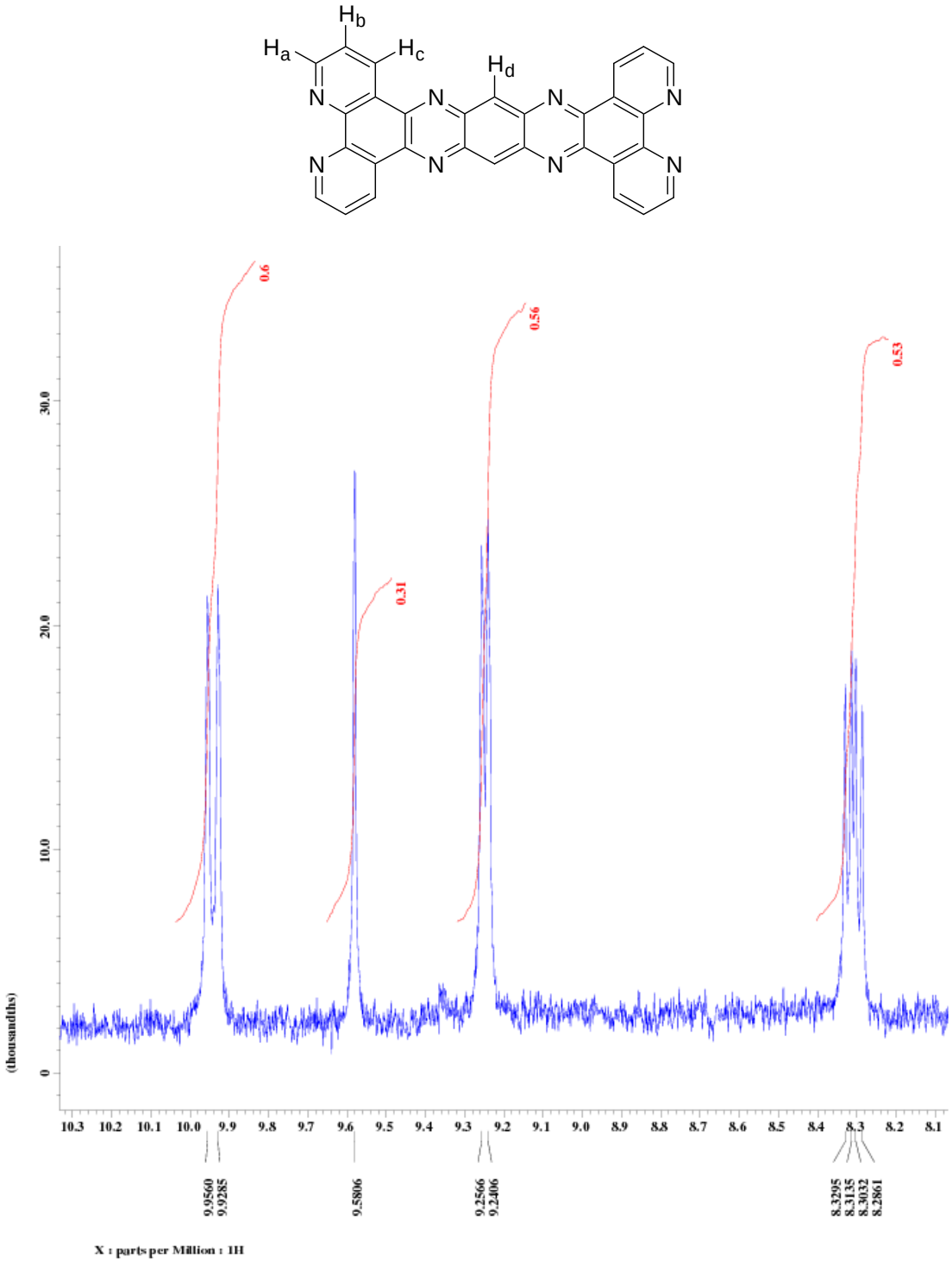

Figure 4.1: 500 MHz NMR of tatpp with $Zn(BF_4)_2$ in d_4-MeCN, where 9.95-9.92 δppm = H_c, 9.58 δppm = H_b, 9.25-9.24 δppm = H_a, and 8.33-8.29 δppm = H_d.

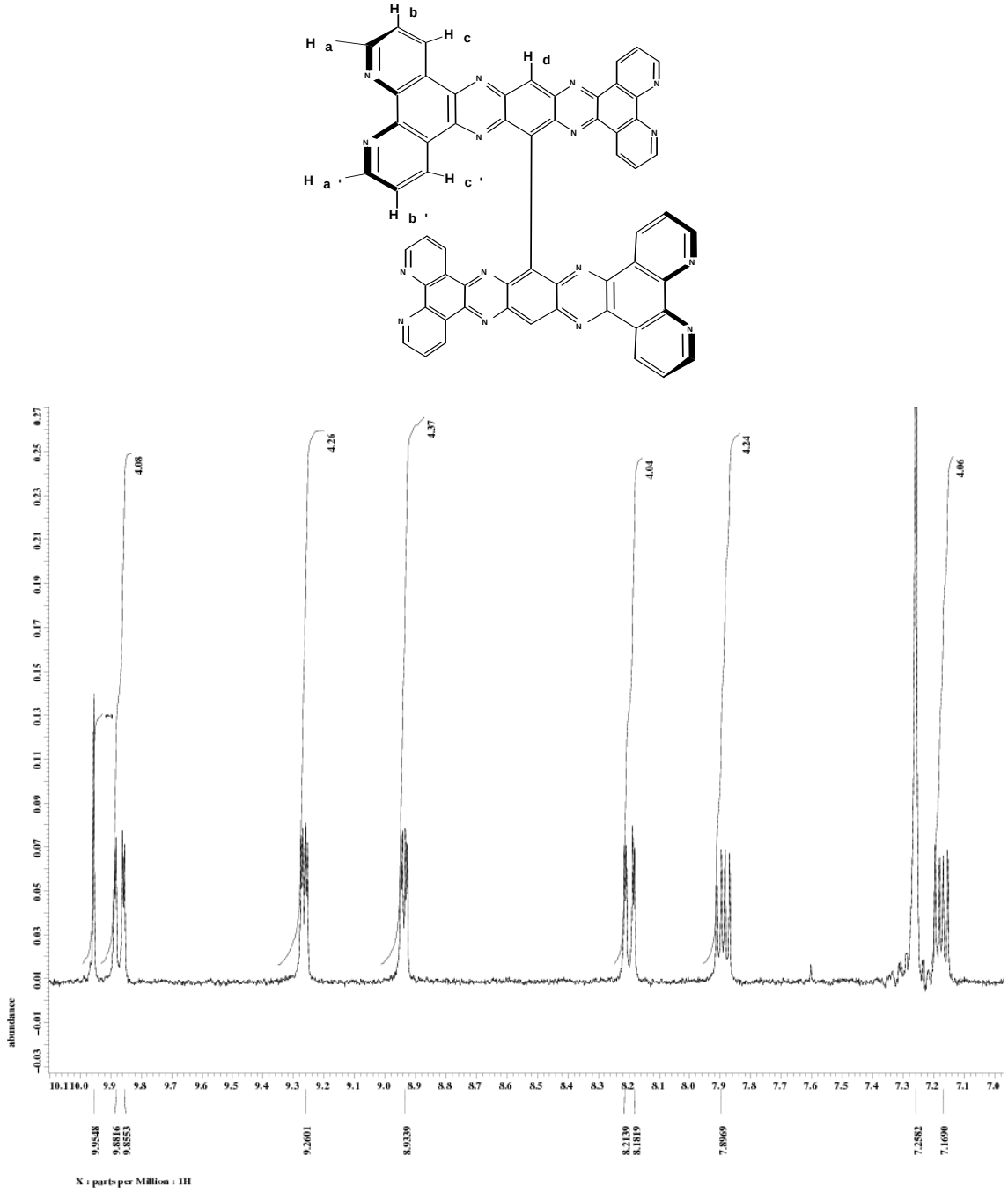

Figure 4.2: 500MHz ^{1}H-NMR of dtatpp with $Zn(BF_4)_2$ in d_1-$CDCl_3$, where 9.95 δppm = H_d, 9.88-9.85 δppm = H_c, 9.26 δppm = H_a, and 8.93 δppm = $H_{a'}$, 8.21 δppm = $H_{c'}$, 7.89 δppm = H_b, and 7.17 δppm = $H_{b'}$.

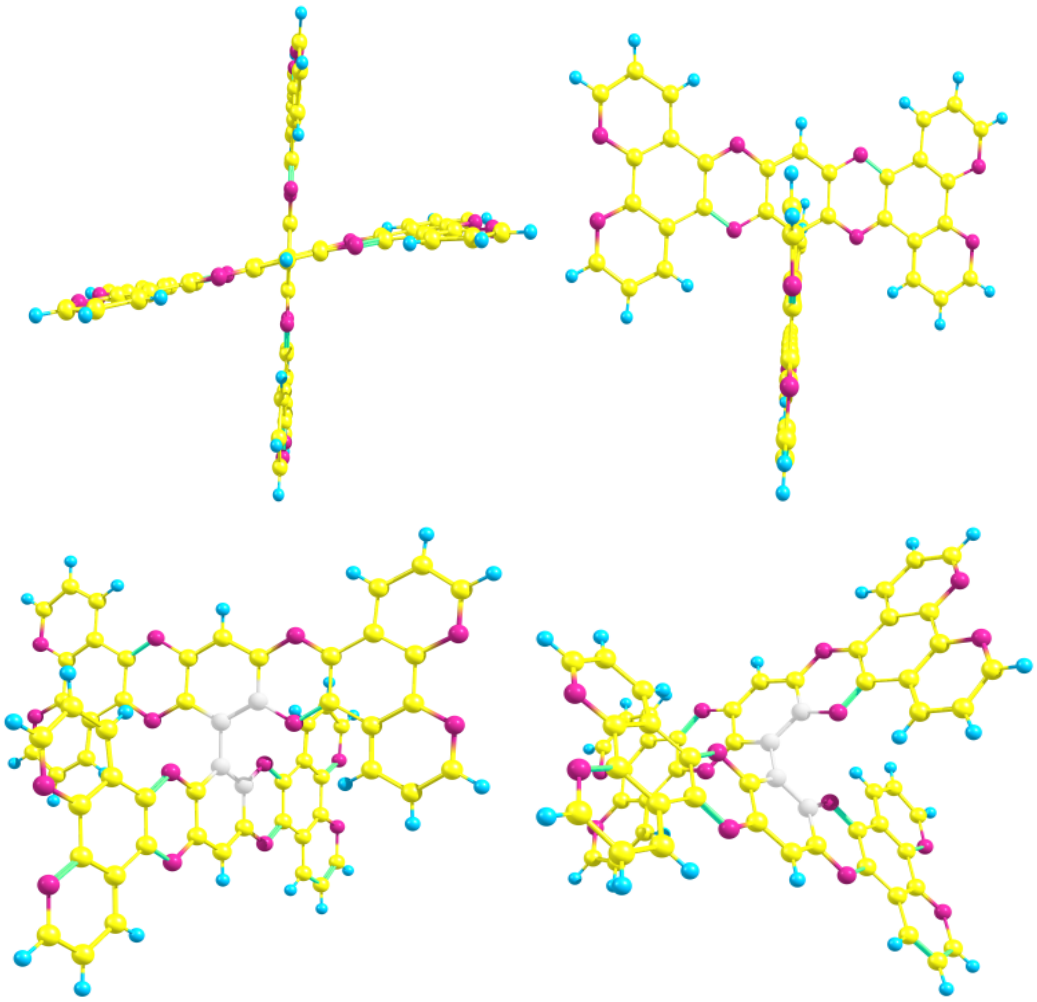

Figure 4.3: Crystal structure of dtatpp in CH_2Cl_2/toluene at varying angles. Crystals suitable for X-Ray analysis were obtained using a layering technique in a 96-well plate, with a CH_2Cl_2/toluene ratio of 3:1 yielding the best quality crystals.

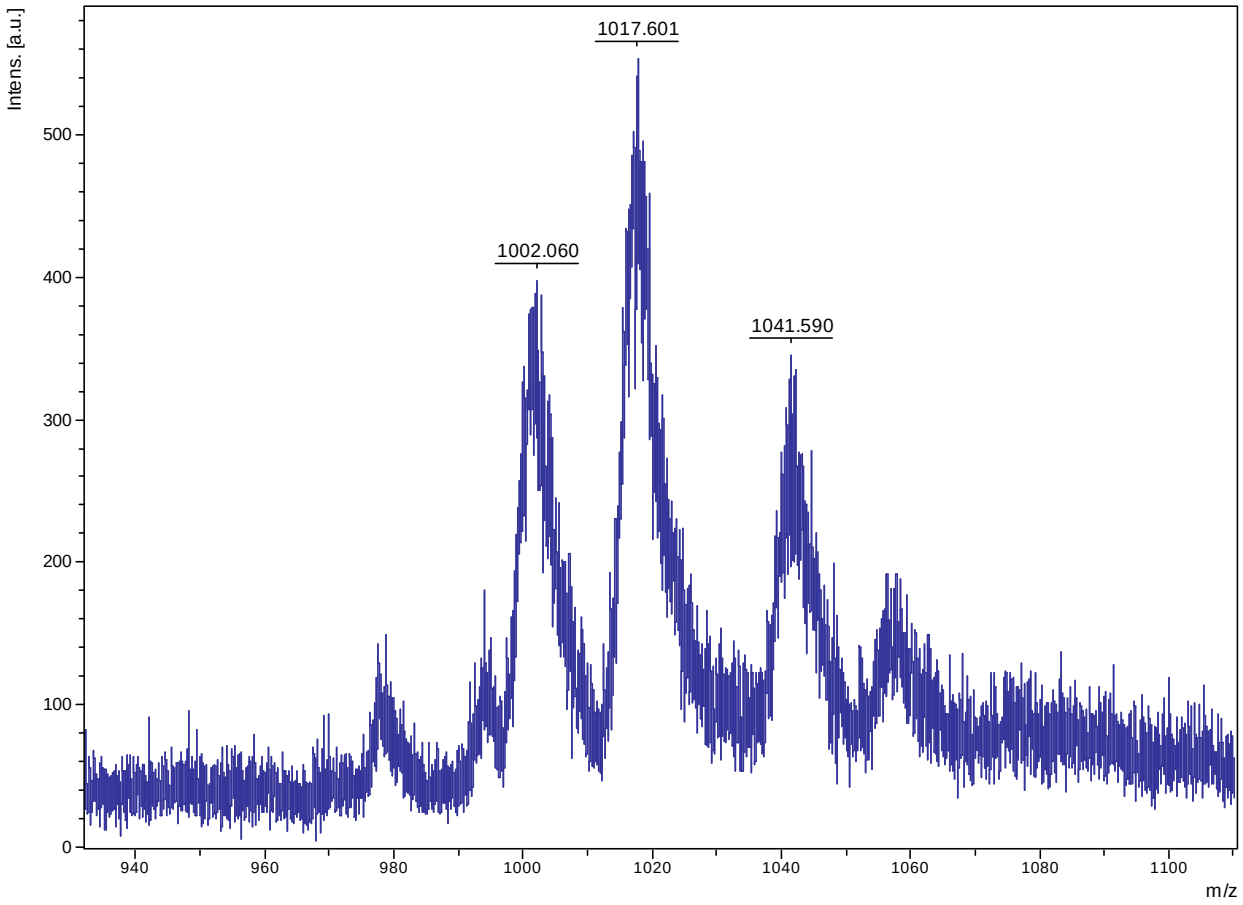

Figure 4.4: MALDI-TOF of dtatpp (MW = 970 g/mol), where the peaks observed at m/z = 1017 and 1041 are sodium adducts representing the ($M + Na^+$) and ($M + 2\ Na^+$) species.

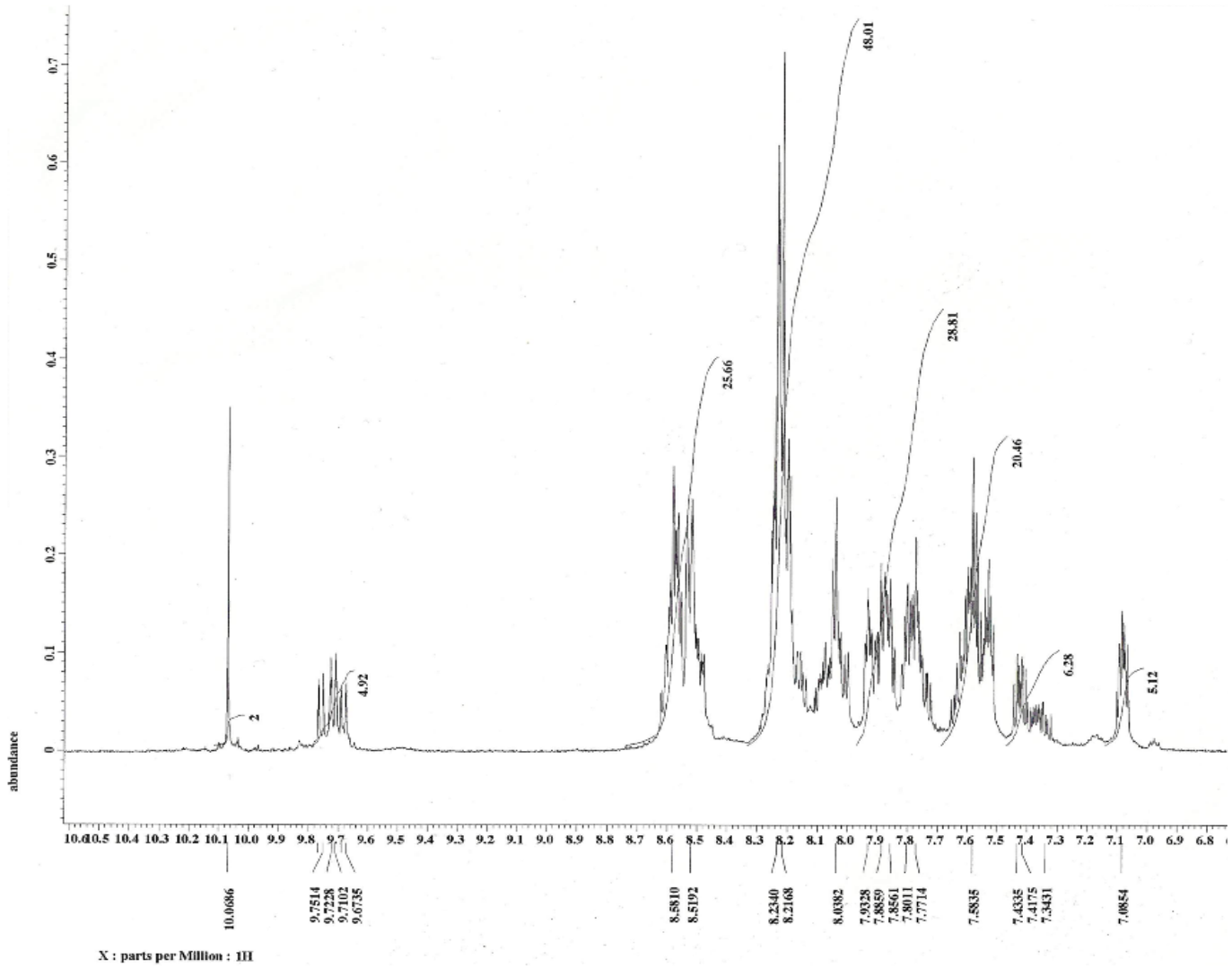

Figure 4.5: 500 MHz ^{1}H-NMR of the $[(Ru(phen)_2)_4(dtatpp)](PF_6)_8$ in d_3-MeCN.

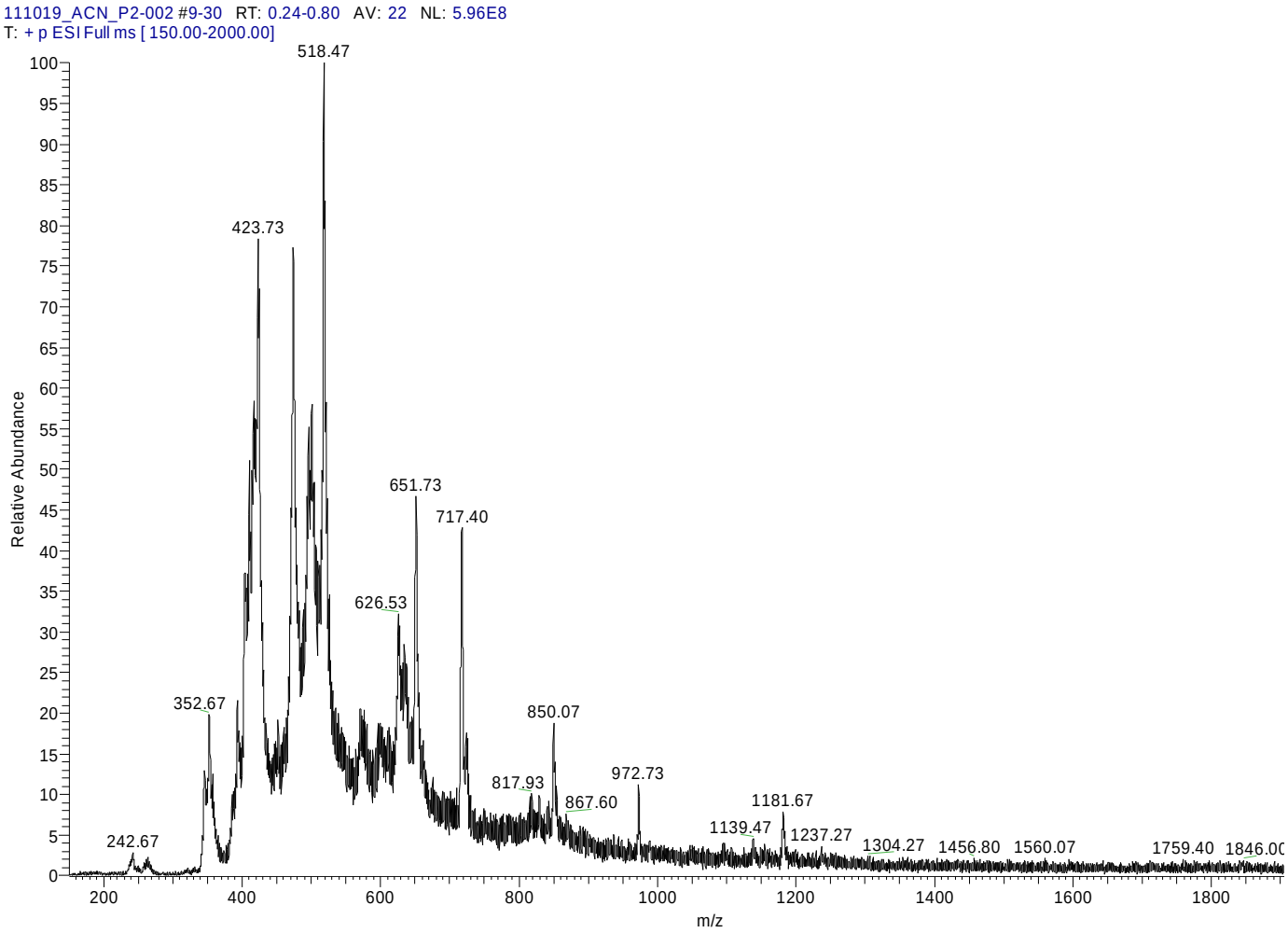

Figure 4.6: ESI-MS of the $[(Ru(phen)_2)_4(dtatpp)](PF_6)_8$ (M = 3976.88).

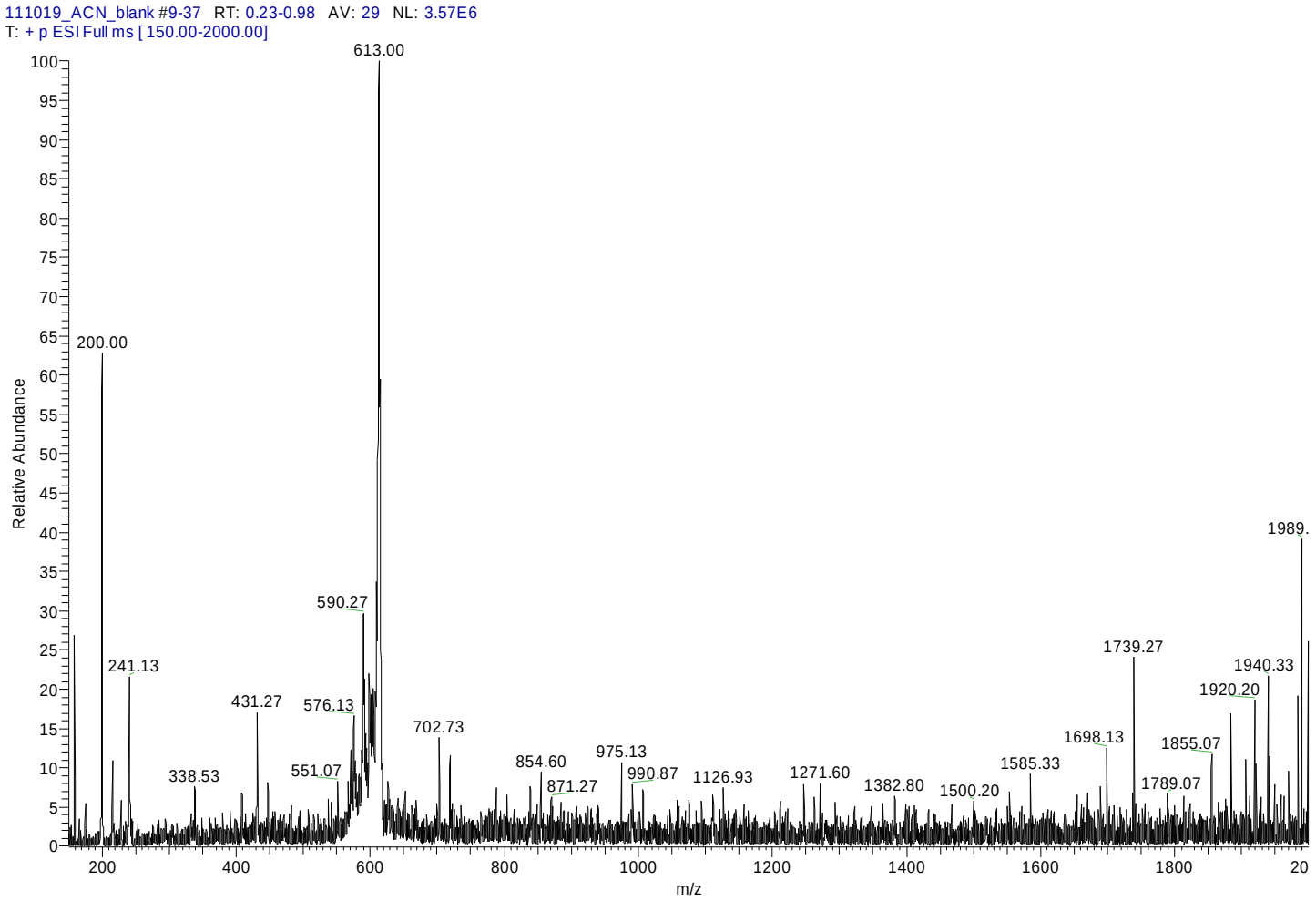

Figure 4.7: ESI-MS of MeCN blank which shows contaminations in the solvent.

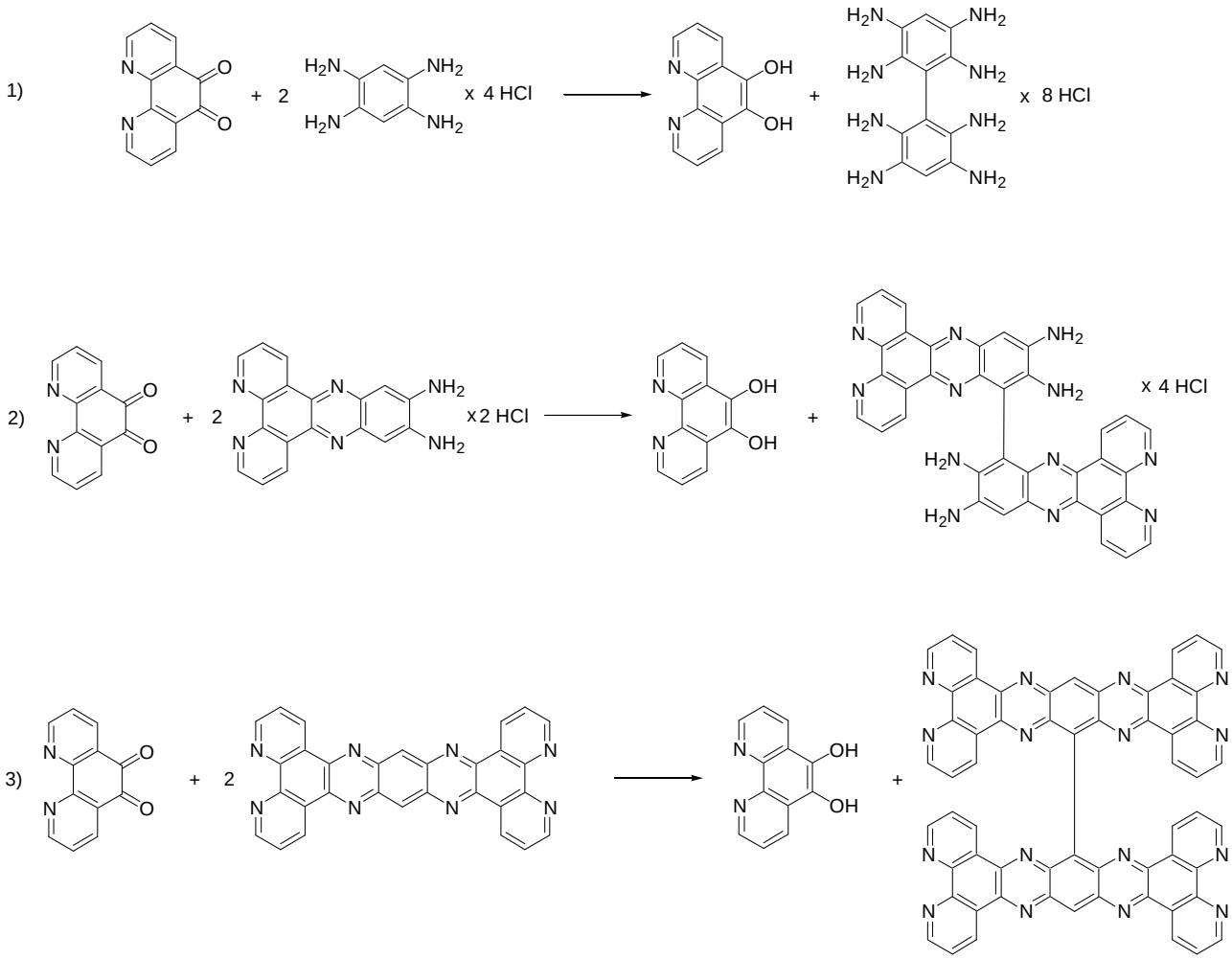

Figure 4.8: Possible pathways by which phendione abstracts 2 e^- and 2 H^+ from either starting material (1), intermediate (2), or product (3) during the condensation reaction between BTA and phendione.

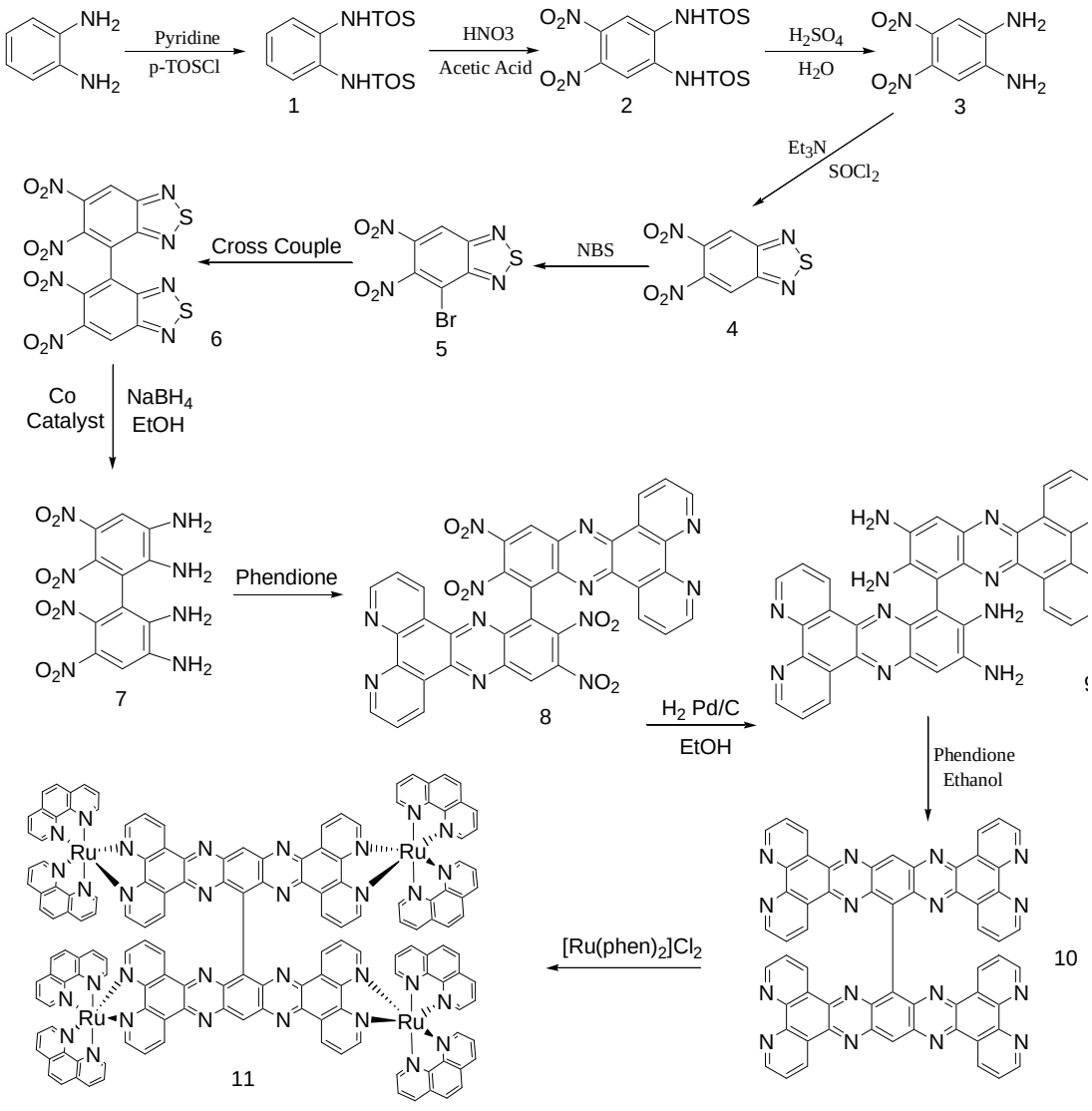

Figure 4.9: Possible synthetic route towards formation of the $[(Ru(phen)_2)_4(dtatpp)](PF_6)_8$

APPENDIX A

NMR SPECTRA OF FREE LIGANDS AND ESI-MS AND NMR SPECTRA OF RU(II) COMPLEXES

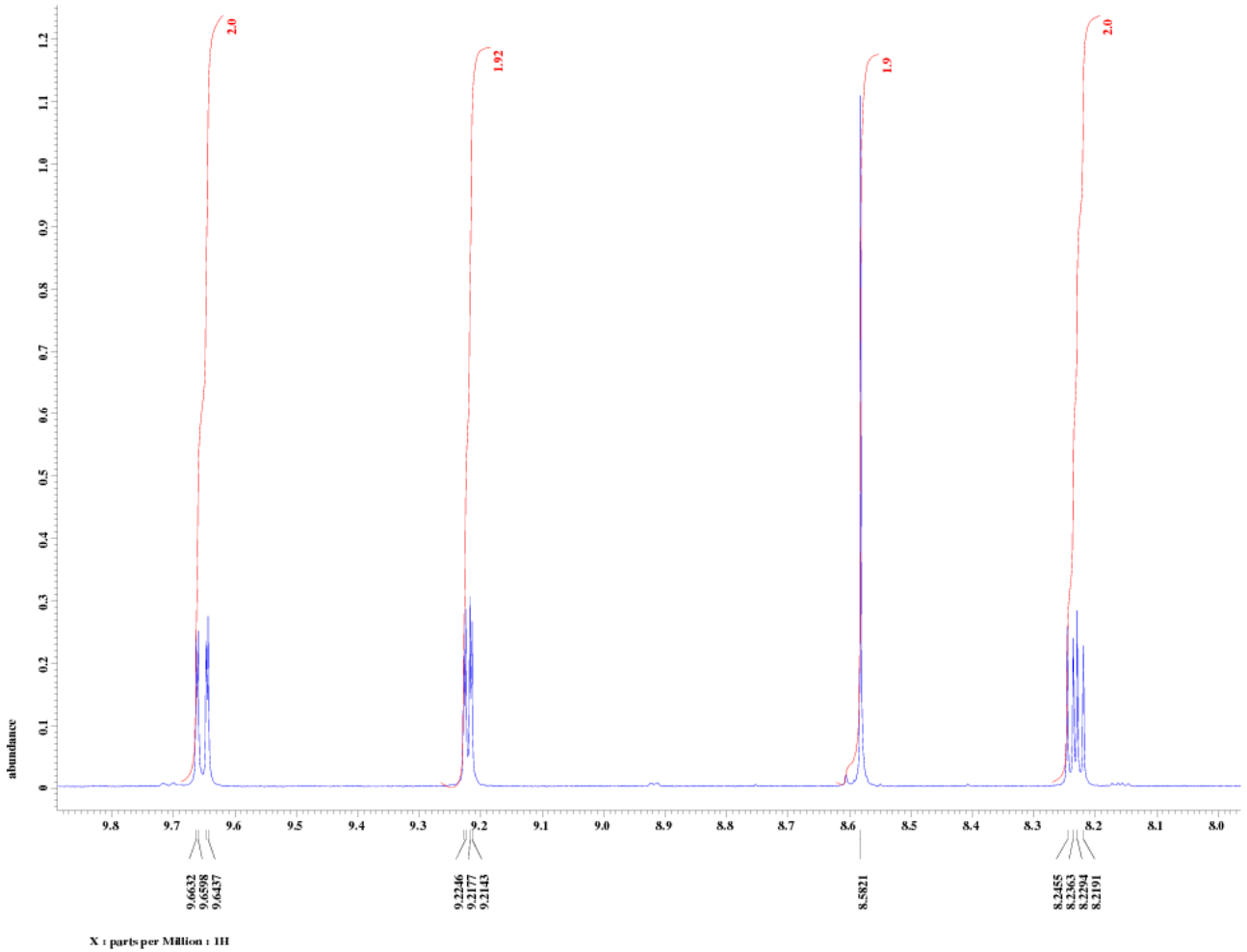

^{1}HNMR of 11,12-dibromodipyrido-[3,2-a:2',3'-c]phenazine using $Zn(BF_4)_2$ in d_3-MeCN

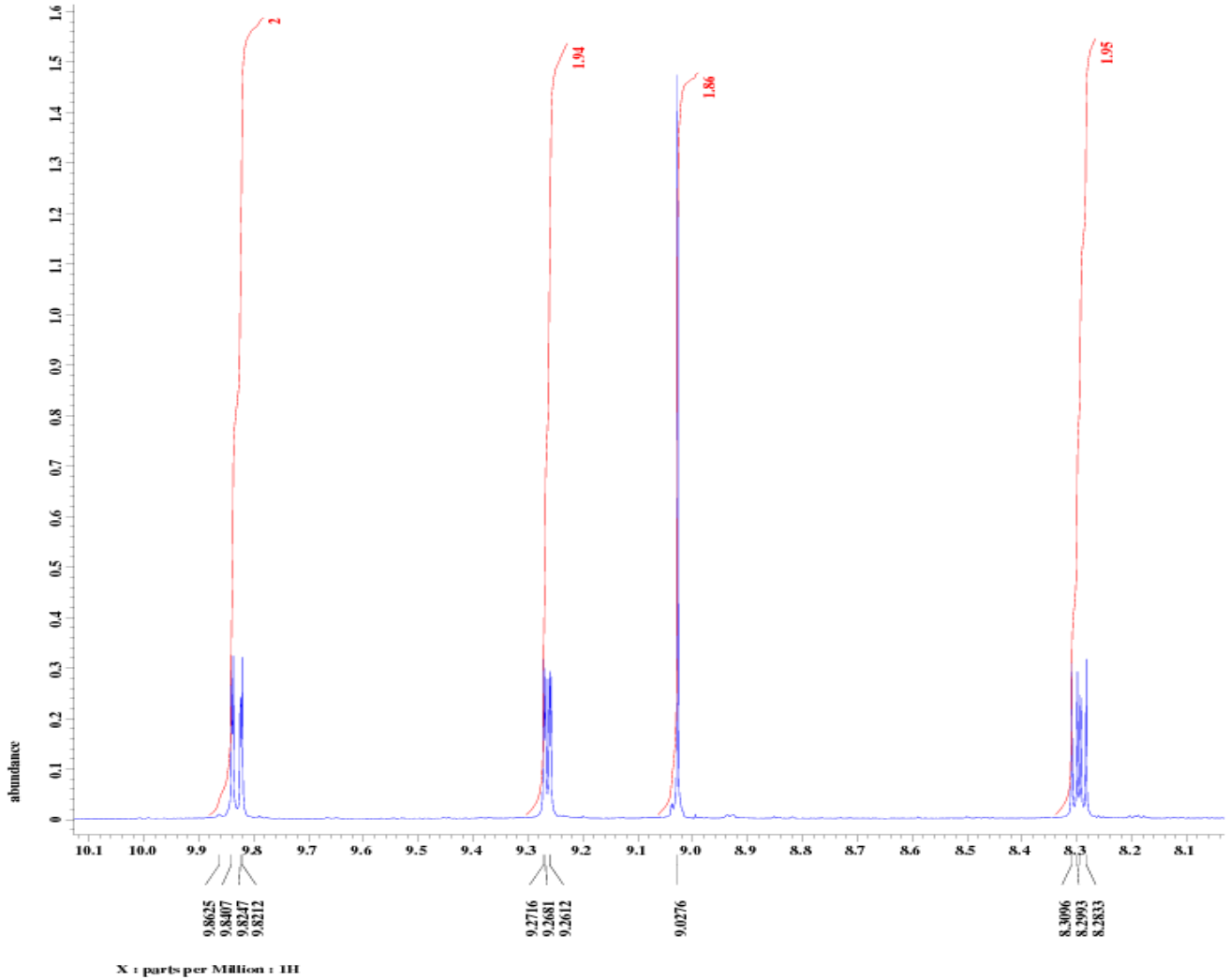

^{1}HNMR of 11,12-dicyanodipyrido-[3,2-a:2',3'-c]phenazine using $Zn(BF_4)_2$ in d_3 - MeCN

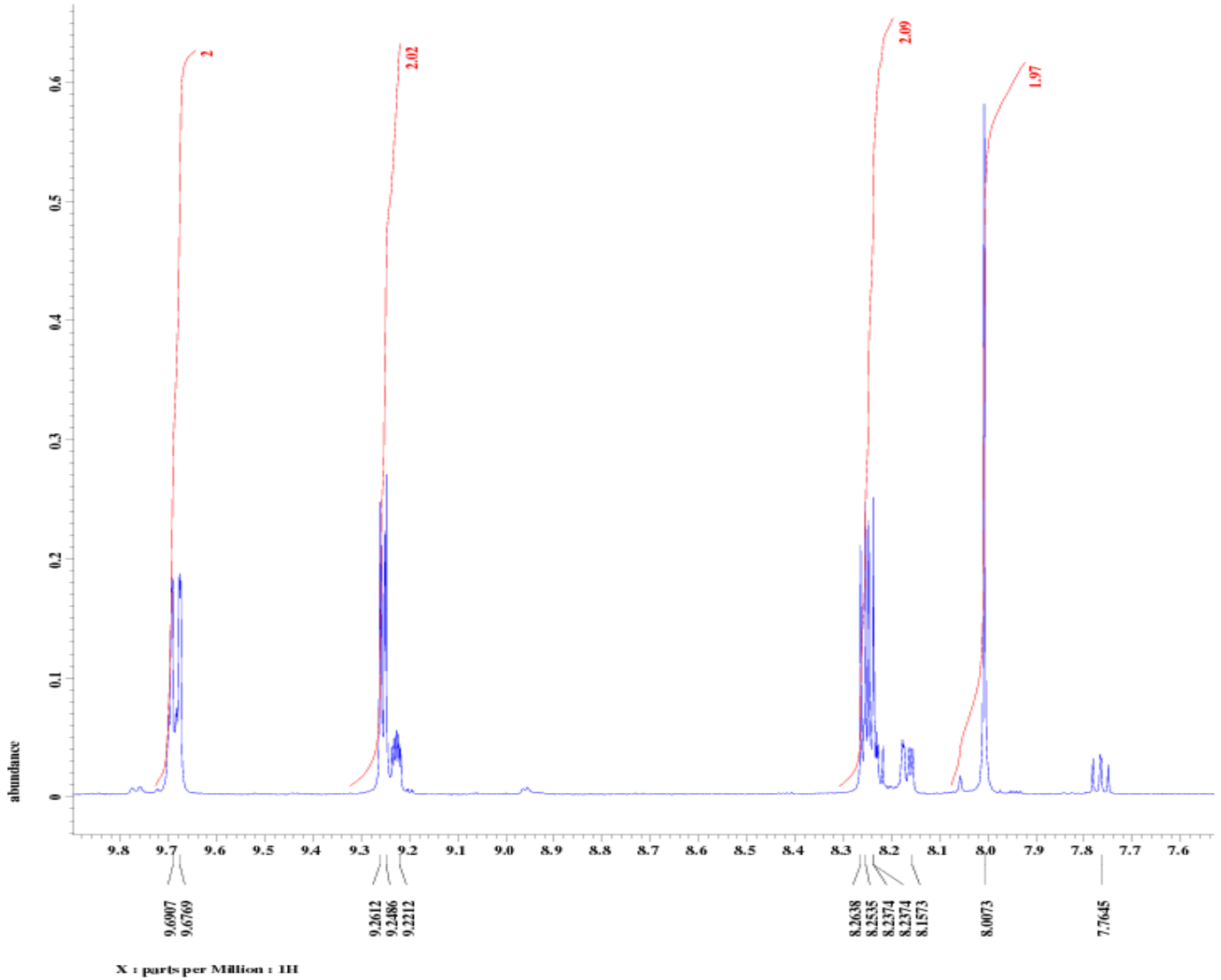

^{1}HNMR of crude 10,13-dibromodipyrido-[3,2-a:2',3'-c]phenazine using $Zn(BF_4)_2$ in d_3 - MeCN. Phendione impurities are present at 9.22 δppm, 8.15 δppm, and 7.76 δppm.

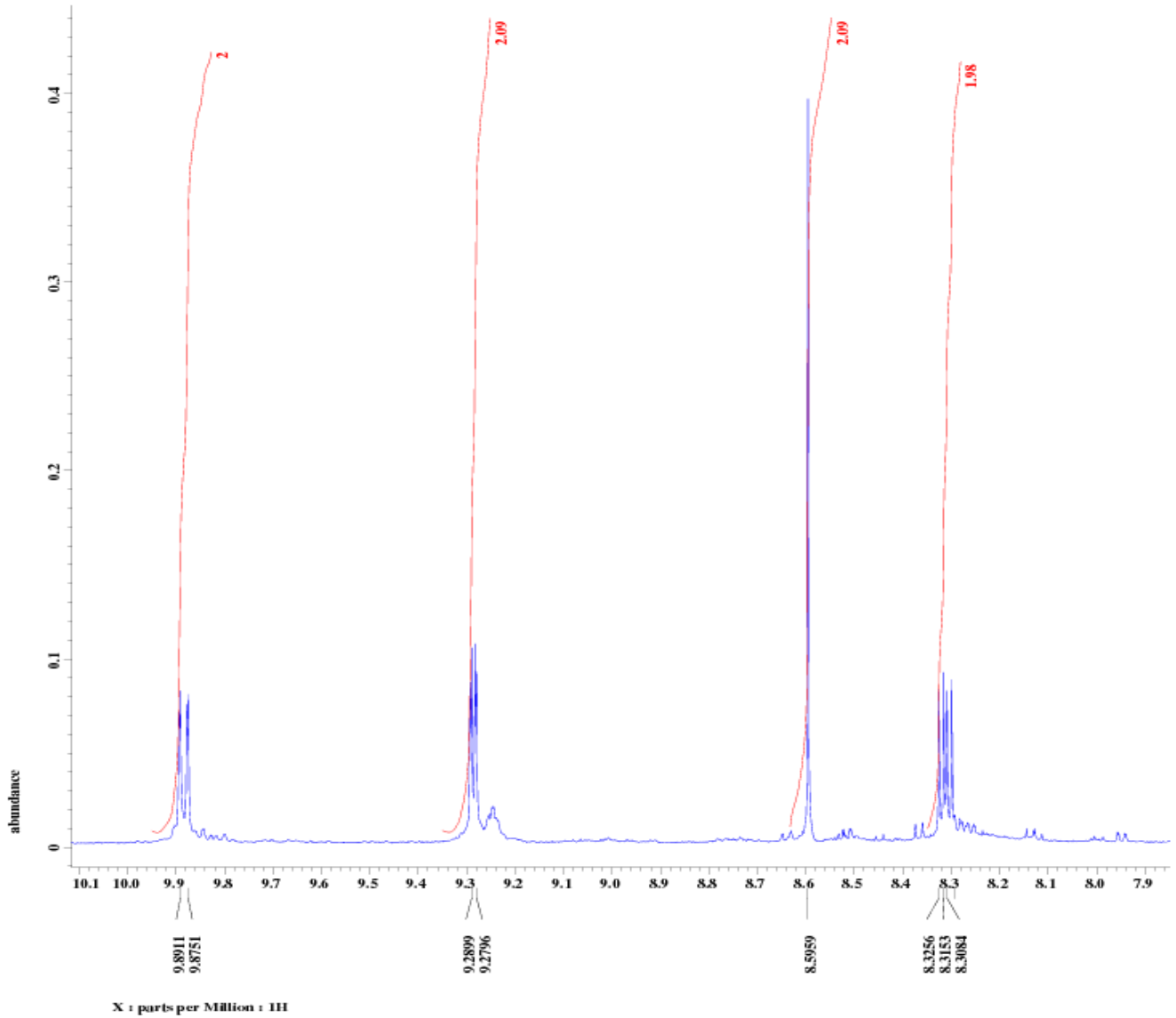

^{1}HNMR of crude 10,13-dicyanodipyrido-[3,2-a:2',3'-c]phenazine using $Zn(BF_4)_2$ in d_3 - MeCN

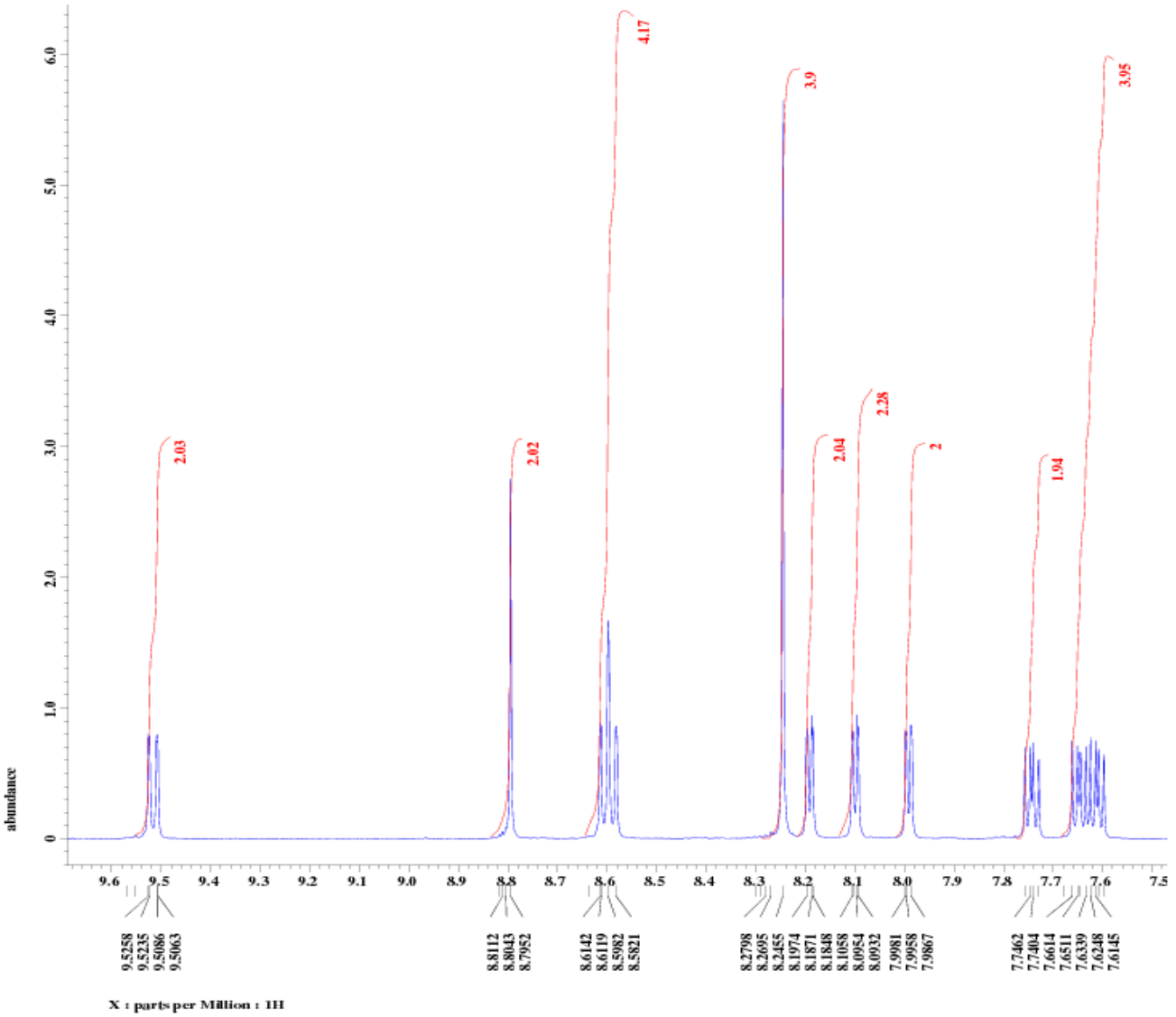

^{1}HNMR of [Ru(phen)$_2$(11,12-dibromodipyrido-[3,2-a:2',3'-c]phenazine)](PF$_6$)$_2$ in d$_3$ - MeCN

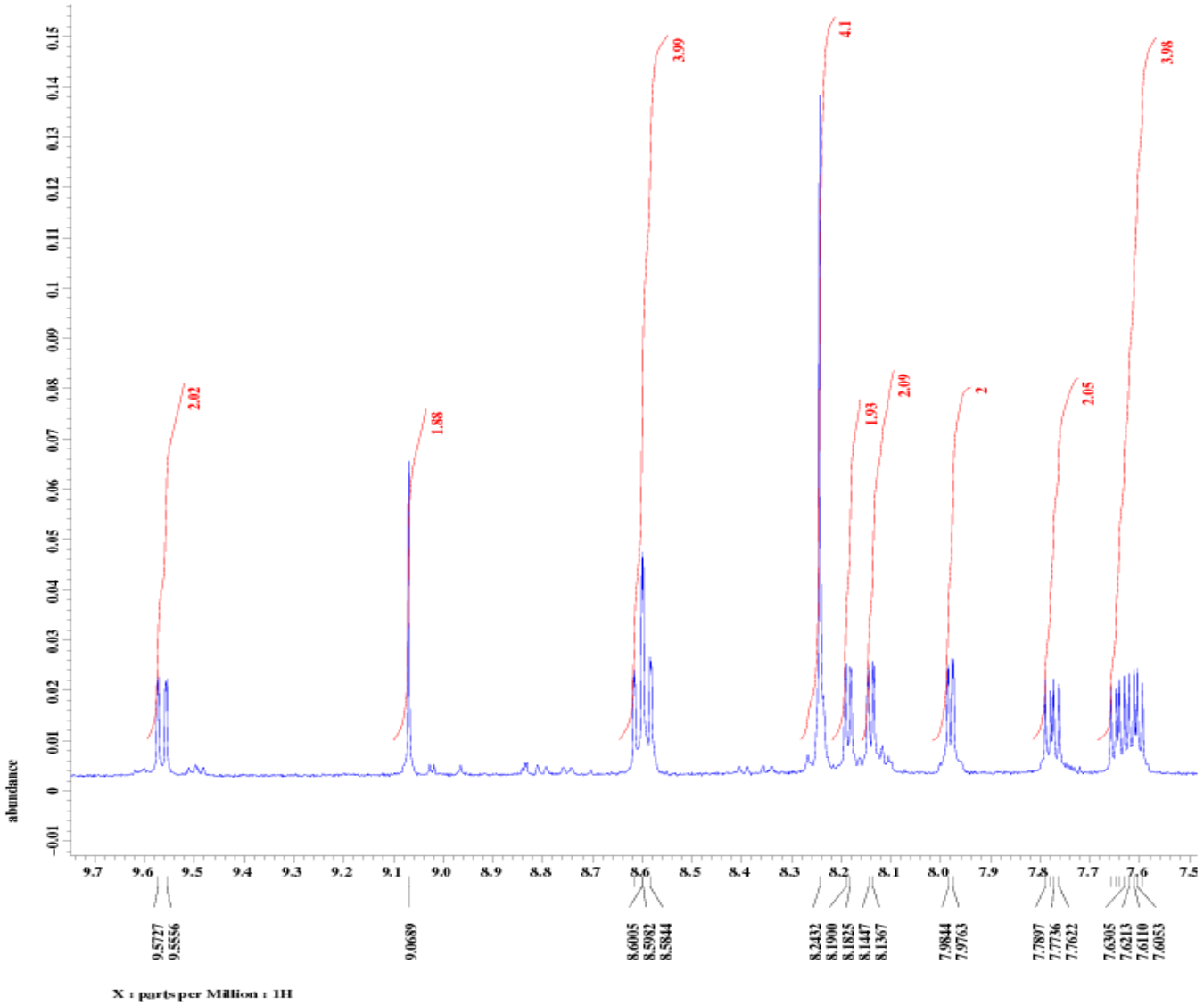

^{1}HNMR of [Ru(phen)$_2$(11,12-dicyanodipyrido-[3,2-a:2',3'-c]phenazine)](PF$_6$)$_2$ in d$_3$ - MeCN

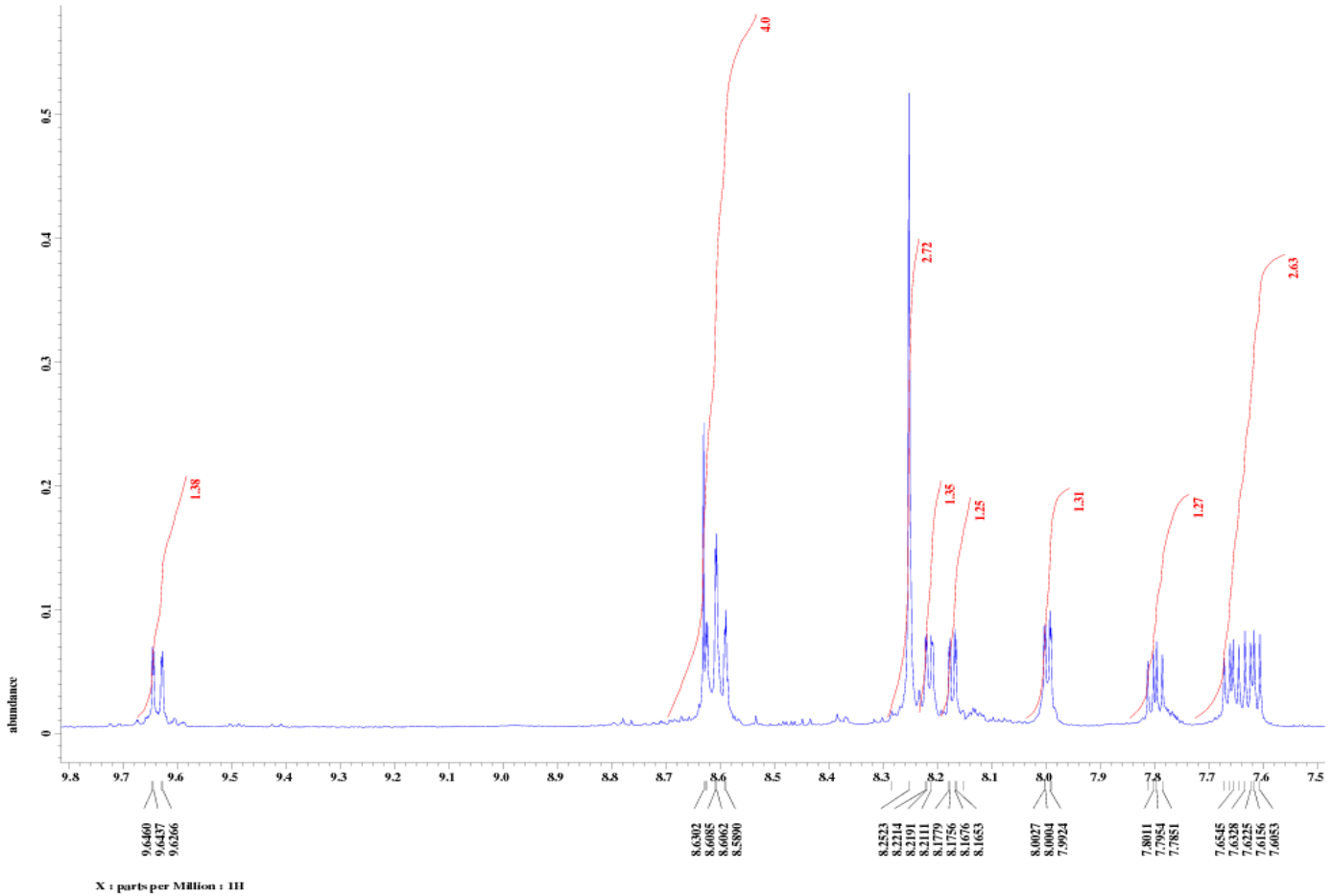

^{1}HNMR of [Ru(phen)$_2$(10,13-dicyanodipyrido-[3,2-a:2',3'-c]phenazine)](PF$_6$)$_2$ in d$_3$ - MeCN

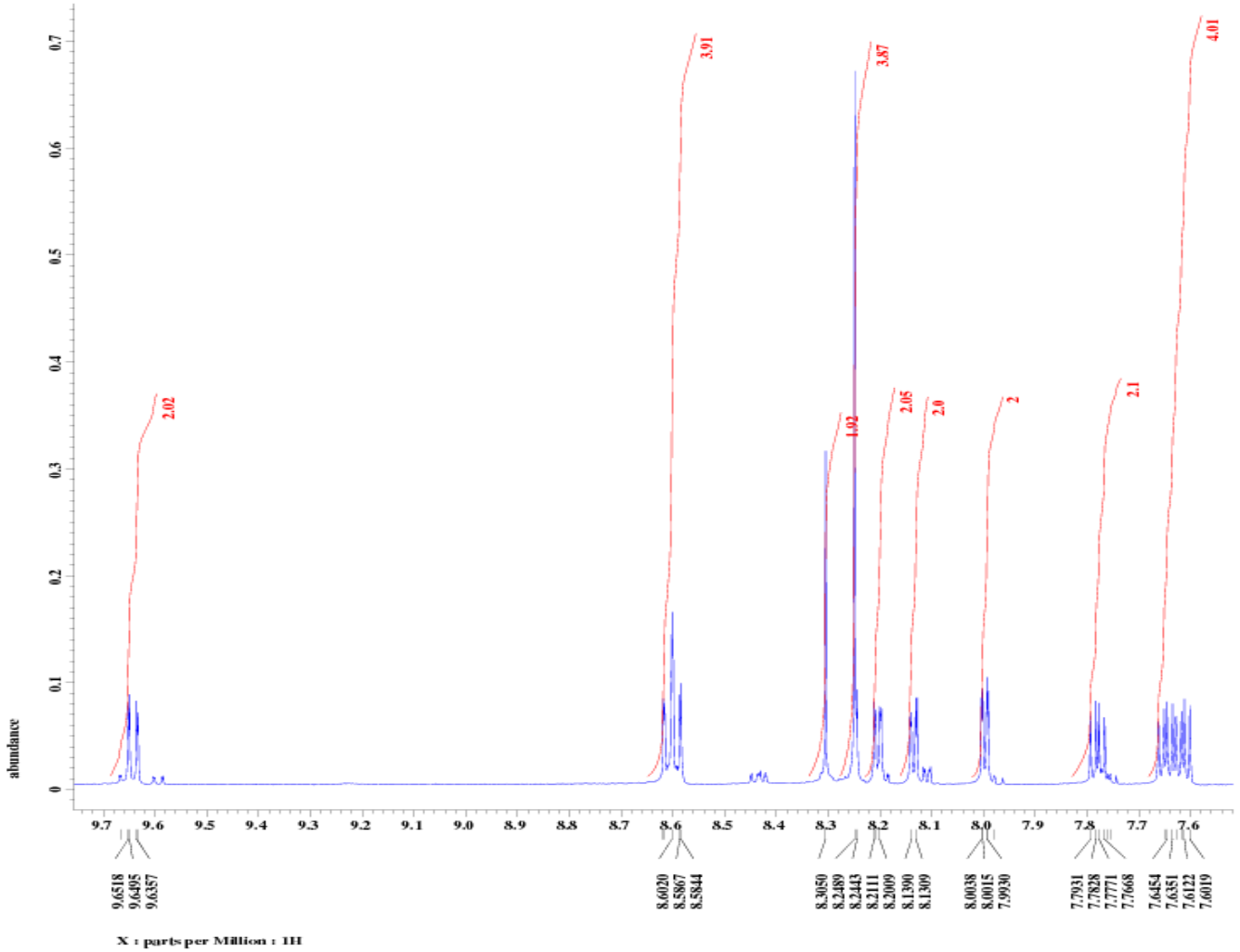

^{1}HNMR of [Ru(phen)$_2$(10,13-dibromodipyrido-[3,2-a:2',3'-c]phenazine)](PF$_6$)$_2$ in d$_3$ - MeCN

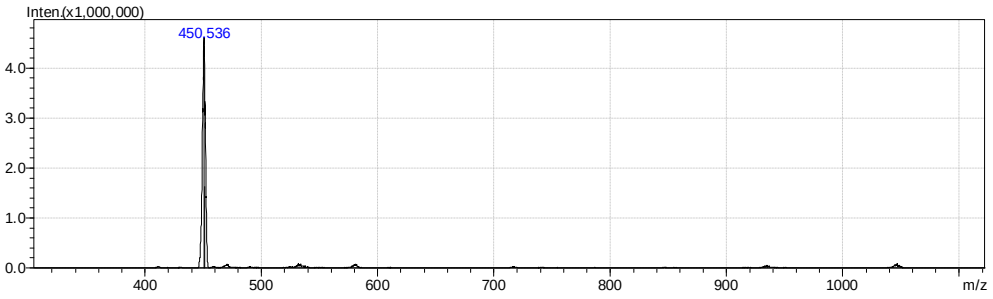

ESI-MS of [Ru(phen)$_2$(11,12-dibromoodipyrido-[3,2-a:2',3'-c]phenazine)](PF$_6$)$_2$

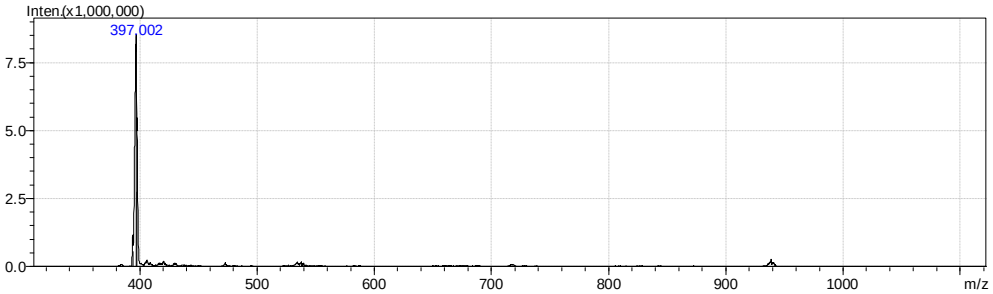

ESI-MS of [Ru(phen)$_2$(11,12-dicyanodipyrido-[3,2-a:2',3'-c]phenazine)](PF$_6$)$_2$

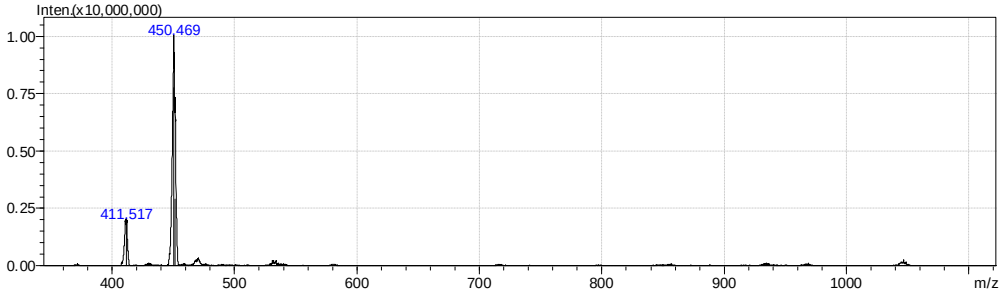

ESI-MS of [Ru(phen)$_2$(10,13-dibromodipyrido-[3,2-a:2',3'-c]phenazine)](PF$_6$)$_2$

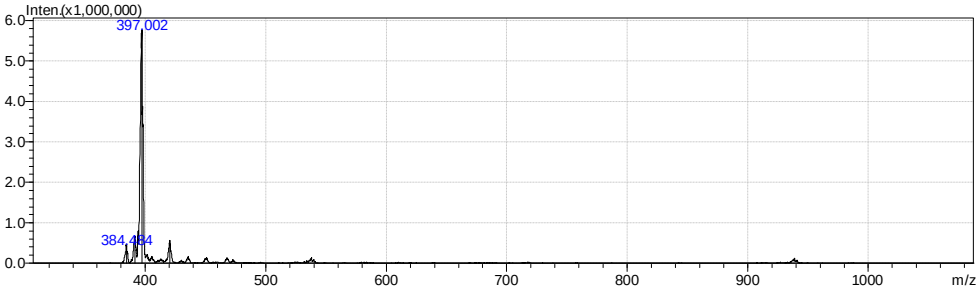

ESI-MS of [Ru(phen)$_2$(10,13-dicyanodipyrido-[3,2-a:2',3'-c]phenazine)](PF$_6$)$_2$

APPENDIX B

X-RAY CRYSTALLOGRAPHY DATA

Crystal data and structure refinement for (C60 H26 N16)*2(C7 H8)*0.5(C6 H6)*3(C H2 Cl2).

Identification code	joe3m	
Empirical formula	C80 H51 Cl6 N16	
Formula weight	1449.07	
Temperature	100(2) K	
Wavelength	0.71073 Å	
Crystal system	Triclinic	
Space group	P-1	
Unit cell dimensions	a = 14.467(4) Å	□= 84.964(5)°.
	b = 15.398(4) Å	□= 84.866(7)°.
	c = 16.493(5) Å	□ = 66.373(7)°.
Volume	3348(463) $Å^3$	
Z	2	
Density (calculated)	1.437 Mg/m^3	
Absorption coefficient	0.319 mm^{-1}	
F(000)	1490	
Crystal size	0.37 x 0.33 x 0.05 mm^3	
Theta range for data collection	1.45 to 25.68°.	
Index ranges	-17<=h<=17, -18<=k<=18, 0<=l<=20	
Reflections collected	12600	
Independent reflections	12600 [R(int) = 0.0945]	
Completeness to theta = 25.68°	99.1 %	
Absorption correction	Semi-empirical from equivalents	
Max. and min. transmission	0.745 and 0.209	
Refinement method	Full-matrix least-squares on F^2	
Data / restraints / parameters	12600 / 111 / 920	
Goodness-of-fit on F^2	1.432	
Final R indices [I>2sigma(I)]	R1 = 0.1580, wR2 = 0.4040	
R indices (all data)	R1 = 0.2126, wR2 = 0.4510	
Largest diff. peak and hole	1.961 and -1.001 e.$Å^{-3}$	

Atomic coordinates (x 10^4) and equivalent isotropic displacement parameters ($Å^2$x 10^3) for (C60 H26 N16)*2(C7 H8)*0.5(C6 H6)*3(C H2 Cl2). U(eq) is defined as one third of the trace of the orthogonalized U^{ij} tensor.

	x	y	z	U(eq)
N(1)	1843(6)	2948(5)	4860(4)	49(2)
N(2)	1421(5)	4833(5)	4812(4)	45(2)
N(3)	420(5)	3022(4)	7593(4)	31(1)
N(4)	-133(5)	5022(4)	7530(4)	30(1)
N(5)	-702(5)	3103(4)	10391(3)	27(1)
N(6)	-1347(5)	5093(4)	10300(3)	30(1)
N(7)	-2118(6)	3242(5)	13137(4)	44(2)
N(8)	-2677(5)	5144(4)	13079(4)	33(2)
N(9)	5156(6)	-414(6)	11216(4)	56(2)
N(10)	4523(5)	1471(5)	11140(4)	45(2)
N(11)	2242(5)	-168(4)	9867(4)	36(2)
N(12)	1611(5)	1843(4)	9742(4)	30(1)
N(13)	-631(5)	124(4)	8516(4)	36(2)
N(14)	-1259(5)	2121(5)	8370(4)	38(2)
N(15)	-3522(6)	460(6)	7128(4)	48(2)
N(16)	-4107(6)	2357(6)	6948(5)	53(2)
C(1)	2078(8)	2021(7)	4875(6)	57(3)
C(2)	1809(8)	1513(7)	5538(6)	56(3)
C(3)	1325(7)	1998(6)	6205(5)	44(2)
C(4)	1089(6)	2954(6)	6219(5)	38(2)
C(5)	586(6)	3494(5)	6933(5)	33(2)
C(6)	-11(5)	3518(5)	8258(4)	28(2)
C(7)	-152(5)	3059(5)	8994(4)	26(2)
C(8)	-574(5)	3570(5)	9683(4)	25(2)
C(9)	-1150(5)	3612(5)	11011(4)	26(2)
C(10)	-1351(6)	3130(5)	11781(4)	29(2)
C(11)	-1035(7)	2161(5)	11838(5)	39(2)

C(12)	-1282(7)	1742(6)	12540(5)	44(2)
C(13)	-1832(8)	2307(6)	13156(6)	53(2)
C(14)	-1876(6)	3661(5)	12451(5)	32(2)
C(15)	-2199(5)	4693(5)	12415(4)	30(2)
C(16)	-2921(6)	6070(6)	13075(5)	38(2)
C(17)	-2708(6)	6607(5)	12413(5)	35(2)
C(18)	-2237(6)	6141(5)	11713(4)	31(2)
C(19)	-1971(5)	5154(5)	11687(4)	29(2)
C(20)	-1486(5)	4636(5)	10976(4)	28(2)
C(21)	-906(5)	4587(5)	9642(5)	29(2)
C(22)	-761(5)	5038(5)	8907(4)	29(2)
C(23)	-317(5)	4554(5)	8243(4)	28(2)
C(24)	332(5)	4510(5)	6916(4)	29(2)
C(25)	598(6)	4967(6)	6155(5)	34(2)
C(26)	381(6)	5951(5)	6123(5)	36(2)
C(27)	692(6)	6334(6)	5433(5)	40(2)
C(28)	1205(8)	5756(7)	4810(6)	53(2)
C(30)	1115(6)	4443(5)	5512(5)	36(2)
C(31)	1357(6)	3403(6)	5520(5)	38(2)
C(32)	5430(8)	-1398(7)	11267(5)	62(3)
C(33)	4916(7)	-1848(6)	10977(5)	49(2)
C(34)	4060(7)	-1332(6)	10610(5)	46(2)
C(35)	3689(6)	-335(5)	10541(5)	37(2)
C(36)	2773(6)	243(5)	10153(5)	36(2)
C(37)	1370(6)	401(5)	9508(4)	34(2)
C(38)	799(6)	-4(5)	9201(5)	38(2)
C(39)	-78(6)	538(5)	8813(4)	32(2)
C(40)	-1460(7)	673(6)	8163(5)	38(2)
C(41)	-2051(7)	234(6)	7821(5)	40(2)
C(42)	-1792(7)	-741(6)	7899(5)	45(2)
C(43)	-2392(8)	-1115(7)	7575(6)	52(2)
C(44)	-3248(8)	-497(8)	7192(6)	59(3)
C(45)	-2943(7)	811(6)	7425(5)	44(2)

C(46)	-3279(7)	1848(6)	7345(5)	43(2)
C(47)	-4363(9)	3274(8)	6843(7)	75(4)
C(48)	-3855(9)	3781(8)	7099(8)	85(4)
C(49)	-2983(8)	3245(7)	7509(7)	74(4)
C(50)	-2697(8)	2268(6)	7654(6)	53(3)
C(51)	-1769(7)	1694(5)	8085(5)	39(2)
C(52)	-399(6)	1572(5)	8732(4)	30(2)
C(53)	172(6)	2005(5)	9051(4)	30(2)
C(54)	1062(6)	1428(5)	9437(4)	29(2)
C(55)	2455(6)	1270(5)	10090(4)	29(2)
C(56)	3042(6)	1691(5)	10447(4)	31(2)
C(57)	2725(6)	2674(5)	10447(5)	35(2)
C(58)	3297(7)	3054(6)	10798(5)	45(2)
C(59)	4199(7)	2433(6)	11135(5)	47(2)
C(60)	3949(6)	1128(6)	10805(5)	40(2)
C(61)	4275(6)	89(5)	10851(4)	39(2)
C(62)	4478(8)	2099(8)	5170(7)	74(3)
Cl(1)	5612(7)	859(8)	4870(6)	254(4)
Cl(2)	4007(4)	1536(4)	6068(4)	155(2)
C(63)	2488(8)	3700(7)	3140(6)	56(3)
Cl(3)	3636(2)	2696(2)	3225(2)	64(1)
Cl(4)	2703(2)	4663(2)	2637(2)	78(1)
C(64)	3725(11)	9766(10)	7620(9)	101(4)
Cl(5)	2689(2)	10820(2)	7817(2)	83(1)
Cl(6)	3433(4)	8948(3)	7188(4)	147(2)
C(65)	6114(13)	4616(13)	624(12)	107(5)
C(66)	6703(13)	4092(15)	-84(12)	124(5)
C(67)	7027(10)	3070(13)	100(10)	99(4)
C(68)	6747(10)	2729(12)	869(10)	96(5)
C(69)	6266(14)	3282(16)	1423(13)	125(6)
C(70)	5951(10)	4214(13)	1275(11)	101(4)
C(71)	5710(30)	5670(30)	750(20)	271(16)
C(72)	8938(10)	346(9)	5849(8)	103(5)

C(73)	9417(9)	903(9)	6132(7)	87(4)
C(74)	8915(10)	1892(9)	6033(8)	99(4)
C(75)	8011(10)	2300(10)	5620(9)	118(6)
C(76)	7576(11)	1751(11)	5356(8)	119(5)
C(77)	8049(9)	801(8)	5438(6)	67(3)
C(78)	9499(13)	-646(12)	5951(9)	115(5)
C(79)	5743(13)	4566(12)	4573(9)	115(5)
C(80)	5149(13)	4063(13)	4290(10)	121(5)
C(81)	4134(14)	4629(13)	4837(11)	134(6)

Bond lengths [Å] and angles [°] for (C60 H26 N16)* 2(C7 H8)*0.5(C6 H6)*3(C H2 Cl2).

N(1)-C(1)	1.326(14)
N(1)-C(31)	1.33(3)
N(2)-C(28)	1.326(14)
N(2)-C(30)	1.37(3)
N(3)-C(5)	1.312(14)
N(3)-C(6)	1.348(17)
N(4)-C(24)	1.30(2)
N(4)-C(23)	1.386(15)
N(5)-C(9)	1.301(19)
N(5)-C(8)	1.355(11)
N(6)-C(20)	1.310(12)
N(6)-C(21)	1.349(18)
N(7)-C(13)	1.327(13)
N(7)-C(14)	1.34(2)
N(8)-C(16)	1.324(13)
N(8)-C(15)	1.33(2)
N(9)-C(61)	1.36(13)
N(9)-C(32)	1.401(15)
N(10)-C(60)	1.33(10)
N(10)-C(59)	1.362(13)
N(11)-C(36)	1.31(9)
N(11)-C(37)	1.37(12)
N(12)-C(55)	1.33(12)
N(12)-C(54)	1.35(9)
N(13)-C(40)	1.31(12)
N(13)-C(39)	1.35(9)
N(14)-C(51)	1.31(8)
N(14)-C(52)	1.35(12)
N(15)-C(45)	1.31(10)
N(15)-C(44)	1.360(15)
N(16)-C(47)	1.309(15)

N(16)-C(46)	1.33(12)
C(1)-C(2)	1.41(3)
C(1)-H(1)	0.9500
C(2)-C(3)	1.36(2)
C(2)-H(2)	0.9500
C(3)-C(4)	1.373(14)
C(3)-H(3)	0.9500
C(4)-C(31)	1.40(2)
C(4)-C(5)	1.46(2)
C(5)-C(24)	1.455(14)
C(6)-C(7)	1.392(12)
C(6)-C(23)	1.473(13)
C(7)-C(8)	1.390(15)
C(7)-C(53)	1.495(12)
C(8)-C(21)	1.439(11)
C(9)-C(20)	1.449(11)
C(9)-C(10)	1.481(16)
C(10)-C(11)	1.371(12)
C(10)-C(14)	1.41(3)
C(11)-C(12)	1.37(2)
C(11)-H(11)	0.9500
C(12)-C(13)	1.37(3)
C(12)-H(12)	0.9500
C(13)-H(13)	0.9500
C(14)-C(15)	1.463(12)
C(15)-C(19)	1.422(19)
C(16)-C(17)	1.40(2)
C(16)-H(16)	0.9500
C(17)-C(18)	1.39(2)
C(17)-H(17)	0.9500
C(18)-C(19)	1.414(13)
C(18)-H(18)	0.9500
C(19)-C(20)	1.44(2)

C(21)-C(22)	1.385(12)
C(22)-C(23)	1.342(19)
C(22)-H(22)	0.9500
C(24)-C(25)	1.48(2)
C(25)-C(30)	1.36(3)
C(25)-C(26)	1.416(14)
C(26)-C(27)	1.36(3)
C(26)-H(26)	0.9500
C(27)-C(28)	1.38(3)
C(27)-H(27)	0.9500
C(28)-H(28)	0.9500
C(30)-C(31)	1.496(14)
C(32)-C(33)	1.34(8)
C(32)-H(32)	0.9500
C(33)-C(34)	1.34(13)
C(33)-H(33)	0.9500
C(34)-C(35)	1.407(11)
C(34)-H(34)	0.9500
C(35)-C(61)	1.41(10)
C(35)-C(36)	1.44(13)
C(36)-C(55)	1.456(12)
C(37)-C(38)	1.37(9)
C(37)-C(54)	1.458(12)
C(38)-C(39)	1.39(13)
C(38)-H(38)	0.9500
C(39)-C(52)	1.467(12)
C(40)-C(51)	1.449(13)
C(40)-C(41)	1.46(10)
C(41)-C(42)	1.390(14)
C(41)-C(45)	1.42(13)
C(42)-C(43)	1.38(10)
C(42)-H(42)	0.9500
C(43)-C(44)	1.39(11)

C(43)-H(43)	0.9500
C(44)-H(44)	0.9500
C(45)-C(46)	1.468(14)
C(46)-C(50)	1.40(10)
C(47)-C(48)	1.38(8)
C(47)-H(47)	0.9500
C(48)-C(49)	1.40(12)
C(48)-H(48)	0.9500
C(49)-C(50)	1.395(14)
C(49)-H(49)	0.9500
C(50)-C(51)	1.48(13)
C(52)-C(53)	1.41(9)
C(53)-C(54)	1.41(13)
C(55)-C(56)	1.44(10)
C(56)-C(57)	1.394(12)
C(56)-C(60)	1.40(13)
C(57)-C(58)	1.38(9)
C(57)-H(57)	0.9500
C(58)-C(59)	1.40(13)
C(58)-H(58)	0.9500
C(59)-H(59)	0.9500
C(60)-C(61)	1.472(14)
C(62)-Cl(2)	1.87(5)
C(62)-Cl(1)	2.02(9)
C(62)-H(62A)	0.9900
C(62)-H(62B)	0.9900
C(63)-Cl(4)	1.76(2)
C(63)-Cl(3)	1.76(14)
C(63)-H(63A)	0.9900
C(63)-H(63B)	0.9900
C(64)-Cl(6)	1.71(4)
C(64)-Cl(5)	1.74(10)
C(64)-H(64A)	0.9900

C(64)-H(64B)	0.9900
C(65)-C(70)	1.24(2)
C(65)-C(66)	1.48(4)
C(65)-C(71)	1.52(4)
C(66)-C(67)	1.46(2)
C(66)-H(66)	0.9500
C(67)-C(68)	1.42(3)
C(67)-H(67)	0.9500
C(68)-C(69)	1.26(3)
C(68)-H(68)	0.9500
C(69)-C(70)	1.33(2)
C(69)-H(69)	0.9500
C(70)-H(70)	0.9500
C(71)-H(71A)	0.9814
C(71)-H(71B)	0.9815
C(71)-H(71C)	0.9815
C(72)-C(77)	1.40(14)
C(72)-C(73)	1.43(7)
C(72)-C(78)	1.42(3)
C(73)-C(74)	1.401(17)
C(73)-H(73)	0.9500
C(74)-C(75)	1.41(14)
C(74)-H(74)	0.9500
C(75)-C(76)	1.36(7)
C(75)-H(75)	0.9500
C(76)-C(77)	1.343(16)
C(76)-H(76)	0.9500
C(77)-H(77)	0.9500
C(78)-H(78A)	0.9800
C(78)-H(78B)	0.9800
C(78)-H(78C)	0.9800
C(79)-C(80)	1.49(10)
C(79)-C(81)#1	1.71(3)

C(79)-H(79)	0.9500
C(80)-C(81)	1.61(13)
C(80)-H(80)	0.9500
C(81)-C(79)#1	1.71(3)
C(81)-H(81)	0.9500
C(1)-N(1)-C(31)	117.6(9)
C(28)-N(2)-C(30)	115.5(10)
C(5)-N(3)-C(6)	117.4(12)
C(24)-N(4)-C(23)	117.6(13)
C(9)-N(5)-C(8)	117.3(11)
C(20)-N(6)-C(21)	118.2(11)
C(13)-N(7)-C(14)	117.0(12)
C(16)-N(8)-C(15)	118.3(8)
C(61)-N(9)-C(32)	114.1(19)
C(60)-N(10)-C(59)	117(4)
C(36)-N(11)-C(37)	118(6)
C(55)-N(12)-C(54)	117(6)
C(40)-N(13)-C(39)	118(6)
C(51)-N(14)-C(52)	118(6)
C(45)-N(15)-C(44)	119(4)
C(47)-N(16)-C(46)	118(2)
N(1)-C(1)-C(2)	123.1(13)
N(1)-C(1)-H(1)	118.4
C(2)-C(1)-H(1)	118.4
C(3)-C(2)-C(1)	117.6(18)
C(3)-C(2)-H(2)	121.2
C(1)-C(2)-H(2)	121.2
C(2)-C(3)-C(4)	120.8(10)
C(2)-C(3)-H(3)	119.6
C(4)-C(3)-H(3)	119.6
C(3)-C(4)-C(31)	117.3(10)
C(3)-C(4)-C(5)	122.2(10)
C(31)-C(4)-C(5)	120.4(15)

N(3)-C(5)-C(24)	121.8(9)
N(3)-C(5)-C(4)	117.7(13)
C(24)-C(5)-C(4)	120.4(9)
N(3)-C(6)-C(7)	120.8(10)
N(3)-C(6)-C(23)	121.7(7)
C(7)-C(6)-C(23)	117.5(9)
C(8)-C(7)-C(6)	120.6(10)
C(8)-C(7)-C(53)	119.6(6)
C(6)-C(7)-C(53)	119.8(9)
N(5)-C(8)-C(7)	119.2(10)
N(5)-C(8)-C(21)	120.1(10)
C(7)-C(8)-C(21)	120.7(6)
N(5)-C(9)-C(20)	123.0(6)
N(5)-C(9)-C(10)	118.7(12)
C(20)-C(9)-C(10)	118.2(11)
C(11)-C(10)-C(14)	119.8(7)
C(11)-C(10)-C(9)	119.8(12)
C(14)-C(10)-C(9)	120.4(13)
C(12)-C(11)-C(10)	118.4(14)
C(12)-C(11)-H(11)	120.8
C(10)-C(11)-H(11)	120.8
C(11)-C(12)-C(13)	118.6(17)
C(11)-C(12)-H(12)	120.7
C(13)-C(12)-H(12)	120.7
N(7)-C(13)-C(12)	124.8(9)
N(7)-C(13)-H(13)	117.6
C(12)-C(13)-H(13)	117.6
N(7)-C(14)-C(10)	121.2(15)
N(7)-C(14)-C(15)	117.8(13)
C(10)-C(14)-C(15)	121.0(7)
N(8)-C(15)-C(19)	123.8(14)
N(8)-C(15)-C(14)	117.4(7)
C(19)-C(15)-C(14)	118.8(12)

N(8)-C(16)-C(17)	123.9(12)
N(8)-C(16)-H(16)	118.0
C(17)-C(16)-H(16)	118.0
C(18)-C(17)-C(16)	117.7(15)
C(18)-C(17)-H(17)	121.2
C(16)-C(17)-H(17)	121.1
C(17)-C(18)-C(19)	120.3(8)
C(17)-C(18)-H(18)	119.8
C(19)-C(18)-H(18)	119.9
C(18)-C(19)-C(15)	115.9(9)
C(18)-C(19)-C(20)	122.7(8)
C(15)-C(19)-C(20)	121.4(13)
N(6)-C(20)-C(19)	119.8(11)
N(6)-C(20)-C(9)	120.2(11)
C(19)-C(20)-C(9)	120.1(6)
N(6)-C(21)-C(22)	120.4(11)
N(6)-C(21)-C(8)	121.2(6)
C(22)-C(21)-C(8)	118.4(10)
C(23)-C(22)-C(21)	121.9(11)
C(23)-C(22)-H(22)	119.1
C(21)-C(22)-H(22)	119.0
C(22)-C(23)-N(4)	120.4(12)
C(22)-C(23)-C(6)	120.9(7)
N(4)-C(23)-C(6)	118.7(10)
N(4)-C(24)-C(5)	122.6(9)
N(4)-C(24)-C(25)	119.8(15)
C(5)-C(24)-C(25)	117.6(9)
C(30)-C(25)-C(26)	119.7(12)
C(30)-C(25)-C(24)	121.0(15)
C(26)-C(25)-C(24)	119.1(9)
C(27)-C(26)-C(25)	117.4(10)
C(27)-C(26)-H(26)	121.3
C(25)-C(26)-H(26)	121.3

C(26)-C(27)-C(28)	119.2(18)
C(26)-C(27)-H(27)	120.4
C(28)-C(27)-H(27)	120.4
N(2)-C(28)-C(27)	125.4(12)
N(2)-C(28)-H(28)	117.3
C(27)-C(28)-H(28)	117.3
C(25)-C(30)-N(2)	122.7(17)
C(25)-C(30)-C(31)	121.4(11)
N(2)-C(30)-C(31)	115.8(10)
N(1)-C(31)-C(4)	123.4(16)
N(1)-C(31)-C(30)	117.7(10)
C(4)-C(31)-C(30)	118.9(10)
C(33)-C(32)-N(9)	126(4)
C(33)-C(32)-H(32)	117.2
N(9)-C(32)-H(32)	117.2
C(34)-C(33)-C(32)	119(5)
C(34)-C(33)-H(33)	120.6
C(32)-C(33)-H(33)	120.6
C(33)-C(34)-C(35)	121.1(13)
C(33)-C(34)-H(34)	119.4
C(35)-C(34)-H(34)	119.5
C(34)-C(35)-C(61)	117(4)
C(34)-C(35)-C(36)	122.7(14)
C(61)-C(35)-C(36)	120(6)
N(11)-C(36)-C(35)	119(6)
N(11)-C(36)-C(55)	122(4)
C(35)-C(36)-C(55)	119.2(18)
C(38)-C(37)-N(11)	119(6)
C(38)-C(37)-C(54)	120(4)
N(11)-C(37)-C(54)	120(2)
C(37)-C(38)-C(39)	122(5)
C(37)-C(38)-H(38)	119.2
C(39)-C(38)-H(38)	119.2

N(13)-C(39)-C(38)	121(5)
N(13)-C(39)-C(52)	120(4)
C(38)-C(39)-C(52)	118.9(17)
N(13)-C(40)-C(51)	121(2)
N(13)-C(40)-C(41)	119(6)
C(51)-C(40)-C(41)	120(4)
C(42)-C(41)-C(45)	118(2)
C(42)-C(41)-C(40)	122(3)
C(45)-C(41)-C(40)	120(5)
C(43)-C(42)-C(41)	119(3)
C(43)-C(42)-H(42)	120.3
C(41)-C(42)-H(42)	120.3
C(42)-C(43)-C(44)	118(6)
C(42)-C(43)-H(43)	120.8
C(44)-C(43)-H(43)	120.7
N(15)-C(44)-C(43)	123(2)
N(15)-C(44)-H(44)	118.6
C(43)-C(44)-H(44)	118.6
N(15)-C(45)-C(41)	123(5)
N(15)-C(45)-C(46)	116(4)
C(41)-C(45)-C(46)	121.1(17)
N(16)-C(46)-C(50)	122(5)
N(16)-C(46)-C(45)	118.8(15)
C(50)-C(46)-C(45)	119(4)
N(16)-C(47)-C(48)	126(4)
N(16)-C(47)-H(47)	116.8
C(48)-C(47)-H(47)	116.8
C(47)-C(48)-C(49)	115(6)
C(47)-C(48)-H(48)	122.3
C(49)-C(48)-H(48)	122.2
C(50)-C(49)-C(48)	120(2)
C(50)-C(49)-H(49)	120.0
C(48)-C(49)-H(49)	120.0

C(49)-C(50)-C(46)	118(4)
C(49)-C(50)-C(51)	120(2)
C(46)-C(50)-C(51)	122(5)
N(14)-C(51)-C(40)	123(4)
N(14)-C(51)-C(50)	119(5)
C(40)-C(51)-C(50)	118.1(17)
N(14)-C(52)-C(53)	119(6)
N(14)-C(52)-C(39)	120.3(18)
C(53)-C(52)-C(39)	120(4)
C(54)-C(53)-C(52)	119(6)
C(54)-C(53)-C(7)	119.6(18)
C(52)-C(53)-C(7)	121(4)
N(12)-C(54)-C(53)	119(6)
N(12)-C(54)-C(37)	121(4)
C(53)-C(54)-C(37)	119.8(19)
N(12)-C(55)-C(56)	118(6)
N(12)-C(55)-C(36)	122(2)
C(56)-C(55)-C(36)	119(4)
C(57)-C(56)-C(60)	117.6(16)
C(57)-C(56)-C(55)	121(4)
C(60)-C(56)-C(55)	121(5)
C(58)-C(57)-C(56)	120(4)
C(58)-C(57)-H(57)	120.1
C(56)-C(57)-H(57)	120.1
C(57)-C(58)-C(59)	119(6)
C(57)-C(58)-H(58)	120.8
C(59)-C(58)-H(58)	120.7
N(10)-C(59)-C(58)	122.6(19)
N(10)-C(59)-H(59)	118.7
C(58)-C(59)-H(59)	118.7
N(10)-C(60)-C(56)	124(5)
N(10)-C(60)-C(61)	117(4)
C(56)-C(60)-C(61)	118.7(18)

N(9)-C(61)-C(35)	123(5)
N(9)-C(61)-C(60)	115.6(15)
C(35)-C(61)-C(60)	121(4)
Cl(2)-C(62)-Cl(1)	93(4)
Cl(2)-C(62)-H(62A)	113.1
Cl(1)-C(62)-H(62A)	113.1
Cl(2)-C(62)-H(62B)	113.1
Cl(1)-C(62)-H(62B)	113.1
H(62A)-C(62)-H(62B)	110.5
Cl(4)-C(63)-Cl(3)	111(7)
Cl(4)-C(63)-H(63A)	109.5
Cl(3)-C(63)-H(63A)	109.5
Cl(4)-C(63)-H(63B)	109.5
Cl(3)-C(63)-H(63B)	109.6
H(63A)-C(63)-H(63B)	108.1
Cl(6)-C(64)-Cl(5)	114(7)
Cl(6)-C(64)-H(64A)	108.8
Cl(5)-C(64)-H(64A)	108.8
Cl(6)-C(64)-H(64B)	108.7
Cl(5)-C(64)-H(64B)	108.7
H(64A)-C(64)-H(64B)	107.6
C(70)-C(65)-C(66)	123(2)
C(70)-C(65)-C(71)	107(2)
C(66)-C(65)-C(71)	129(2)
C(65)-C(66)-C(67)	110.1(16)
C(65)-C(66)-H(66)	124.9
C(67)-C(66)-H(66)	125.0
C(68)-C(67)-C(66)	119.8(19)
C(68)-C(67)-H(67)	120.1
C(66)-C(67)-H(67)	120.1
C(69)-C(68)-C(67)	122(2)
C(69)-C(68)-H(68)	119.0
C(67)-C(68)-H(68)	119.1

C(68)-C(69)-C(70)	120(2)
C(68)-C(69)-H(69)	120.1
C(70)-C(69)-H(69)	120.0
C(65)-C(70)-C(69)	125(2)
C(65)-C(70)-H(70)	117.3
C(69)-C(70)-H(70)	117.4
C(65)-C(71)-H(71A)	109.5
C(65)-C(71)-H(71B)	109.7
H(71A)-C(71)-H(71B)	109.3
C(65)-C(71)-H(71C)	109.6
H(71A)-C(71)-H(71C)	109.3
H(71B)-C(71)-H(71C)	109.3
C(77)-C(72)-C(73)	119(5)
C(77)-C(72)-C(78)	126.6(17)
C(73)-C(72)-C(78)	114(6)
C(74)-C(73)-C(72)	117(6)
C(74)-C(73)-H(73)	121.5
C(72)-C(73)-H(73)	121.5
C(73)-C(74)-C(75)	120.5(14)
C(73)-C(74)-H(74)	119.8
C(75)-C(74)-H(74)	119.8
C(76)-C(75)-C(74)	121(5)
C(76)-C(75)-H(75)	119.5
C(74)-C(75)-H(75)	119.5
C(77)-C(76)-C(75)	119(6)
C(77)-C(76)-H(76)	120.3
C(75)-C(76)-H(76)	120.3
C(76)-C(77)-C(72)	122.6(12)
C(76)-C(77)-H(77)	118.7
C(72)-C(77)-H(77)	118.7
C(72)-C(78)-H(78A)	109.5
C(72)-C(78)-H(78B)	109.5
H(78A)-C(78)-H(78B)	109.5

C(72)-C(78)-H(78C)	109.4
H(78A)-C(78)-H(78C)	109.5
H(78B)-C(78)-H(78C)	109.5
C(80)-C(79)-C(81)#1	152(2)
C(80)-C(79)-H(79)	104.3
C(81)#1-C(79)-H(79)	104.2
C(79)-C(80)-C(81)	95(8)
C(79)-C(80)-H(80)	132.3
C(81)-C(80)-H(80)	132.5
C(80)-C(81)-C(79)#1	113(6)
C(80)-C(81)-H(81)	123.3
C(79)#1-C(81)-H(81)	123.5

Symmetry transformations used to generate equivalent atoms:

#1 -x+1,-y+1,-z+1

Anisotropic displacement parameters ($Å^2 x\ 10^3$) for (C60 H26 N16)*2(C7 H8)*0.5(C6 H6)*3(C H2 Cl2). The anisotropic displacement factor exponent takes the form: $-2\pi^2[h^2 a^{*2} U^{11} + ... + 2 h k a^* b^* U^{12}]$

	U^{11}	U^{22}	U^{33}	U^{23}	U^{13}	U^{12}
N(1)	56(5)	41(4)	43(4)	1(3)	4(4)	-13(4)
N(2)	54(4)	43(4)	33(4)	7(3)	2(3)	-16(4)
N(3)	31(3)	26(3)	33(3)	3(3)	-6(3)	-9(3)
N(4)	35(3)	24(3)	32(3)	9(3)	-7(3)	-13(3)
N(5)	37(3)	18(3)	25(3)	4(2)	-8(3)	-9(3)
N(6)	40(4)	20(3)	26(3)	4(2)	-5(3)	-9(3)
N(7)	59(5)	37(4)	31(4)	5(3)	3(3)	-18(4)
N(8)	38(4)	26(3)	34(4)	2(3)	-6(3)	-11(3)
N(9)	53(5)	47(5)	39(4)	7(3)	-13(4)	10(4)
N(10)	41(4)	45(4)	32(4)	-4(3)	-6(3)	3(3)
N(11)	46(4)	17(3)	31(3)	7(3)	-8(3)	2(3)
N(12)	32(3)	21(3)	30(3)	1(3)	-9(3)	0(3)
N(13)	51(4)	21(3)	38(4)	2(3)	-1(3)	-18(3)
N(14)	50(4)	31(4)	36(4)	12(3)	-10(3)	-20(3)
N(15)	70(5)	53(5)	38(4)	-10(3)	3(4)	-41(4)
N(16)	63(5)	57(5)	57(5)	16(4)	-24(4)	-40(4)
C(1)	86(7)	42(5)	45(5)	-18(4)	16(5)	-28(5)
C(2)	69(6)	41(5)	47(6)	-5(4)	2(5)	-11(5)
C(3)	49(5)	34(5)	43(5)	3(4)	1(4)	-12(4)
C(4)	39(4)	37(5)	34(4)	-2(3)	-7(3)	-10(4)
C(5)	33(4)	33(4)	30(4)	8(3)	-8(3)	-10(3)
C(6)	32(4)	21(4)	35(4)	6(3)	-9(3)	-13(3)
C(7)	29(4)	16(3)	29(4)	-1(3)	-6(3)	-3(3)
C(8)	26(4)	18(3)	30(4)	3(3)	-7(3)	-8(3)
C(9)	35(4)	12(3)	30(4)	9(3)	-13(3)	-7(3)
C(10)	43(4)	19(3)	26(4)	2(3)	-3(3)	-12(3)
C(11)	57(5)	25(4)	36(4)	5(3)	-12(4)	-17(4)

C(12)	67(6)	22(4)	43(5)	8(4)	-12(4)	-16(4)
C(13)	74(7)	33(5)	43(5)	14(4)	5(5)	-17(5)
C(14)	35(4)	25(4)	37(4)	5(3)	-6(3)	-13(3)
C(15)	31(4)	23(4)	32(4)	5(3)	-8(3)	-7(3)
C(16)	34(4)	39(5)	37(4)	-3(4)	-12(3)	-8(4)
C(17)	43(5)	18(3)	38(4)	6(3)	-13(4)	-4(3)
C(18)	40(4)	18(3)	27(4)	2(3)	-7(3)	-4(3)
C(19)	29(4)	23(4)	36(4)	5(3)	-10(3)	-12(3)
C(20)	35(4)	16(3)	37(4)	4(3)	-12(3)	-12(3)
C(21)	28(4)	17(3)	39(4)	3(3)	-9(3)	-7(3)
C(22)	32(4)	19(3)	35(4)	7(3)	-5(3)	-9(3)
C(23)	26(4)	24(4)	37(4)	4(3)	-13(3)	-10(3)
C(24)	30(4)	27(4)	28(4)	9(3)	-7(3)	-12(3)
C(25)	28(4)	35(4)	38(4)	9(3)	-9(3)	-11(3)
C(26)	39(4)	28(4)	37(4)	5(3)	-4(3)	-10(3)
C(27)	54(5)	30(4)	35(5)	9(3)	-8(4)	-17(4)
C(28)	73(7)	44(5)	41(5)	22(4)	-11(5)	-26(5)
C(30)	40(4)	31(4)	32(4)	9(3)	-7(3)	-9(4)
C(31)	41(5)	29(4)	41(5)	6(4)	-5(4)	-12(4)
C(32)	60(6)	50(6)	30(5)	8(4)	-6(4)	24(5)
C(33)	55(6)	34(5)	35(5)	11(4)	-9(4)	5(4)
C(34)	63(6)	22(4)	38(5)	6(3)	-12(4)	-1(4)
C(35)	43(5)	23(4)	28(4)	3(3)	-8(3)	5(4)
C(36)	40(4)	26(4)	29(4)	-2(3)	1(3)	1(4)
C(37)	47(5)	17(4)	27(4)	1(3)	-4(3)	-1(3)
C(38)	55(5)	18(4)	34(4)	3(3)	-2(4)	-9(4)
C(39)	43(4)	23(4)	28(4)	8(3)	-8(3)	-12(3)
C(40)	59(5)	33(4)	29(4)	5(3)	-7(4)	-26(4)
C(41)	60(6)	34(4)	37(4)	-4(4)	2(4)	-29(4)
C(42)	48(5)	38(5)	53(5)	2(4)	5(4)	-22(4)
C(43)	61(6)	45(5)	59(6)	-23(5)	6(5)	-29(5)
C(44)	70(7)	75(7)	54(6)	-14(5)	-4(5)	-49(6)
C(45)	59(6)	46(5)	34(4)	5(4)	2(4)	-31(5)

C(46)	52(5)	52(5)	34(4)	8(4)	-10(4)	-31(5)
C(47)	67(7)	74(8)	94(8)	51(7)	-49(6)	-41(6)
C(48)	78(8)	60(7)	134(11)	38(7)	-67(8)	-40(6)
C(49)	74(7)	50(6)	117(9)	47(6)	-63(7)	-43(6)
C(50)	67(6)	40(5)	60(6)	25(4)	-24(5)	-30(5)
C(51)	53(5)	25(4)	36(4)	8(3)	-7(4)	-14(4)
C(52)	46(4)	19(4)	24(4)	1(3)	-9(3)	-10(3)
C(53)	39(4)	16(3)	32(4)	7(3)	-5(3)	-7(3)
C(54)	37(4)	19(4)	23(4)	0(3)	1(3)	-3(3)
C(55)	40(4)	15(3)	22(4)	5(3)	-1(3)	-1(3)
C(56)	37(4)	16(3)	24(4)	0(3)	-8(3)	4(3)
C(57)	40(4)	21(4)	35(4)	-4(3)	-10(3)	-1(3)
C(58)	47(5)	36(5)	42(5)	-8(4)	-10(4)	-3(4)
C(59)	49(5)	45(5)	40(5)	-11(4)	-9(4)	-7(4)
C(60)	35(4)	40(5)	27(4)	-1(3)	-4(3)	3(4)
C(61)	45(5)	28(4)	23(4)	4(3)	-3(3)	8(4)
C(62)	63(7)	69(7)	97(9)	12(6)	-33(6)	-30(6)
Cl(1)	195(6)	308(8)	248(7)	-95(6)	-58(5)	-63(6)
Cl(2)	127(4)	146(4)	190(5)	-81(4)	3(3)	-41(3)
C(63)	71(7)	49(6)	52(6)	11(4)	-13(5)	-30(5)
Cl(3)	78(2)	44(1)	69(2)	-13(1)	18(1)	-26(1)
Cl(4)	105(2)	66(2)	88(2)	36(2)	-48(2)	-60(2)
C(64)	101(8)	85(7)	107(8)	-28(6)	-23(6)	-18(6)
Cl(5)	66(2)	88(2)	56(2)	15(2)	-4(1)	7(2)
Cl(6)	170(5)	102(3)	192(5)	-22(3)	-75(4)	-60(3)
C(65)	104(6)	103(6)	123(7)	-15(5)	-21(5)	-45(5)
C(66)	106(8)	160(10)	142(10)	16(8)	-45(7)	-86(8)
C(67)	70(7)	128(9)	110(8)	-34(7)	-23(6)	-41(6)
C(68)	73(9)	110(11)	110(12)	-28(10)	-39(8)	-30(8)
C(69)	113(9)	142(10)	139(10)	-33(8)	-33(7)	-60(8)
C(70)	64(6)	125(9)	129(9)	-32(7)	-25(6)	-45(6)
C(72)	110(8)	108(8)	71(7)	16(6)	24(6)	-30(7)
C(73)	106(8)	96(7)	77(7)	6(6)	13(6)	-65(7)

C(74)	97(8)	109(8)	98(8)	36(6)	-6(6)	-55(7)
C(75)	117(13)	178(17)	93(11)	17(11)	20(9)	-106(14)
C(76)	117(9)	133(9)	82(8)	1(7)	26(7)	-33(8)
C(77)	82(8)	83(8)	40(6)	-16(5)	11(5)	-37(7)
C(78)	114(9)	122(9)	90(8)	-4(7)	7(7)	-30(7)
C(79)	121(9)	97(8)	83(7)	62(6)	-1(6)	-12(7)
C(80)	121(9)	120(9)	95(8)	50(7)	-5(7)	-31(7)
C(81)	119(9)	126(9)	109(8)	68(7)	-8(7)	-15(7)

Hydrogen coordinates (x 10^4) and isotropic displacement parameters ($Å^2$x 10^3) for (C60 H26 N16)*2(C7 H8)*0.5(C6 H6)*3(C H2 Cl2).

	x	y	z	U(eq)
H(1)	2446	1684	4415	68
H(2)	1960	855	5520	67
H(3)	1148	1671	6668	52
H(11)	-653	1790	11399	47
H(12)	-1077	1072	12600	53
H(13)	-2023	2008	13631	63
H(16)	-3260	6388	13551	46
H(17)	-2881	7268	12442	42
H(18)	-2092	6487	11249	37
H(22)	-982	5709	8873	35
H(26)	32	6329	6567	43
H(27)	556	6993	5381	48
H(28)	1423	6041	4339	64
H(32)	6032	-1779	11528	74
H(33)	5154	-2521	11032	59
H(34)	3698	-1645	10392	55
H(38)	1009	-675	9255	45
H(42)	-1208	-1146	8171	54
H(43)	-2223	-1780	7613	62
H(44)	-3658	-753	6964	71
H(47)	-4958	3626	6562	90
H(48)	-4082	4450	7002	102
H(49)	-2585	3545	7690	89
H(57)	2118	3080	10204	42
H(58)	3084	3722	10812	54
H(59)	4601	2693	11370	57
H(62A)	4722	2576	5320	89
H(62B)	3982	2373	4745	89

H(63A)	2022	3547	2832	67
H(63B)	2168	3876	3691	67
H(64A)	4227	9916	7251	122
H(64B)	4045	9481	8138	122
H(66)	6850	4377	-586	149
H(67)	7423	2636	-295	119
H(68)	6926	2066	970	115
H(69)	6129	3031	1945	150
H(70)	5570	4607	1701	121
H(71A)	5274	5811	1256	406
H(71B)	5320	6031	290	406
H(71C)	6277	5858	797	406
H(73)	10048	617	6377	104
H(74)	9184	2290	6244	119
H(75)	7702	2970	5526	141
H(76)	6942	2035	5115	142
H(77)	7769	424	5207	81
H(78A)	9117	-982	5761	172
H(78B)	9622	-822	6529	172
H(78C)	10146	-819	5633	172
H(79)	6376	4308	4273	138
H(80)	5311	3578	3918	145
H(81)	3530	4526	4833	160

REFERENCES

1. Ruiz, G. T.; Juliarena, M. P.; Lezna, R. O.; Feliz, M. R.; Ferraudi, G. *J. Photochem. Photobiol., A* **2006**, *179*, 289-297.

2. McGovern, D. A.; Selmi, A.; O'Brien, J. E.; Kelly, J. M.; Long, C. *Chem. Commun. (Camb)* **2005**, 1402-1404.

3. Molnar, S. M.; Nallas, G.; Bridgewater, J. S.; Brewer, K. J. *J. Am. Chem. Soc.* **1994**, *116*, 5206-5210.

4. Brewer, K. J. B., VA, US), Elvington, Mark (Blacksburg, VA, US); Virginia Tech Intellectual Properties, Inc. (Blacksburg, VA, US): United States, **2009**.

5. Schilling, M. A.; Esmundo, M. *Energy Policy* **2009**, *37*, 1767-1781.

6. Arifin, K.; Majlan, E. H.; Wan Daud, W. R.; Kassim, M. B. *Int. J. Hydrogen Energy* **2012**, *37*, 3066-3087.

7. Kalyanasundaram, K.; Graetzel, M. *Curr. Opin. Biotechnol.* **2010**, *21*, 298-310.

8. Chow, W. S.; Eaton-Rye, J. J., Tripathy, B. C., Sharkey, T. D., Eds.; Springer Netherlands: **2012**; Vol. 34, p 607-622.

9. van de Krol, R.; Grätzel, M. *Photoelectrochemical Hydrogen Production*; Springer, **2011**.

10. Lewis, N. S.; Nocera, D. G. *Proceedings of the National Academy of Sciences* **2006**, *103*, 15729-15735.

11. Esswein, A. J.; Nocera, D. G. *Chem. Rev.* **2007**, *107*, 4022-4047.

12. Alstrum-Acevedo, J. H.; Brennaman, M. K.; Meyer, T. J. *Inorg. Chem.* **2005**, *44*, 6802-6827.

13. Meyer, T. J. *Acc. Chem. Res.* **1989**, *22*, 163-170.

14. Morris, A. J.; Meyer, G. J.; Fujita, E. *Acc. Chem. Res.* **2009**, *42*, 1983-1994.

15. Danielson, E.; Elliott, C. M.; Merkert, J. W.; Meyer, T. J. *J. Am. Chem. Soc.* **1987**, *109*, 2519-2520.

16. Treadway, J. A.; Chen, P.; Rutherford, T. J.; Keene, F. R.; Meyer, T. J. *The Journal of Physical Chemistry A* **1997**, *101*, 6824-6826.

17. MacDonnell, F. M. *Solar Hydrogen GenerationToward a Renewable Energy Future*; Springer New York, **2008**.

18. Fees, J.; Kaim, W.; Moscherosch, M.; Matheis, W.; Klima, J.; Krejcik, M.; Zalis, S. *Inorg. Chem.* **1993**, *32*, 166-174.

19. Fees, J.; Ketterle, M.; Klein, A.; Fiedler, J.; Kaim, W. *J. Chem. Soc., Dalton Trans.* **1999**, 2595-2600.

20. Choi, C.-S.; Mutai, T.; Arita, S.; Araki, K. *J. Chem. Soc., Perkin Trans. 2* **2000**, 243-247.

21. Olofsson, J.; Önfelt, B.; Lincoln, P. *J. Phys. Chem. A* **2004**, *108*, 4391-4398.

22. Tan, L. F.; Liang, X. L.; Liu, X. H. *J. Inorg. Biochem.* **2009**, *103*, 441-447.

23. Kuhnt, C.; Karnahl, M.; Tschierlei, S.; Griebenow, K.; Schmitt, M.; Schafer, B.; Krieck, S.; Gorls, H.; Rau, S.; Dietzek, B.; Popp, J. *Phys. Chem. Chem. Phys.* **2010**, *12*, 1357-1368.

24. Kim, M. J.; Konduri, R.; Ye, H.; MacDonnell, F. M.; Puntoriero, F.; Serroni, S.; Campagna, S.; Holder, T.; Kinsel, G.; Rajeshwar, K. *Inorg. Chem.* **2002**, *41*, 2471-2476.

25. de Tacconi, N. R.; Lezna, R. O.; Konduri, R.; Ongeri, F.; Rajeshwar, K.; MacDonnell, F. M. *Chem. Eur. J.* **2005**, *11*, 4327-4339.

26. de Tacconi, N. R.; Chitakunye, R.; MacDonnell, F. M.; Lezna, R. O. *J. Phys. Chem. A* **2008**, *112*, 497-507.

27. Lezna, R. O.; Tacconi, N. R.; Janaratne, T.; Zuniga, M.; MacDonnell, F. M. *J. Argent. Chem. Soc.* **2009**, *97*.

28. Arachchige, S. M.; Brown, J. R.; Chang, E.; Jain, A.; Zigler, D. F.; Rangan, K.; Brewer, K. J. *Inorg. Chem.* **2009**, *48*, 1989-2000.

29. Fukuzumi, S.; Koumitsu, S.; Hironaka, K.; Tanaka, T. *J. Am. Chem. Soc.* **1987**, *109*, 305-316.

30. Gajiwala, H. M.; Zand, R. *Polymer* **2000**, *41*, 2009-2015.

31. Dickenson, J. E.; Summers, L. A. *Aust. J. Chem.* **1970**, *23*.

32. Murov, S. L.; Hug, G. L.; Carmichael, I. *Handbook Of Photochemistry*; M. Dekker, **1993**.

33. Nielsen, S. S. *Food Analysis*; Springer, **2010**.

34. Wilson, K.; Walker, J. *Principles and Techniques of Biochemistry and Molecular Biology*; Cambridge University Press, **2010**.

35. Jordan, R. B. *Reaction Mechanisms of Inorganic and Organometallic Systems*; Oxford University Press, **2007**.

36. Balaceanu, J. C. *Investigation of Rates and Mechanisms of Reaction*; Interscience Publishers, **1961**; Vol. 8.

37. Bergquist, C.; Parkin, G. *Inorg. Chem.* **1999**, *38*, 422-423.

38. Bergquist, C.; Storrie, H.; Koutcher, L.; Bridgewater, B. M.; Friesner, R. A.; Parkin, G. *J. Am. Chem. Soc.* **2000**, *122*, 12651-12658.

39. Brombacher, H.; Vahrenkamp, H. *Inorg. Chem.* **2004**, *43*, 6042-6049.

40. Kimura, E.; Shionoya, M.; Hoshino, A.; Ikeda, T.; Yamada, Y. *J. Am. Chem. Soc.* **1992**, *114*, 10134-10137.

41. Kvassman, J.; Larsson, A.; Pettersson, G. *Eur. J. Biochem.* **1981**, *114*, 555-563.

42. LeBrun, L. A.; Park, D.-H.; Ramaswamy, S.; Plapp, B. V. *Biochemistry* **2004**, *43*, 3014-3026.

43. Sakurai, M.; Furuki, T.; Inoue, Y. *J. Phys. Chem.* **1995**, *99*, 17789-17794.

44. Schmidt, J.; Chen, J.; DeTraglia, M.; Minkel, D.; McFarland, J. T. *J. Am. Chem. Soc.* **1979**, *101*, 3634-3640.

45. Guo, W.; Obare, S. O. *Tetrahedron Lett.* **2008**, *49*, 4933-4936.

46. Chatterjee, C.; Stephen, M. *Polyhedron* **2001**, *20*, 2917-2924.

47. Friess, S. L.; Lewis, E. S.; Weissberger, A. *Investigation of Rates and Mechanisms of Reactions: Volume VIII*; Wiley-Interscience, **1971**.

48. Bailey, D. N.; Roe, D. K.; Hercules, D. M. *J. Am. Chem. Soc.* **1968**, *90*, 6291-6297.

49. Heyes, D. J.; Levy, C.; Sakuma, M.; Robertson, D. L.; Scrutton, N. S. *J. Biol. Chem.* **2011**, *286*, 11849-11854.

50. Lu, Y.; Qu, F.; Moore, B.; Endicott, D.; Kuester, W. *J. Org. Chem.* **2008**, *73*, 4763-4770.

51. Lu, Y.; Qu, F.; Zhao, Y.; Small, A. M.; Bradshaw, J.; Moore, B. *J. Org. Chem.* **2009**, *74*, 6503-6510.

52. Liu, Y.; Yamamoto, S.; Sueishi, Y. *J. Photochem. Photobiol., A* **2001**, *143*, 153-159.

53. Scrutton, N. S.; Louise Groot, M.; Heyes, D. J. *Phys. Chem. Chem. Phys.* **2012**, *14*, 8818-8824.

54. Heyes, D. J.; Sakuma, M.; de Visser, S. P.; Scrutton, N. S. *J. Biol. Chem.* **2009**, *284*, 3762-3767.

55. Heyes, D. J.; Heathcote, P.; Rigby, S. E. J.; Palacios, M. A.; van Grondelle, R.; Hunter, C. N. *J. Biol. Chem.* **2006**, *281*, 26847-26853.

56. Davis, G. A.; Gresser, J. D.; Carapellucci, P. A. *J. Am. Chem. Soc.* **1971**, *93*, 2179-2182.

57. Martell, A. E.; Hancock, R. D. *Metal Complexes in Aqueous Solutions*; Springer, **1996**.

58. Garcia-Espana, E.; Nuzzi, F.; Sabatini, A.; Vacca, A. *Gazz. Chim. Ital.* **1985**, *115*, 607-611.

59. Banks, C. V.; Bystroff, R. I. *J. Am. Chem. Soc.* **1959**, *81*, 6153-6158.

60. Dillow, G. W.; Kebarle, P. *Can. J.Chem.* **1989**, *67*.

61. Kuimova, M. K.; Alsindi, W. Z.; Blake, A. J.; Davies, E. S.; Lampus, D. J.; Matousek, P.; McMaster, J.; Parker, A. W.; Towrie, M.; Sun, X.-Z.; Wilson, C.; George, M. W. *Inorg. Chem.* **2008**, *47*, 9857-9869.

62. Koley, D.; Arunan, E.; Ramakrishnan, S. *J. Comput. Chem.* **2012**, 1762-1772.

63. Zade, S. S.; Zamoshchik, N.; Reddy, A. R.; Fridman-Marueli, G.; Sheberla, D.; Bendikov, M. *J. Am. Chem. Soc.* **2011**, *133*, 10803-10816.

64. Norton, J. E.; Northrop, B. H.; Nuckolls, C.; Houk, K. N. *Org. Lett.* **2006**, *8*, 4915-4918.

65. Allakhverdiev, S. I.; Kreslavski, V. D.; Thavasi, V.; Zharmukhamedov, S. K.; Klimov, V. V.; Ramakrishna, S.; Nishihara, H.; Mimuro, M.; Carpentier, R.; Nagata, T. *Photosynthetic Energy Conversion: Hydrogen Photoproduction by Natural and Biomimetic Means*, **2010**.

66. Koca, A.; Kasimsener, M.; Kocak, M.; Gul, A. *Int. J. Hydrogen Energy* **2006**, *31*, 2211-2216.

67. Larsen, A. S.; Wang, K.; Lockwood, M. A.; Rice, G. L.; Won, T.-J.; Lovell, S.; Sadílek, M.; Turec□ek, F.; Mayer, J. M. *J. Am. Chem. Soc.* **2002**, *124*, 10112-10123.

68. Losse, S.; Vos, J. G.; Rau, S. *Coord. Chem. Rev.* **2010**, *254*, 2492-2504.

69. Nada, A.; Hamed, H.; Barakat, M.; Mohamed, N.; Veziroglu, T. *Int. J. Hydrogen Energy* **2008**, *33*, 3264-3269.

70. Ng, Siu M.; Yin, C.; Yeung, Chi H.; Chan, Tak C.; Lau, Chak P. *Eur. J. Inorg. Chem.* **2004**, *2004*, 1788-1793.

71. Sakai, K.; Ozawa, H. *Coord. Chem. Rev.* **2007**, *251*, 2753-2766.

72. Arounaguiri, S.; Easwaramoorthy, D.; Ashokkumar, A.; Dattagupta, A.; Maiya, B. G. *Proc. - Indian Acad. Sci., Chem. Sci.* **2000**, *112*.

73. Giordano, P. J.; Bock, C. R.; Wrighton, M. S. *J. Am. Chem. Soc.* **1978**, *100*, 6960-6965.

74. Kim, M. J.; MacDonnell, F. M.; Gimon-Kinsel, M. E.; Du Bois, T.; Asgharian, N.; Griener, J. C. *Angew. Chem., Int. Ed. Engl.* **2000**, *39*, 615-619.

75. Rusanova, J.; Decurtins, S.; Rusanov, E.; Stoeckli-Evans, H.; Delahaye, S.; Hauser, A. *J. Chem. Soc., Dalton Trans.* **2002**, 4318-4320.

76. Singh, S.; de Tacconi, N. R.; Boston, D.; MacDonnell, F. M. *Dalton transactions* **2010**, *39*, 11180-11187.

77. Kato, T.; Masu, H.; Takayanagi, H.; Kaji, E.; Katagiri, K.; Tominaga, M.; Azumaya, I. *Tetrahedron* **2006**, *62*, 8458-8462.

78. Cheeseman, G. W. H. *J. Chem. Soc. (Resumed)* **1962**, 1170-1176.

79. Bockman, T. M.; Kochi, J. K. *J. Org. Chem.* **1990**, *55*, 4127-4135.

80. Burmester, C.; Faust, R. *Synthesis* **2008**, 1179-1181.

81. DaSilveira Neto, B. A.; Lopes, A. S.; Wuest, M.; Costa, V. E. U.; Ebeling, G.; Dupont, J. *Chem. Inform.* **2006**, *37*.

82. Mancilha, F. S.; DaSilveira Neto, B. A.; Lopes, A. S.; Moreira, P. F.; Quina, F. H.; Gonçalves, R. S.; Dupont, J. *Eur. J. Org. Chem.* **2006**, *2006*, 4924-4933.

83. Edelmann, M. J.; Raimundo, J.-M.; Utesch, N. F.; Diederich, F.; Boudon, C.; Gisselbrecht, J.-P.; Gross, M. *Helv. Chim. Acta* **2002**, *85*, 2195-2213.

84. Moerkved, E. H.; Neset, S. M.; Bjoerlo, O.; Kjoesen, H.; Hvistendahl, G.; Mo, F. *ChemInform* **1996**, *27*, no-no.

85. Robbins, J. L.; Edelstein, N.; Spencer, B.; Smart, J. C. *J. Am. Chem. Soc.* **1982**, *104*, 1882-1893.

86. Konishi, A.; Hirao, Y.; Nakano, M.; Shimizu, A.; Botek, E.; Champagne, B. t.; Shiomi, D.; Sato, K.; Takui, T.; Matsumoto, K.; Kurata, H.; Kubo, T. *J. Am. Chem. Soc.* **2010**, *132*, 11021-11023.

87. Lambert, C. *Angew. Chem., Int. Ed. Engl.* **2011**, *50*, 1756-1758.

88. Kubo, T.; Shimizu, A.; Uruichi, M.; Yakushi, K.; Nakano, M.; Shiomi, D.; Sato, K.; Takui, T.; Morita, Y.; Nakasuji, K. *Org. Lett.* **2006**, *9*, 81-84.

89. Porter, W. W.; Vaid, T. P.; Rheingold, A. L. *J. Am. Chem. Soc.* **2005**, *127*, 16559-16566.

90. Lund, A.; Shiotani, M. *Epr of Free Radicals in Solids: Trends in Methods and Applications*; Kluwer Academic, **2003**.

91. Zheng, R. H.; Guo, H. C.; Jiang, H. J.; Xu, K. H.; Liu, B. B.; Sun, W. L.; Shen, Z. Q. *Chin. Chem. Lett.* **2010**, *21*, 1270-1272.

92. Inc., B. A. X.-r. S. Madison, WI.

93. Kyzioł, J. B.; Zaleski, J. *Acta Crystallogr., Sect. E: Struct. Rep. Online* **2007**, *63*, 1235-1237.

94. D'Alessandro, D. M.; Keene, F. R. *Dalton Trans.* **2006**, 1060-1072.

95. Ullmann, F.; Bielecki, J. *Ber. der Deut. Chem. Ges.* **1901**, *34*, 2174-2185.

96. Tamao, K.; Sumitani, K.; Kumada, M. *J. Am. Chem. Soc.* **1972**, *94*, 4374-4376.

97. King, A. O.; Okukado, N.; Negishi, E.-i. *J. Chem. Soc., Chem. Commun.* **1977**, 683-684.

98. Miyaura, N.; Suzuki, A. *J. Chem. Soc., Chem. Commun.* **1979**, 866-867.

BIOGRAPHICAL INFORMATION

Joseph Aslan was born on January 7th, 1985 in Mountain View, California. He received his Bachelor's Degree from the University of Texas at Arlington in May 2007, and decided to continue his research under the supervision of Dr. Frederick MacDonnell. After his unconditional acceptance into the Ph.D. program in August 2009, he presented his research at various meetings such as the Gordon Research Conference in August 2010, and the Annual Celebration of Excellence by Students in April 2011. During his graduate school career he was awarded the Charles K. Baker Character Fellowship award, in a unanimous decision by the department faculty.

In May 2011, he was awarded an internship opportunity with SABIC Innovative Plastics for 12-weeks, where he filed 3 patent disclosure statements and contributed to the success of the sustainability program. In February 2012, he was re-invited to attend a second internship starting in May 2012, where by the end of June 2012 he finished filing 3 new patent disclosure statements, all of which have the potential to be commercialized on an industrial scale.

Joseph plans to begin a full-time position with SABIC after his internship ends in August 2012. He plans on living in Indiana with his future wife Casey Freeman, who is a registered nurse and currently works in Ft. Worth, Texas.